Dilute Surfactant Methods for Carbonate Formations

ID Number: DE-FC26-02NT 15322

Final Report

Reporting Period Start Date: 7-1-2002

Reporting Period End Date: 11-24-2005

Submitted to the

U.S. Department of Energy

Kishore K. Mohanty

Department of Chemical Engineering

University of Houston

4800 Calhoun Road

Houston, Texas 77204-4004

February, 2006

Disclaimer

Abstract

There are many fractured carbonate reservoirs in US (and the world) with light oil. Waterflooding is effective in fractured reservoirs, if the formation is water-wet. Many fractured carbonate reservoirs, however, are mixed-wet and recoveries with conventional methods are low (less than 10%). The process of using dilute anionic surfactants in alkaline solutions has been investigated in this work for oil recovery from fractured oil-wet carbonate reservoirs both experimentally and numerically. This process is a surfactant-aided gravity drainage where surfactant diffuses into the matrix, lowers IFT and contact angle, which decrease capillary pressure and increase oil relative permeability enabling gravity to drain the oil up.

Anionic surfactants have been identified which at dilute concentration of 0.05 wt% and optimal salinity can lower the interfacial tension and change the wettability of the calcite surface to intermediate/water-wet condition as well or better than the cationic surfactant DTAB with a West Texas crude oil. The force of adhesion in AFM of oil-wet regions changes after anionic surfactant treatment to values similar to those of water-wet regions. The AFM topography images showed that the oil-wetting material was removed from the surface by the anionic surfactant treatment. Adsorption studies indicate that the extent of adsorption for anionic surfactants on calcite minerals decreases with increase in pH and with decrease in salinity. Surfactant adsorption can be minimized in the presence of Na_2CO_3.

Laboratory-scale surfactant brine imbibition experiments give high oil recovery (20-42% OOIP in 50 days; up to 60% in 200 days) for initially oil-wet cores through wettability alteration and IFT reduction. Small (<10%) initial gas saturation does not affect significantly the rate of oil recovery in the imbibition process, but larger gas saturation decreases the oil recovery rate. As

the core permeability decreases, the rate of oil recovery reduces, and this reduction can be scaled by the gravitational dimensionless time.

Mechanistic simulation of core-scale surfactant brine imbibition matches the experimentally observed imbibition data. In-situ distributions observed through simulation indicate that surfactant diffusion (which depends on temperature and molecular weight) is the rate limiting step. Most of the oil is recovered through gravitational forces. Oil left behind at the end of this process is at its residual oil saturation. The capillary and Bond numbers are not large enough to affect the residual oil saturation.

At the field-scale, 50% of the recoverable oil is produced in about 3 years if the fracture spacing is 1 m and 25% if 10 m, in the example simulated. Decreasing fracture spacing and height, increasing permeability, and increasing the extent of wettability alteration increase the rate of oil recovery from surfactant-aided gravity drainage. This dilute surfactant aided gravity-drainage process is relatively cheap. The chemical cost for a barrel of oil produced is expected to be less than $1.

TABLE OF CONTENTS

List of Figures

Executive Summary

There are many fractured carbonate reservoirs in US (and the world) with light oil. Waterflooding is effective in fractured reservoirs, if the formation is water-wet. Many fractured carbonate reservoirs, however, are mixed-wet and recoveries with conventional methods are low (less than 10%). The process of using dilute anionic surfactants in alkaline solutions has been investigated in this work for oil recovery from fractured oil-wet carbonate reservoirs both experimentally and numerically. This process is a surfactant-aided gravity drainage where surfactant diffuses into the matrix, lowers IFT and contact angle, which decrease capillary pressure and increase oil relative permeability enabling gravity to drain the oil up.

Anionic surfactants have been identified which at dilute concentration of 0.05 wt% and optimal salinity can lower the interfacial tension and change the wettability of the calcite surface to intermediate/water-wet condition as well or better than the cationic surfactant DTAB with a West Texas crude oil. The force of adhesion in AFM of oil-wet regions changes after anionic surfactant treatment to values similar to those of water-wet regions. The AFM topography images showed that the oil-wetting material was removed from the surface by the anionic surfactant treatment. Adsorption studies indicate that the extent of adsorption for anionic surfactants on calcite minerals decreases with increase in pH and with decrease in salinity. Surfactant adsorption can be minimized in the presence of Na_2CO_3.

Laboratory-scale surfactant brine imbibition experiments give high oil recovery (20-42% OOIP in 50 days; up to 60% in 200 days) for initially oil-wet cores through wettability alteration and IFT reduction. Small (<10%) initial gas saturation does not affect significantly the rate of oil recovery in the imbibition process, but larger gas saturation decreases the oil recovery rate. As the core permeability decreases, the rate of oil recovery reduces, and this reduction can be scaled by the gravitational dimensionless time.

Mechanistic simulation of core-scale surfactant brine imbibition matches the experimentally observed imbibition data. In-situ distributions observed through simulation indicate that surfactant diffusion (which depends on temperature and molecular weight) is the rate limiting step. Most of the oil is recovered through gravitational forces. Oil left behind at the end of this process is at its residual oil saturation. The capillary and Bond numbers are not large enough to affect the residual oil saturation.

At the field-scale, 50% of the recoverable oil is produced in about 3 years if the fracture spacing is 1 m and 25% if 10 m, in the example simulated. Decreasing fracture spacing and height, increasing permeability, and increasing the extent of wettability alteration increase the rate of oil recovery from surfactant-aided gravity drainage. This dilute surfactant aided gravity-drainage process is relatively cheap. The chemical cost for a barrel of oil produced is expected to be less than $1.

Introduction

About half-of the world's known oil reserves are in carbonate reservoirs.[1] Many of these carbonate reservoirs are naturally fractured. Many fractured reservoirs are poorly understood and recovery from fractured reservoirs is typically lower than those from unfractured reservoirs. Fractured reservoirs with high matrix porosity and low matrix permeability need a secondary or EOR technique to achieve maximum production, according to a recent review of 100 fractured reservoirs.[2] Recovery factor in these reservoirs depends on matrix permeability, wettability, fracture intensity and fluid properties.

Water-flooding is an effective technique for fractured reservoirs, if the formation is water-wet. The positive capillary pressure helps in imbibing water into the matrix and expelling the oil. However, many carbonate reservoirs (about 80%) are mixed-wet or oil-wet.[3] Positive zeta potential on carbonate surfaces at a typical pH (~7),[4] presence of sufficient number of negatively charged / asphaltenic molecules in oil,[5] and high capillary pressure during oil migration into the reservoir often render mixed-wettability to the reservoir rocks.[6] Waterflooding does not lead to a significant amount of oil recovery from the matrix porosity because the capillary pressure curve is predominantly negative. Surfactant flooding (or huff-n-puff) is being tested[7] to improve oil recovery from mixed-wet, fractured carbonate formations and is the subject of this study.

Surfactant or micellar-polymer flooding has been developed for sandstone reservoirs in the last four decades. It has been shown to be highly effective in laboratory studies[8] and holds the promise for recovering a significant amount of light oil in a favorable oil price scenario. A slug of anionic/nonionic surfactant solution is injected in these methods to create ultralow interfacial tension between oil and water thus mobilizing oil. A polymer solution is injected to push the surfactant slug. In some formulations, polymer is added to the surfactant slug itself.

Many surfactant flood field tests have been conducted over the past three decades [9-10]. Some have been technically successful; others have taught some important lessons. It has been shown that preflushes to remove excessive salinity are mostly ineffective and both surfactants and polymers need to be compatible with the reservoir brine [9-10]. It has been demonstrated that the effective and timely oil recovery from surfactant-polymer field tests correlates well with the integrity of surfactant slug and polymer buffer[11].

Chemical slugs tend to break down in reservoirs because of adsorption, phase trapping, dispersion, dilution, and viscous/heterogeneity fingering. Adsorption and phase trapping have been studied extensively[12] and chemicals are being developed to minimize adsorption. Anionic surfactants are used in sandstones because the surface charge in sandstones is primarily negative. Dispersion in multiphase flow has been studied [13-14]. Surfactant-polymer flooding often involves flood fronts with adverse mobility ratios[15]. Reservoir heterogeneity and viscous fingering can lead to oil bypassing by the surfactant bank. It is important to design surfactant banks to minimize this bypassing.

There are two kinds of designs for surfactant-polymers floods and minimizing bypassing is important to both the designs. The first design uses a high concentration of surfactant (> 5 wt%), but a small slug (<0.2 PV). These floods are often referred to as microemulsion floods and have been field tested by Exxon[9] and Marathon[16-17], for example. In the second design, a larger slug (>0.2 PV) of low concentration surfactant (< 1 wt%) is injected. It is often referred to as Low Tension Flood and has been field tested by Mobil, for example. In microemulsion floods, there are two displacement fronts of adverse mobility ratio. One is the displacement of multi-phase water-oil bank by single-phase microemulsion. The second is the displacement of polymer bank by water. Reppert et al. [9] studied the total mobility variation in several one-dimensional microemulsion corefloods. It was demonstrated that the oil-bank–microemulsion front cannot be

made stable by adding diesel to the microemulsion phase. Polymer had to be added to the surfactant bank to bring about favorable mobility to this flood front. The technical success of the Loudon field test [9] can be ascribed, at least partly, to this stabilization. The instability at the polymer-water front is well recognized and is mitigated by having graded viscosity in the polymer bank. The front-end cost is very high in these processes, because surfactant is injected early in the process. The economic return comes at a later stage when the incremental oil is produced. This high cost is justified if the initial oil saturation is high enough, the residual oil saturation is reduced to near zero, adsorption is minimal, sweep efficiency is high, oil bank is produced fast and oil price is high. This process carries a high risk. Recently, researchers have sought for a less risky surfactant process which is described next.

The Low Tension Floods also suffer from adverse mobility ratio at the oil bank-surfactant bank flood front. The failure of Mobil's field test in 1960's is blamed partly on this instability. Recently, [8] mobility control is given to the low tension flood by adding polymer to the surfactant bank in what they refer to as "Low Tension Polymer Flood" (LTPF). The effectiveness of LTPF has been demonstrated at the laboratory scale. The basic LTPF scheme involves the injection of up to 0.7 PV of surfactant-polymer mixture (~3000 ppm surfactant and ~750 ppm polymer) in brine. This is followed by 0.5 PV of graded viscosity polymer buffer, followed by brine. LTPF combines the mobility control of polymer flooding with the high displacement efficiency of surfactant flooding. Its effectiveness at the field scale remains to be tested. Because of the low concentration of the chemicals and large slug size, this process offers the hope of being relatively inexpensive and robust.

Fractured carbonates are different from sandstones in many respects. The zeta potential on carbonate minerals is positive (negative on silica at normal pH), pore structure is more heterogeneous (presence of fractures, vugs and dead-end pores), and permeability (of the matrix)

can be significantly lower. Wettability alteration to water-wet or intermediate-wet conditions is an important mechanism for improving oil recovery in fractured media.

Flooding with cationic surfactants is quite attractive because they bear the same charge as the surface of the carbonate minerals. Austad and coworkers have conducted a series of studies[18-21] on oil recovery from oil-wet chalk cores by use of surfactant solutions. They have shown that cationic surfactants, such as dodecyl trimethyl ammonium bromide (DTAB), are quite effective (recovery ~70% OOIP) in imbibing water into originally oil-wet cores at concentrations higher than their CMC (~1 wt%). The imbibition mechanism is proposed as (i) the formation of ion-pairs by the interaction between surfactant monomers and adsorbed organic carboxylates from the crude oil, (ii) water-wettability of the solid surface due to dissolution of the ion-pairs in the oil phase and micelles, (iii) counter-current imbibition of brine due to capillary pressure. The imbibition rate increases with temperature and decreases with a connate water saturation. The interfacial tension between the surfactant solution and oil was high (> 0.1 mN/m). They found that most of the anionic surfactants tested were not able to desorb the adsorbed organic carboxylates. Ethoxylated sulfonates have the ability to displace oil by a spontaneous imbibition of brine. A propoxy ethoxy sulfate surfactant displaced oil when the buoyancy force exceeded the capillary force caused by low interfacial tension (~0.08 mN/m). But the recovery with the anionic surfactants was slow compared to those with the cationic surfactants. The air-water contact angle on the surfactant adsorbed calcite surface showed low angles (12°-28°) for the cationic surfactants, but higher angles (39°-63°) for the anionic surfactants. Water-oil contact angles were not measured for these surfactants.

In 2003, Austad and coworkers[22-24] identified several cheap commercial cationic surfactants, $C_{10}NH_2$ and bioderivatives from the coconut palm termed Arquad and Dodigen (priced at 3 US$

per kg), which were able to recover 50-90% of oil. The higher cost and the needed concentration (about 1 wt%) of cationic surfactants necessitates evaluating other surfactants.

The higher cost of cationic surfactants compared to anionic surfactants (which are usually priced at ~1 US$ per kg) and relatively higher concentration required (~1 wt%) has encouraged others to evaluate anionic surfactants for fractured carbonates[25-26] in the presence of a low concentration potential determining ions. Chen et al.[27] have performed dilute (~0.35 wt%) surfactant imbibition tests for carbonate cores from the Yates field with a nonionic surfactant and an anionic surfactant. Computerized Tomography (CT) scans indicated that enhanced imbibition is possible due to counter-current flow at the beginning and gravity-driven[28] flow during the later stages. Spinler et al.[29] conducted spontaneous imbibition and adsorption tests with a surfactant which was an ammonium salt of ethoxylated and sulfated alcohols at very low concentrations (~0.05 wt%) and a high reservoir temperature (~131 °C). It was found to be effective in improving imbibition in North Sea chalk cores and adsorption was low. Hirasaki and Zhang[26] have evaluated several ethoxylated and propoxylated sulfates in the presence of a low concentration potential determining ions (~0.3 M Na_2CO_3).

Though most of these studies have given favorable results in the laboratory-scale experiments, their field-scale performance is not well understood. Imbibition and drainage of wetting and non-wetting phases from the matrix blocks of fractured reservoirs are driven by some combination of capillary, gravity and viscous forces. Imbibition of brine (surfactant free) into matrix blocks has been studied for the last 50 years. Zhou et al.[31] and Morrow et al.[32] have reviewed oil recovery from spontaneous imbibition dealing especially with the influence of rock wettability and scaling of the imbibition process. Mattax and Kyte[33] were the first to propose a scaling group for capillarity-controlled imbibition. Ma et al.[22] have proposed a modified scaling group which is given as:

$$t_{Pc} = \frac{\sqrt{\frac{k}{\phi}}\sigma}{\sqrt{\mu_o \mu_w} L_c^2} t \,,\; L_c = \frac{Ld}{2\sqrt{d^2 + 2L^2}} \tag{1}$$

where, t_{Pc} is dimensionless time, k is the rock permeability, ϕ is the porosity, σ is the interfacial tension, μ_w and μ_o are the viscosities of water and oil phases, respectively. L_c is the characteristic length for imbibition (often termed as the shape factor), and t is the actual time of imbibition. The imbibition experiments conducted by Morrow et al.[31] and Ma et al.[33] for water-wet cases all fitted into a unique curve using this dimensionless time, which is referred to as the very strongly water wet (VSWW) curve.

Cuiec et al.[34] examined imbibition at low IFT in short low permeability (1-3mD) chalk samples. They found that lowering IFT reduces the rate of imbibition in accordance with Eq. (1). The balance of the capillary and gravitational forces was investigated and reported by Du Prey.[35] The ratio of the capillary to gravitational forces termed as macroscopic inverse Bond number, is given by

$$N_B^{-1} = C \frac{\sqrt{\frac{\phi}{k}}\sigma}{\Delta\rho g L} \tag{2}$$

It can be seen that when N_B^{-1} is large, the gravitational forces dominate the flow. The numerator of N_B^{-1} is a measure of the capillary entry pressure. Schechter et al.[28] found that for N_B^{-1} < 1, gravity segregation dominates the flow and that for high values of N_B^{-1} >1, capillary forces are dominant. Hagoort[36] has analyzed the 1-D gravity driven oil drainage by a gas, and the expressions for dimensionless time and recovery are:

$$t_{Dg} = \frac{k k_{ro}^o \Delta\rho g}{(S_{oi} - S_{or})\phi \mu_o L} \tag{3}$$

$$E_R = \frac{(S_{oi} - \bar{S}_o)}{(S_{oi} - S_{or})} \tag{4}$$

The fractional recovery for a totally 1-D gravity-driven process with these dimensionless groups is given by

$$E_R = t_{Dg}, \text{ for } t_{Dg} < t_{BT}$$

and (5)

$$E_R = 1 - \frac{1 - \frac{1}{n}}{\left(n t_{Dg}\right)^{\frac{1}{n-1}}}, \text{ for } t_{Dg} > t_{BT}$$

where $t_{BT} = \frac{1}{n}$. The exponent *n*, is the Corey exponent in Hagoort's[36] analysis, and it determines the degree of curvature in the oil relative permeability relationship: the lower the *n*, the more favorable will be recovery. *n* is the only adjustable parameter in the above expression.

The combined effects of both gravitational and capillary forces on residual saturations has been considered by Morrow et al.[37] Li and Horne[38] more recently have analytically developed a general scaling group incorporating both capillary and gravity forces besides general parameters like mobility and capillary pressure. They tested their model on the imbibition data from Schechter et al;[28] the fit was quite good for a large range of permeabilities.

The above scaling groups do not apply to imbibition processes with changing wettability and IFT. Numerical simulators have been developed in the past for chemical flooding where IFT changes along the reservoir with time. The UTCHEM simulator[39] incorporates oil/surfactant/brine phase behavior using Hand's rule, trapping number model for relative permeability, adsorption of surfactants, flow, and dispersion for describing the and trapping

number model for relative permeability. Shutang et al.[40] have predicted the alkaline surfactant polymer (ASP) performance for a pilot in Daqing oil field in China using the GCOMP simulator. It, however, did not include all the interactions between alkali, surfactant, and the minerals. They used a simplified model based on the interfacial tension contour maps as a function of surfactant and alkaline concentration to match field results. Most of the simulation studies were also focused on the study of chemical EOR in non-fractured reservoirs without wettability alteration. In this study, a simulator is developed that incorporates variation of IFT and wettability due to diffusion and imbibition of surfactant solutions into a matrix block.

The goal of this research is to evaluate dilute surfactant methods for carbonate formations and identify conditions under which they can be effective. Laboratory experiments have been conducted to understand the physicochemical mechanisms of oil recovery by anionic surfactant treatment. Mechanistic simulations have been conducted to understand the laboratory experiments. Field-scale simulations are also conducted to identify criteria under which dilute surfactant methods are feasible without active mobility control. This final report summarizes our results for the period of July, 2002 through November, 2005.

Experimental

Material. Surfactant properties are listed in Table 1. Surfactants 4-22, 5-166 and S-6566 are alkyl aryl sulfonates (two of them were ethoxylated) and the surfactants Alf-mn are alkyl propoxylated sulfates. In the nomenclature Alf-mn, the second digit n (e.g., 5 in Alf-35) indicates the number of propoxy groups present. Alf-3n series has a carbon chain length of 14 and Alf-6n series has a carbon chain length of 12-13. There are four ethoxy sulfates. Of the fourteen surfactants evaluated one of them is a cationic surfactant, Dodecyl trimethyl ammonium bromide (DTAB), used as a reference. Surfactants were used as supplied.

Calcite (Iceland spar), lithographic limestone, marble, and dolomite plates were supplied by Scientific Ward. Synthetic calcite powder, consisting of 5 μm particles, was supplied by AESAR (Johnson Mathey Inc.). The surface area for the calcite powder is 1.67 m^2/g. The oil was from a West Texas fractured carbonate field. It had 28.2 °API, 19.1 cp viscosity, 0.2 acid number and 1.17 base number. It was similar to the oil MY3 used by Hirasaki and Zhang.[26] Reformulated reservoir brine (Table 2) was used for the evaluation of the cationic surfactant. Synthetic brine composed of Na_2CO_3 was used for the anionic surfactants to lower adsorption and surfactant requirement. Ideally, the reservoir brine should have been used. However, the reservoir brine consists of divalent ions that are likely to precipitate in the presence of Na_2CO_3. In the actual field conditions, the problem is less severe because the brine is in equilibrium with the mineral rock and addition of more CO_3^{2-} in fact suppresses the Ca^{2+} in the brine. In a study on the chemical composition during chemical flooding, Cheng[24] found significantly lower ion exchange and mineral dissolution in the presence of Na_2CO_3 as compared to caustic and sodium silicate. Further, the permeability reduction due to precipitation was also found to be the lowest for Na_2CO_3.

Experimental Procedure. The following experiments were conducted for evaluation of the surfactants: phase behavior study, interfacial tension measurement, wettability test, and adsorption.

Phase Behavior Study. Dilute solutions of anionic surfactants (0.05 active wt%) were prepared with varying concentrations of sodium carbonate (Na_2CO_3). These solutions were equilibrated with equal volumes of oil on a tube shaker for a period of two days. Thereafter the tubes were removed and left to settle for a day. The number of phases and the color of the phases were observed, which indicated the shift from Winsor type II- to type II+ phase behavior with the increase in salinity of the solution.

Interfacial Tension Measurement. The IFT between the equilibrated brine and oil phases was measured with the help of a spinning drop tensiometer. The equilibrated brine solutions and the equilibrated oil from the phase behavior study were used to determine the interfacial tension between the synthetic brine and oil. This led to the identification of the region of lowest interfacial tension or optimal salinity of the given system. The subsequent wettability experiments were performed at the optimal salinity obtained from these measurements.

Wettability Test. The wettability tests were done on mineral plates (2 cm x 1 cm x 0.2 cm). The plates were polished on a 600 mesh diamond lap and equilibrated with synthetic brine for a day. The initial wettability state of the plate was determined by measuring advancing and receding contact angles of oil with the plate immersed in brine. The contact angle measurements were made with the help of a Kruss goniometer. The plate was removed from brine and aged with oil at an elevated temperature (~80 °C) in the oven for about two days to make it oil-wet. The

reservoir temperature is close to the room temperature (~30 °C), but the elevated temperature aging is done to compensate for the short aging time (compared with the geological time). After removing from the oven, the plate (with oil stuck around it) was contacted with synthetic (sodium carbonate) brine for an hour and the advancing contact angle was measured. Thereafter, the synthetic brine was replaced by the surfactant-brine solution and the evolution of contact angle was studied for a period of two days by imaging the drops attached to the plate. In the cases where the drops were too small (<<0.1 mm), it was difficult to measure an accurate contact angle and a post-wettability test was performed. In the post-wettability test, the plate was washed with brine following the surfactant treatment. This plate was then placed in the brine solution and an oil drop was deposited on the bottom of the surface with the help of an inverted needle (oil drops did not attach to the top of the plate in these cases). The contact angle was then measured. This gave the final wettability state of the plate. The contact angle measured in the postwettability test is a receding contact angle, which is lower than the advancing contact angles. Drops were deposited on several parts of the plate and the range of the contact angles was noted. For the cationic surfactant, a similar procedure was followed except that the reformulated field brine replaced the synthetic brine.

Atomic Force Microscopy. In AFM force measurements, a tip is brought close to a surface and the deflection of the cantilever is measured as a function of tip-sample distance as shown in Fig. 1. At large tip-sample separations (position 1), there are no detectable interaction forces. As the separation distance decreases (position 2), forces such as electrostatic, van der Waals, specific interactions etc. come into play. As the tip is brought closer to the sample, at some point (position 3) the gradient of the attractive force exceeds the spring constant of the cantilever and the cantilever tip jumps into contact with the sample (position 4). This vertical distance between

(position 3) and (position 4) gives us a measure of the jump to contact force. From position (position 4) to (position 5), the tip and the sample remain in contact with each other until the tip starts to retract. As the tip retracts, at a particular point (position 6) the spring constant exceeds the gradient of the force of adhesion between the tip and the sample and the tip suddenly breaks away from the sample to its equilibrium position (position 7). The value of the spring force at position 6 is called the force of adhesion or pull-off force or jump-off contact force. This force of adhesion can be related to the surface energy using the JKR theory of adhesion mechanics as[41,42]

$$F_{adh}=(3/2)\pi R W_{abc} \qquad (6)$$

where W_{abc} is the work of adhesion to pull the tip off the sample, R is the radius of curvature of the tip, a represents the cantilever tip, b represents the medium and c is the surface. W_{abc} can be expressed as a function of surface energies as $W_{abc}= W_{ab} +W_{bc} -W_{ac}$, where W_{ab} is the tip surface free energy in equilibrium with the medium, W_{bc} is the sample surface free energy in equilibrium with the medium and W_{ac} is the interfacial free energy of the tip-sample contact interface.

The interaction forces in water between chemically modified spherical tips and the oil treated surfaces in water were measured using the AFM. Cantilevers with 1μm diameter, COOH-terminated borosilicate spherical tips (from Novascan Technologies Inc.) were used. These cantilevers had a nominal spring constant of 0.32 N/m. When the spherical tip is brought close to the sample, there are issues of water drainage from the thin water film and when the tip retracts, water suction into the film occurs. The film dynamics are quite complicated to model. As an alternative, we use the adhesion force or pull-off force to characterize the surface. Force Measurements were done in the contact mode. While measuring the interaction forces, the whole

tip was kept inside water in the fluid cell. Moreover, the tip was wetted with water before it was placed on AFM in order to avoid trapping of any air bubble at the tip or capillary effects. The force of adhesion also depends on Z scan rate[43], which was taken to be 0.199 Hz in these experiments. The scan rate is kept low in order to minimize the effects of viscosity.

Calcite cannot be used for AFM study because it is not atomically smooth. Fig. 2 shows a 5 μm x 5 μm scan of a calcite surface. The z-scale is of the order of 20 nm. (Z-scale is defined as the difference in height between the highest and bottom most point on the area scanned). It should be mentioned that on cleaving the calcite surface, we obtain some very smooth areas on the calcite plate but it is very difficult to locate these areas after aging the calcite surface with oil. So we use mica coated with APTES (3-aminopropyltriethoxy silane) or AP mica as a substitute for calcite surface. The choice of this substrate was justified by contact angle experiments. The water-crude oil contact angle on a calcite surface was found to be 35^{o} whereas for AP mica the contact angle was 33^{o}. Calcite was obtained from Ward's Scientfic Inc., AP mica from Novascan Technologies Inc. and microscope glass slides from Corning Glass Works.

AP mica is aged in synthetic brine (0.5 % sodium chloride) for a day. An oil droplet is placed on it using an inverted needle as shown in Fig. 3 and aged for 21 days. The excess oil is then washed with water and the surface was scanned and force measurements were done using AFM. The AP mica was then treated with different surfactants for a day and the surfaces were scanned and force measurements were done again.

Adsorption. Surfactant solutions in the concentration range of 10^{-2} M were prepared with and without the presence of 0.3 M Na_2CO_3. These solutions were then equilibrated with 10 grams calcite powder in 50 ml vials. The vials were corked and gently shaken so that the calcite powder comes into contact with the surfactant solution thoroughly. The solutions were allowed to

equilibrate with the calcite powder for 48 hours with gentle periodic shakings. The slurry was then centrifuged at 1200 rpm for 20 minutes to separate the solid particles from the liquid solution. The supernatant was carefully pipetted out while avoiding the solid particles. The supernatant was then centrifuged again for 20 minutes to obtain particle free supernatant. The pH of all the supernatant solutions was measured. UV spectrometry and titration analysis were used to determine the residual surfactant concentration in the supernatant liquid. The adsorbed surfactant concentration was calculated by material balance. To study the effect of pH on adsorption, the surfactant solution was prepared in different pH buffer solutions and the same method was adopted to measure the degree of adsorption. Similarly, experiments were performed at different temperatures to study the effect of temperature. Also, experiments were performed at different salinities to study the effect of salinity on adsorption.

Capillary Number Dependence. For obtaining capillary desaturation curve, the following procedure was undertaken. Surfactant (Alf-38, 0.05 wt% in 0.3 M Na_2CO_3) was equilibrated with crude oil in 1:1 ratio for a period of 2 days, with gentle mixing. The equilibrated solutions were used as the aqueous and oil phase for the capillary number curve. The IFT between the two was obtained as 10^{-2} mN/m. The contact angle on calcite was observed as 33^{o}, essentially rendering the calcite surface water-wet. The core used for this study had a porosity of 22.5% and permeability of 120 mD. The core was vacuum dried and then flooded with equilibrated surfactant brine to obtain 100% aqueous saturation. The equilibrated oil was injected into this core and a final oil saturation of 80% was obtained. The capillary number dependence was studied by flooding this core with equilibrated surfactant solution at various flow rates and calculating the residual oil saturation by material balance.

Spontaneous Imbibition. Outcrop limestone 1.5 inch diameter and 6 inch long cores were used in most of the experiments. Air permeability of these cores were about 150 mD. Porosity was 22.5%. Each core was first completely saturated with a 0.1 N NaCl brine. 5 PV of crude oil was injected to drive the core to connate water saturation. Oil saturation at the end of this oil flood was ~72%. The core was immersed in the crude oil and aged for 18 days at 80 °C. The imbibition cell was filled with the surfactant-Na_2CO_3 solution. The aged core was placed in an imbibition cell and the oil production by spontaneous imbibition was monitored.

Modeling Methods

The effect of alkaline surfactant solution on oil production from an oil-wet fracture block was studied with a 3-D numerical simulator. The capillary pressure between oil and brine phase, the relative permeabilities and the residual saturation of both phases were considered as functions of IFT and wettability. These were in turn correlated to the surfactant and salt concentrations with the data obtained from laboratory experiments.

Phase behavior. This study was based on an isothermal system. Four components were considered: hydrocarbon, water, surfactant and salt. It was assumed that the overall surfactant concentration is low, less than 0.1 wt%. Experiments indicated that the amount of the third micro-emulsion phase was small; so only two fluid phases were considered: oil phase and aqueous phase. Based on this assumption, the following equation must be satisfied:

$$S_a + S_o = 1 \tag{7}$$

where the subscript “a” represents the aqueous phase, “o” represents the oil phase, and S is the phase saturation.

According to the experimental observations,[3] the following assumptions were made regarding the distribution of components among different phases:

- Hydrocarbon can exist in oil phase and aqueous phase;

- Water can exist in aqueous phase and oil phase;
- Surfactant can exist in aqueous phase and oil phase, and on the solid surface;
- Salt can exist in aqueous phase and can be absorbed onto matrix surface.

Based on these assumptions, the mass balances at any position can be described with:

$$w_a^w + w_a^h + w_a^{sf} + w_a^{st} = 1 \tag{8a}$$

$$w_o^w + w_o^h + w_o^{sf} = 1 \tag{8b}$$

$$\phi C^{sf} = \phi\left(\rho_a S_a w_a^{sf} + \rho_o S_o w_o^{sf}\right) + A_s C_r^{sf} \tag{8c}$$

$$\phi C^{st} = \phi \rho_a S_a w_a^{st} + A_s C_r^{st} \tag{8d}$$

where the superscript "w" represents the water component, "h" represents the hydrocarbon component, "sf" represents the surfactant and "st" refers to the salt component. ϕ is the porosity; ρ_j is the density of phase j; w_j^i is the mass fraction of component i in phase j; C^{sf} and C^{st} (kg/m^3) are overall concentrations of surfactant and salt in kg per unit volume; C_r^{sf} and C_r^{st} (kg/m^2) are the concentrations of surfactant and salt absorbed on matrix surface in kg per unit area; A_s is the specific matrix surface area (m^2/m^3 matrix).

For a local site in the medium, if the matrix properties (ϕ and A_s), the phase densities (ρ_j), either of the phase saturations (S_o in this study) and the overall concentrations of surfactant and salt (C^{sf} and C^{st}) were given, there were 10 unknowns in Eqs. (7) and (8a) – (8d): S_a, w_a^w, w_a^h, w_a^{sf}, w_a^{st}, w_o^w, w_o^h, w_o^{sf}, C_r^{sf} and C_r^{st}. Local equilibrium was assumed for the distribution of any component among different phases. Under this assumption, Eqs. (7) and (8a) – (8d) were closed by the phase diagram, which determined the partition of each component among the aqueous phase, oil phase and matrix phase. In this work, the following correlations were needed:

$$w_a^h = w_a^h\left(C^{sf}, C^{st}, S_o, \rho_o, S_a, \rho_a, \phi, A_s\right) \tag{9a}$$

$$w_a^{sf} = w_a^{sf}\left(C^{sf}, C^{st}, S_o, \rho_o, S_a, \rho_a, \phi, A_s\right) \tag{9b}$$

$$w_a^{st} = w_a^{st}\left(C^{sf}, C^{st}, S_o, \rho_o, S_a, \rho_a, \phi, A_s\right) \tag{9c}$$

$$w_o^{w} = w_o^{w}\left(C^{sf}, C^{st}, S_o, \rho_o, S_a, \rho_a, \phi, A_s\right) \tag{9d}$$

$$w_o^{sf} = w_o^{sf}\left(C^{sf}, C^{st}, S_o, \rho_o, S_a, \rho_a, \phi, A_s\right) \tag{9e}$$

For a certain system, the correlations described by Eqs. (9a) – (9e) can be determined from experimental data. From these five correlations along with Eqs. (7) and (8a) – (8d), the distribution of each component among different phases was determined. The effect of pressure on density was incorporated by considering the compressibility of oil phase:

$$\rho_o = \rho_o^0 + \beta\left(p_o - 101325\right) \tag{10}$$

where ρ_o^0 was the oil density at 1 atmosphere (101,325Pa) and β was the compressibility of oil. The values of ρ_o^0 and β were dependent on the type of oil. The aqueous phase was assumed to be incompressible.

Mass transfer models. In this study, we neglected the effect of hydraulic dispersion and assumed that the overall mass flux of each component was a linear summation of convection and molecular diffusion:[44]

$$\overline{F}_i = \rho_a \bar{v}_a w_a^i + \rho_o \bar{v}_o w_o^i - D_a^{i,e} \nabla w_a^i - D_o^{i,e} \nabla w_o^i \tag{11}$$

The phase velocity, $\bar{v}_j$ was determined from Darcy's law:

$$\bar{v}_j = -\frac{k_{rj}}{\mu_j} \overline{\overline{K}} \cdot \left(\nabla p_j + \rho_j \bar{g}\right) \tag{12}$$

Here $\overline{\overline{K}}$ was the absolute permeability tensor; k_{rj} was the relative permeability of phase j; μ_j was the viscosity of phase j; p_j was the phase pressure; $\bar{g}$ was the gravitational acceleration. In a

system of two-phase (oil-aqueous phase) flow, the pressure difference between oil and aqueous phase was the capillary pressure:

$$p_c = p_o - p_a \tag{13}$$

The effective diffusivity of component *i* in phase *j* in porous media, $D_j^{i,e}$, was evaluated with:[45]

$$D_j^{i,e} = \phi^{4/3} S_j^{10/3} \rho_j D_j^i \tag{14}$$

where D_j^i (m^2/s) was the molecular diffusion coefficient of component i in phase j in bulk phase.

Effects of surfactant and salt on flow functions. For an initially oil-wet reservoir, the improved oil recovery by introduction of surfactant into brine is ultimately due to the alteration of flow functions, including capillary pressure, relative permeability and residual saturations. Surfactant, along with the salt (either artificially introduced into or originally resident in the reservoir), can lower the IFT and also alter the wettability of matrix to intermediate-wet or water-wet through removal of oil-wetting components from the matrix surface. IFT and matrix wettability are the factors that control residual saturations, capillary pressure and relative permeability.

A set of models[46] has been proposed by the research group in University of Texas at Austin (called UT models in this paper) to correlate the trapping number with the residual saturation and relative permeability. The trapping number N_T is defined as: [46]

$$N_T = \frac{\left| \overline{\overline{K}} \cdot \left(\nabla p_o + \overline{g} \left(\rho_a - \rho_o \right) \right) \right|}{\sigma} \tag{15}$$

It can be seen from Eq. (15) that the trapping number essentially combines the effects of capillary number and Bond number. Note, as proposed by Pope et al.[46], the evaluation of N_T is based on the displaced phase, which is oil phase in the present study.

The following equation is used to correlate residual saturation with the trapping number (Pope et al. [46]):

$$S_{rj} = S_{rj}^{high} + \frac{S_{rj}^{low} - S_{rj}^{high}}{1 + T_j N_T} \tag{16}$$

where S_{rj} is the residual saturation of phase *j* and T_j is the trapping parameter for phase *j*. The superscript "low" or "high" respectively refers to the parameter value at low or high trapping number. In this equation, S_{rj}^{high} is typically[46] 0. Given the values of S_{rj}^{low} and T_j, which can be obtained by fitting experimental data, Eq. (16) yields the desaturation curve ($S_r - N_T$ curve) that is similar to the CDC curve (capillary desaturation curve) described by Lake.[44] S_{rj}^{low} has the similar meaning as the plateau value of residual saturation as described by Lake[44] and the trapping number plays the role of capillary number. The value of trapping parameter T_j determines the critical trapping number (the trapping number where residual saturation begins to decrease from the plateau value) and the total desaturation trapping number (the trapping number where the residual saturation becomes 0) and it typically has higher value for non-wetting phase and lower value for wetting phase.[46] Note, Eq. (16) has been modified according to the feature of the system under present study, i.e., the hydrocarbon components are simply considered as one pseudo-component.

The effect of wettability was not considered in the trapping number, and therefore it was not incorporated into Eq. (16). In the present study, a simple interpolation technique was used to consider the wettability effect on residual saturation:

$$\frac{S_{rj}^{low} - S_{r,b1}^{low}}{\cos\theta - \cos\theta_0} = \frac{S_{r,b2}^{low} - S_{r,b1}^{low}}{\cos(\pi - \theta_0) - \cos\theta_0}, \tag{17a}$$

$$\frac{\ln T_j - \ln T_{b1}}{\cos\theta - \cos\theta_0} = \frac{\ln T_{b2} - \ln T_{b1}}{\cos(\pi - \theta_0) - \cos\theta_0} \quad . \tag{17b}$$

To apply Eqs. (17a) and (17b), one should have the values of S_r^{low} and T for a pair of base phases, which are represented with subscripts "b1" and "b2" in the equations. Note that oil and aqueous phases are treated in a similar way. The contact angle for base phase b1 was θ_0, and consequently, the contact angle for base phase b2 was π-θ_0. The plateau value S_{rj}^{low} and the trapping parameter T_j for phase *j*, of which the contact angle is θ, can be calculated from Eqs. (17a) and (17b), respectively. The values of S_{rj}^{low} and T_j were used to calculate the residual saturation with Eq. (16). Fig. 4 shows a family of desaturation curves ($S_r - N_T$ curves) that are calculated from two base curves for two base phases with contact angle 0 for phase b1 and π for phase b2 (i.e., the medium is totally wetted by base phase b1). For base phase b1, which is the wetting phase, $S_{r,b1}^{low} = 0.2$ and $T_{b1} = 300$. For the non-wetting base phase b2, $S_{r,b2}^{low} = 0.3$ and $T_{b2} = 6 \times 10^4$. The desaturation curves for a pair of phases with wetting phase contact angle $\theta=\pi/3$ and non-wetting phase $\theta=2\pi/3$ can then be obtained through Eqs. (16), (17a), and (17b). As can be seen from Fig. 4, two important features about the wettability effects on CDC curves discussed by Lake[44] have been qualitatively captured. First, the wetting phase has a lower plateau value than the non-wetting phase. For example, the plateau value of the $\theta=\pi/3$ curve (0.225) is lower than that of $\theta=2\pi/3$ (0.275). Second, the wetting phase has higher critical trapping number and total desaturation trapping number. In Fig. 4, the critical trapping number and total desaturation trapping number for the curve $\theta=\pi/3$ are around 10^{-4} and 10^{-1}, respectively, and for the curve $\theta=2\pi/3$, they are 10^{-5} and 10^{-2}. It should be pointed out that Eqs. (17a) and (17b) are just conceptual models for lack of any other models based on experimental data.

In the present study, a modified Brooks-Corey model was used to describe relative permeability:[44]

$$k_{rj} = k_{rj}^{0}\left(S_j^*\right)^{n_j} \tag{18}$$

where k_{rj}^{0} is the endpoint of the relative permeability k_{rj} and n_j is the exponential parameter that determines the shape of $k_{rj} - S_j$ curve. The normalized phase saturation S_j^* is defined as:

$$S_j^* = \frac{S_j - S_{jr}}{1 - S_{ar} - S_{or}} \quad . \tag{19}$$

The endpoint value k_{rj}^{0} and the exponential parameter n_j for phase *j* are correlated to the residual saturation of phase *j'* through linear interpolation in the UT model. Here phase *j'* is the conjugate phase of phase *j*. For example, in this system, oil is the conjugate phase of aqueous phase and vice versa. Detail investigations of the results in previous studies indicate that the conjugate phase residual saturation may not be a good predictor for k_{rj}^{0} and n_j, especially when wettability alteration is involved (Anderson[47], Fulcher et al.[48], Masalmesh,[49] and Tang et al. [50]). In the present study, the relative permeability curves were assumed for a pair of base phases with contact angle θ_0 for phase b1 and π-θ_0 for phase b2 at a certain trapping number N_{T0}. The following equations were used to correlate the relative permeability curves with trapping number N_T and contact angle θ:

$$k_{rj}^{0} = 1 + \left(k_{r,b1}^{0} + \frac{\cos\theta - \cos\theta_0}{\cos(\pi - \theta_0) - \cos\theta_0}\left(k_{r,b2}^{0} - k_{r,b1}^{0}\right) - 1 \right) \frac{1 + T_{j'} N_{T0}}{1 + T_{j'} N_T} \tag{20}$$

$$n_j = 1 + \left(n_{b1} + \frac{\cos\theta - \cos\theta_0}{\cos(\pi - \theta_0) - \cos\theta_0}\left(n_{b2} - n_{b1}\right) - 1 \right) \frac{1 + T_{j'} N_{T0}}{1 + T_{j'} N_T} \tag{21}$$

Eqs. (20) and (21) are just conceptual models that qualitatively capture the typical trends observed in previous studies[47-51] of the effects of capillary number (trapping number in this

work) and wettability on relative permeabilities. Note, $T_{j'}$ is the trapping parameter of the conjugate phase of phase *j* and its value is evaluated with Eq. (17b) using the contact angle π-θ, where θ is the contact angle of phase *j*.

Fig. 5 shows a family of relative permeability curves calculated from a pair of base curves with Eqs. (16) – (21). The wetting phase saturation is plotted on x-axis and the relative permeability on the y-axis. As the contact angle θ increases from (wetting) 0 to π, the relative permeability alters along with the residual saturations.

According to the Leverett J-function,[44] the effects of IFT and contact angle on capillary pressure are described with the following equation:

$$p_c = p_{c0}\left(S_a\right)\frac{\sigma\cos\theta}{\sigma_0\cos\theta_0} \quad . \tag{22}$$

Here p_{c0} is the capillary pressure between oil and aqueous phase in the base system where aqueous phase contact angle is θ_0 and the IFT is σ_0. It is generally correlated to the normalized aqueous phase saturation S_a. p_c is capillary pressure for the real system where the aqueous phase contact angle is θ and the IFT is σ.

Governing Equations and Numerical Techniques. The mass balance equations for all the components can be written as:

$$\frac{\partial}{\partial t}\left[\phi\left(\rho_a S_a w_a^h + \rho_o S_o w_o^h\right)\right] + \nabla\cdot\overline{F}^h = q^h \tag{23a}$$

$$\frac{\partial}{\partial t}\left[\phi\left(\rho_a S_a w_a^w + \rho_o S_o w_o^w\right)\right] + \nabla\cdot\overline{F}^w = q^w \tag{23b}$$

$$\frac{\partial}{\partial t}\left(\phi C^{sf}\right) + \nabla\cdot\overline{F}^{sf} = q^{sf} \tag{23c}$$

$$\frac{\partial}{\partial t}\left(\phi C^{st}\right)+\nabla\cdot\overline{F}^{st}=q^{st} \tag{23d}$$

In Eqs. (23a) – (23d), the mass flux term $\overline{F}^{i}$ is evaluated with Eqs. (7) and (8a) –8(d). We neglected any in-situ source for any component, e.g., the in-situ generation of surfactant, so the source term q^i is determined solely by boundary conditions.

Eqs. (23a) – (23d) were spatially discretized with a finite volume method.[52,53] One-point upstream averaging was employed in the evaluation of phase mobility. The interblock-interphase diffusions were considered with the help of the discretization method of diffusion term described by Pruess et al.[54] This spatial discretization method provides the simulator with flexibility in treatment of 1D, 2D and 3D problems under any coordinate systems (Cartesian coordinates, cylindrical coordinates and irregular coordinates). The backward Euler method was used to approximate the partial derivative of time. This discretization method generated a fully implicit scheme in which 4n nonlinear algebraic equations were solved simultaneously. Here n is the number of grid blocks into which the medium is discretized. For each grid block, four unknowns were solved. Physical appropriateness and numerical stability were two factors that were considered in selection of unknowns. In the present study, we chose the oil phase pressure (p_o), oil phase saturation (S_o), overall surfactant concentration (C^{sf}) and overall salt concentration (C^{st}) as the primary unknowns to be directly solved from the governing equations. Newton-Raphson method was employed to solve the equation system.[53] A linear solver based on the iterative methods proposed Moridis et al.[53] was used to solve the sparse linear system.

Results and Discussion

Phase Behavior. Fig. 6 shows the phase behavior of crude oil - brine (Na_2CO_3) - surfactant system for three typical cases. Water-oil ratio is kept at 1:1 in all cases shown. Fig. 6(a) shows the phase behavior without addition of any synthetic surfactant, i.e., crude oil - Na_2CO_3 brine. The number underneath each test tube specifies the Na_2CO_3 concentration in the brine. Two phases (aqueous and oleic) are seen in this case. As the Na_2CO_3 concentration increases, the bottom (aqueous) phase first becomes darker and then clarifies beyond an Na_2CO_3 concentration of 0.15 M. Na_2CO_3 reacts with some of the napthenic acid molecules in the crude oil to make in situ surfactants. Some of these surfactants solubilize in the brine and make micelles. These micelles can solubilize some oil into the aqueous phase giving it a darker color. As Na_2CO_3 in brine increases, the solubility of the surfactants in brine decreases (because of high salinity); the surfactants partition back to the oleic phase. Thus the aqueous phase clarifies above a certain Na_2CO_3 concentration.

Fig. 6(b) shows the phase behavior typical of sulfonate surfactants studied. The concentration of the surfactant 5-166 is kept constant at 0.05 wt% and the Na_2CO_3 concentration is increased from 0 to 0.6 M. As the caustic concentration increases, the darkness of the aqueous phase increases, reaches a maximum and then decreases. In this case, the aqueous phase is observed to be the darkest at a Na_2CO_3 concentration of 0.2 M. An optimal salinity is defined in the next section on the basis of the lowest water-oil interfacial tension; 0.2 M salinity is close to the optimal. A small, middle phase microemulsion is also observed in the near-optimal region. Since we are operating at a very dilute surfactant concentration (0.05 wt%) the middle-phase microemulsion layer formed is very thin, too small for any analysis. The aqueous phase becomes clear at the Na_2CO_3 concentration of 0.4 M indicating Winsor type II+ microemulsion. At this point, the system is in the over-optimal salinity regime.

Fig. 6(c) shows the phase behavior typical of propoxylated sulfate surfactants. The concentration of the surfactant Alf-38 is kept constant at 0.05 wt% and the Na_2CO_3 concentration is increased from 0 to 0.5 M. Again, as the Na_2CO_3 concentration increases, the darkness of the aqueous phase increases, reaches a maximum and then decreases. The third phase is more distinct in this case at Na_2CO_3 concentrations of 0.25 M and 0.3 M.

Fig. 6(d) shows the phase behavior of crude oil - brine (Na_2CO_3) - surfactant system for a typical alkyl ethoxylated surfactant, B-330. Water-oil ratio is kept at 1:1 in all the cases shown. The concentration of the surfactants used was kept constant at 0.05 wt% and the Na_2CO_3 concentration is increased from 0 to 1.2 M. The number underneath each test tube specifies the Na_2CO_3 concentration in the brine. As the caustic concentration increases, the aqueous phase becomes cloudier, reaches a maximum cloudiness and then becomes clearer. An optimal salinity is defined on the basis of the lowest water-oil interfacial tension. A small, middle phase microemulsion is also observed in the near-optimal region, similar to those seen for alkyl propoxylated surfactants.[14] Since we are operating at a very dilute surfactant concentration (0.05 wt%), the middle-phase microemulsion layer formed is often thin and too small for any analysis. The aqueous phase becomes clear at higher Na_2CO_3 concentration indicating Winsor type II+ microemulsion. At this point, the system is in the over-optimum salinity regime.

Interfacial Tension. Fig. 7 shows the interfacial tension (IFT) between the aqueous and the oleic phases as a function of Na_2CO_3 concentration in these crude oil - brine (Na_2CO_3) - surfactant systems. Water-oil ratio is again kept at 1:1 in all cases shown. The anionic surfactant concentration is also kept constant at 0.05 wt% in Fig. 7 (a-e) except for the case with no surfactant.

The IFT of the crude oil - brine (Na_2CO_3) system is shown in Fig. 7(a). As the caustic concentration increases, the IFT decreases to slightly below 10^{-1} mN/m at 0.2 M and then increases. The presence of the in situ surfactants in the aqueous phase is responsible for the decrease in IFT. Optimal salinity is defined as the salinity at the minimum IFT, i.e., 0.2 M in this case. Fig. 7(a) also shows IFTs in crude oil - brine - surfactant systems with 0.05 wt% sulfonate surfactants. The ethoxylated sulfonates 4-22 and SS-6566 could lower the IFT of the system to about 10^{-2} mN/m. However, amongst the three sulfonates, lowest IFT (of the order of 10^{-3} mN/m) was obtained with surfactant 5-166, an alkyl aryl sulfonate. The lowest IFT samples corresponded to those with middle phases. Optimal salinity is about 0.2 M Na_2CO_3. IFTs of the order of 10^{-2} mN/m and lower are capable of mobilizing oil by buoyancy.

Fig. 7(b) shows the IFTs for the Alf-3n series of propoxylated sulfate surfactants. The overall trend was similar to that of the other surfactants, i.e., the IFT decreased with increasing Na_2CO_3 concentration before reaching a minimum and then increased. The optimal salinity changed from 0.2 to 0.3 M Na_2CO_3 for the three surfactants. The minimum IFT was 10^{-3} mN/m for Alf-33, $3x10^{-2}$ mN/m for Alf-35, and $9x10^{-3}$ mN/m for Alf-38. The IFT did not change monotonically with the number of propoxy groups in this series of experiments.

Fig. 7(c) shows the IFTs for the Alf-6n series of propoxylated sulfate surfactants. Hydrocarbon chain length is smaller for this series of Alf-than the Alf-3n series. The optimal salinity changed from 0.3 to 0.5 M Na_2CO_3 for the three surfactants. The minimum IFT was 10^{-1} mN/m for Alf-63, $2x10^{-2}$ mN/m for Alf-65, and $7x10^{-4}$ mN/m for Alf-68. The IFT decreased monotonically with the number of propoxy groups in this series of experiments.

Fig. 7 (d) shows the interfacial tension (IFT) between the aqueous and the oleic phases as a function of Na_2CO_3 concentration in these crude oil - brine (Na_2CO_3) - surfactant systems. The equilibrated tubes from the phase behavior study are used to measure the equilibrium IFT

between the oil and the aqueous phase. The surfactant concentration is fixed at 0.05 wt%. The ethoxylated sulfates studied could lower the IFT of the system to about 10^{-3}-10^{-2} mN/m. The lowest IFT samples corresponded to those with middle phases, with two ethoxy groups. Thus low tensions can be generated with anionic surfactants at very low concentrations.

The IFT measurements for the cationic surfactant, DTAB were carried out for varying surfactant concentrations in the field brine at a water-oil ratio of 1:1. The IFT, shown in Fig. 7(e), decreases with the increase of surfactant concentration, but reaches a plateau of about $4x10^{-2}$ mN/m at a surfactant concentration of 2 wt%. At 1 wt% DTAB (a typical value used by Austad and co-workers), IFT is about 0.5 mN/m. Thus low interfacial tension is not the mechanism for high spontaneous imbibition with 1 wt% DTAB solutions.[15] Among all the surfactants studied here, low IFT ($<10^{-2}$ mN/m) was obtained with surfactants 5-166, Alf-33, Alf-38, Alf-68, CS-230 and B-330 S. Very low tensions can be generated with anionic surfactants, but not with cationic surfactants, below a concentration of 1 wt%.

Wettability. Wettability was evaluated by measuring water-oil contact angles. All the contact angle measurements for the anionic surfactants were made at a surfactant concentration of 0.05 active wt%, at the optimal salinity obtained from the IFT experiments. Fig. 8 shows the contact angles measured at different stages of the wettability experiment for the calcite plate with surfactant SS-6566. 0.3 M Na_2CO_3 solution brine was used. Before aging with oil, the mineral plate is found to be intermediate-wet with advancing contact angle greater than 90° and receding contact angle less than 90° (the first two points in Fig. 8). After aging the calcite plate with the crude oil at an elevated temperature for 44 hrs, the mineral plate becomes completely oil-wet with an advancing contact angle close to 160° (the 3rd, 4th and 5th points in Fig. 8). The oil-aged plate is immersed in brine and the oil-water contact line on the calcite plate is photographed to

obtain this data. The brine is then replaced with a surfactant solution at its optimal salinity. When exposed to the surfactant - brine solution, (much of the oil is released from the plate) the advancing contact angle decreases with time and stabilizes at a value of about 58°-88° depending on the drop size (the last four points in Fig. 8).

Fig. 9 shows the calcite plate upper surface at different times after the oil-aged surface was exposed to the surfactant (5-166)-brine solution. The equilibrium IFT was lower than 10^{-2} mN/m for this surfactant. Oil leaves the surface because of low IFT. After 1 hour, the calcite plate does not look water-wet. The wettability was found to be in the intermediate to oil-wet state even after 48 hours (The photograph is not shown here).

The error bars on the last four points (in Fig. 8) indicate the variation of contact angle between different drops in the same experiment. Drop size is proportional to the square root of the interfacial tension and is a function of the contact angle.[23] Fig. 10 (a) shows the state of the calcite plate surface at the end of 48 hours for surfactant SS-6566. Drop sizes varied between ~0.1 mm and ~1 mm. The contact angle generally increased with increasing drop size and varied between 58°-88°. The wettability varies along the surface of the plate because of the nonuniformity in initial oil contact with the plate.

In some cases, most of the oil leaves the plate within 48 hours, thus it is difficult to get a contact angle at this stage. In such cases, the plate was further washed with brine and a drop of crude oil was placed at the bottom of the plate. This contact angle is a receding contact angle and is referred to as the "post-wettability" test. Fig. 10 (b) shows such an example, for 0.5 wt% Alf-38. The contact angle is about 32°, typical of the water-wet calcite before aging with the crude oil. The post wettability-test was conducted for Alf-35, 38, 63, 65, and 68, and B-27. It should be noted that the post-wettability test measures receding contact angles, which is expected to be lower than the advancing contact angles (measured before the post-wettability tests).

Wettability tests for the DTAB were conducted with the field brine at 1 and 0.5 wt%. Fig. 10 (c) shows the calcite plate after 48 hours of contact with 1 wt% surfactant. Oil drops attached are bigger than those seen with the Alf-surfactants; this is a result of higher IFT. The contact angles of these oil drops are between 70°-100°. For the 0.5 wt% surfactant solution, the contact angles were about 140° (photo not shown). Thus DTAB does not change the wettability, if the concentration is small. At about 1 wt%, wettability changes to intermediate / water-wet.

Fig. 11 shows the contact angle at the end of wettability tests (including the post wettability-tests for Alf-35, 38, 63, 65, 68) for all the surfactants studied. Amongst the sulfonates, SS-6566 altered the wettability of the oil-wet carbonate surface to moderately water-wet state. Amongst the propoxylated sulfates, Alf-38 changed the wettability to a near water-wet state. Except for Alf-33, all other propoxylated sulfates resulted in intermediate / water-wet wettability. DTAB at 1 wt% also changed the wettability to intermediate / water- wet state. Lower concentrations of DTAB were not effective in changing wettability. Among the ethoxylated surfactants, B-27 changes wettability to preferentially water-wet, where as B-330 and CS-230 change the wettability to intermediate /water wet regime. CS-130 changes the wettability to intermediate/oil-wet regime.The error bar shows the variation of contact angle between several drops in each case.

Effect of different carbonate surfaces on wettability alteration was studied with only one anionic surfactant 4-22 (0.05 wt% active). The four different surfaces studied were lithographic limestone, calcite, marble and dolomite. The initial state of all the mineral surfaces except for the limestone, determined after aging the surfaces in synthetic brine, was found to be intermediate-wet. Lithographic limestone was found to be oil-wet. After aging the surfaces at elevated temperature in crude oil for two days all the surfaces exhibited close to oil-wet state. When contacted with the anionic surfactant 4-22, significant amount of oil was seen leaving the surface

possibly due to lowered interfacial tension. However, the evolution of contact angles monitored over a period of two days showed that all the four mineral surfaces had been altered to an intermediate-wet state (Table 3).

Atomic Force Microscopy. Force measurements were also conducted after the AP mica was treated with surfactants. The idea behind force measurements is that if the surfactant actually removes the oil molecules from the surface, the force of adhesion between the functionalized tip and the initially oil-wet area would become similar to the water-wet area. Fig. 12 shows the force of adhesion for AP mica surfaces aged with crude oil for 15 days and 50 days using COOH terminated tip. Fig. 12 also shows the adhesion force for the oil-aged AP mica surfaces treated with different surfactants. It was observed that the adhesion force for the oil wet and water wet area became similar for the case of Alf-38 and Alf-68. But there was no change in the force values when the surface was treated with DTAB. This implies that DTAB was not effective in removing oil molecules from the AP mica surface. This was further confirmed by AFM scans (see the next section). It was also observed that the force of adhesion for the oil-wet area before surfactant treatment was approximately the same when the surface was aged for 15 days or 50 days. This could mean that the adsorption of polar components of oil onto AP mica reaches equilibrium in less than 15 days.

A similar trend was also observed when the force measurements were done with an NH_2 terminated tip. Fig. 13 shows the force of adhesion for oil-aged AP mica surface and oil-aged AP mica surfaces which have been treated with different surfactants. However in this case, the force of adhesion between the initially oil-wet area and NH_2 terminated tip was higher than 50 nN and could not be measured using the tip with a spring constant of 0.32 N/m. This was also observed when the oil-wet area was treated with DTAB. This implies that there is still a large amount of

oil molecules adsorbed on the AP mica surface after treating with DTAB. This is in conjunction with the force measurements using COOH terminated tip.

After washing the excess oil on the AP mica surface by water, the oil-wet and water-wet regions were scanned. Fig. 14 represents a 25 μm x 25 μm scan. The left half-shows an area which was exposed to oil and thus was oil-wet. The white dots represent the oil-wet patches. The z scale of the white dots is of the order of 700 nm. The right side of Fig. 14, which has very few white dots, represents the water-wet area. The same area as viewed in Fig. 14 is scanned (Fig. 10) after treatment with Alf-38 for 15 minutes, followed by washing with water. Fig. 15 shows that the number of white dots (oil-wet patches) has greatly reduced. The z scale of Fig. 10 is only 100 nm. This signifies that the surfactant actually removes the adsorbed oil molecules.

The AP mica was again dipped in surfactant for a day and scanned after washing off the excess surfactant with water. Fig. 16 represents a 5 μm x 5 μm scan of the oil-wet area treated with Alf-38 for a day. The z scale is 50 nm and it is clearly seen that Alf-38 has removed a lot of adsorbed oil molecules. The oil-wet patches (shown by white dots) have diameters around 50 nm. Fig 17 and Fig 18 show the oil-wet areas which have been treated with Alf-38 and DTAB respectively. The z-scales are 100 nm and 200 nm respectively. The Alf-68 treated surface shows oil adsorbed patches with radius ranging from 50 nm to 500 nm whereas the DTAB treated surface show oil-adsorbed regions of radius from 50 nm to 1 μm. It is obvious from the Figs. 16, 17 and 18 that DTAB is least effective in removing oil molecules from the oil-wet surface as compared to Alf-38 and Alf-68.

Adsorption. Surfactant loss due to adsorption is one of the important criteria that govern the economics of the dilute surfactant flooding methods for carbonate formations. The adsorption of surfactants on minerals more typical of sandstone reservoirs has been studied extensively.

However there is little published literature on the adsorption of surfactants on the carbonate minerals.[25] Fig. 19 shows the adsorption isotherm for the anionic surfactants 4-22, 5-166 and SS-6566 in the absence and presence of Na_2CO_3. In the absence of Na_2CO_3, the adsorption is low at low surfactant concentration, increases nonlinearly with the increase in surfactant concentration and then reaches a plateau adsorption value above the CMC of the surfactants. This plateau adsorption value is the highest (~3.5 mg/m^2 of calcite) for 5-166 among the sulfonates studied. For the ethoxylated sulfonates 4-22 and SS-6566, the plateau adsorption values are ~0.9 mg/m^2 and ~1.3 mg/m^2, respectively. These adsorption values are similar to those found for SDS on calcite and dolomite surfaces by Tabatabal et al.[25] The pHs of all the surfactant solutions used for the adsorption experiment were found to be between 6 and 7 before contacting the calcite powder. However, after adsorption the pH values of the supernatant were found to be around 8.

Fig. 19 also shows the adsorption isotherm for the anionic surfactants in the presence of 0.3 M Na_2CO_3. Surfactant adsorption decreases dramatically in the presence of the Na_2CO_3. In the case of surfactant 5-166, the plateau adsorption is reduced to ~0.15 mg/m^2 from ~3.5 mg/m^2. For the other two anionic surfactants, the adsorption was negligible in the presence of Na_2CO_3. The presence of 0.3 M Na_2CO_3 raises the pH of the solution to 10.3. This pH is higher than the point of zero charge for the calcite, which was found to be about 8.2 by Somasundaran and Agar.[26] This causes the surface to acquire negative charges and repel the like charged anionic polar head group of the surfactant. Thus the adsorption of anionic surfactants can be suppressed by the use of the potential determining ions like carbonates.[12,25]

The adsorption densities reach a plateau value when the concentration of the surfactant exceeds the CMC. The surfactant concentration that are used for oil recoveries using surfactant brine imbibition are far above the CMC. Hence, the important adsorption parameters are the plateau values of the adsorption on calcite mineral surface. Fig. 20 shows the plateau adsorption

values for the propoxy and ethoxy sulfates with and without the presence of Na_2CO_3. The plateau values are shown for the Alf-series in Fig. 20 (a). Fig. 20 (b) shows the adsorption densities for the alkyl ethoxylated surfactants in the absence and presence of Na_2CO_3. These adsorption values are similar to those found for SDS on calcite and dolomite surfaces by Tabatabal et al.[34] and Seethepalli et al.[14] In one of the cases, negative adsorption was found, this was also reported earlier by Somasundaran et al.[35] Anionic surfactants can be repelled near the negatively charged calcite surface at that pH. They accumulate in the bulk solution, thereby increasing the local surfactant concentration. This leads to the negative adsorption numbers by titration calculations. Practically, it means negligible adsorption on the calcite surface.

Fig. 21 shows the effect of important field parameters like pH, salinity and temperature on the plateau adsorption values of the surfactant adsorption density. Fig. 21 (a) shows the effect of pH on the adsorption density of anionic surfactants on calcite mineral. The point of zero charge for the calcite was found to be about 8.2 by Somasundaran and Agar.[35] Increasing pH beyond this level causes the surface to acquire negative charges and repel the like charged anionic polar head group of the surfactant. Thus, the adsorption of anionic surfactants can be suppressed by the use of the potential determining carbonate ions.[34] According to DLVO theory, higher electrolyte concentration lowers the Debye screening length $1/\kappa$ which implies higher shielding effect and lesser repulsion between the adsorbed molecules. Hence, increasing the salinity would increase the adsorption of surfactants on mineral surface. Fig. 21 (b) shows an increase in adsorption experimentally for the increase of salinity (achieved by increasing the NaCl concentration). Multivalent ions would further reduce the thickness of the electric double layer (for a symmetric electrolyte $1/\kappa \propto 1/Z$), decrease the repulsion and thus increase the adsorption.

Fig. 21 (c) shows the effect of temperature on surfactant adsorption. Increasing temperature increases the enthalpy and entropy of the system. If the adsorption is enthalpy driven as is the

case with surfactants with low density of adsorption, then increasing temperature increases the adsorption density. On the other hand, if the adsorption of surfactants is entropy driven, as is the case with surfactants with high density of adsorption, increasing the temperature would lead to a decrease in adsorption.[35] Fig. 21 (c) shows that for surfactants with low density of adsorption, an increase in temperature leads to increase in the adsorption density, whereas for surfactants with high density of adsorption, an increase in temperature leads to a decrease in the adsorption density.

Capillary Number Dependence. The capillary number is defined as $N_c = V\mu / \gamma$, where μ is viscosity of the displacing fluid, γ is the interfacial tension between the two fluids and V is the superficial fluid velocity. Values of V were chosen such that N_c varied from 10^{-5} to 10^{-2}. The residual oil phase saturation is plotted in Fig. 22 as a function of the capillary number. At $N_c = 10^{-5}$ oil saturation is reduced to 36% from the original saturation of 80%. But with increase of N_c varied from 10^{-5} to 10^{-2}, the Sor does not decrease much (only ~6%). The pore structure of the carbonate rock may be responsible for the high residual oil saturation. The capillary number or the Bond number does not become very high in the surfactant-aided gravity drainage process (as shown by simulation, later in this report). The remaining oil saturation at the end of this process is close to low capillary number residual saturation.

Spontaneous Imbibition. Fig. 23 shows the imbibition cell set up. The oil recovery obtained by spontaneous imbibition conducted with three surfactants (Alf-35, 38 and 68) and brine is shown in Fig. 24. The surfactant concentration was 0.05 wt% and the Na_2CO_3 concentration was at the optimal values determined from IFT measurements. As seen earlier, Alf-35 and 38 are good wettability altering agents and Alf-68 lowers the IFT considerably. An additional spontaneous

imbibition test was done with 0.1 M NaCl brine to demonstrate the oil-wetness of the aged cores. The oil production due to spontaneous imbibition is shown in Fig. 24. The spontaneous imbibition volumes for Alf-35 and 38 solutions are about the same and higher than those for the other two cases. About 50% of the oil is produced in about 100 days of spontaneous imbibition with Alf-35 and 38. The final recovery is about 62% OOIP. These two surfactants are good wettability altering agents for the calcite plate, as seen in Fig. 11. The production for Alf-68 is about 35% in 100 days. Alf-68 induces spontaneous imbibition, but to a lower extent compared to the first two cases. Alf-68 lowers the IFT considerably, as seen in Fig. 7(c). There was very little imbibition with the NaCl brine. This indicates that the core was oil-wet at the start of spontaneous imbibition tests.

The imbibition obtained with these surfactants can be compared to the literature values. Standness and Austad[18] obtained about 15% OOIP recovery at 40 °C and about 45% OOIP recovery at 70 °C from spontaneous imbibition with 1 wt% DTAB for chalks with Swi=26%. Xie et al. [27] have used nonionic surfactants to enhance oil recovery from dolomitic Class II reservoirs. They observed about 5-10% recovery. Hirasaki and Zhang[23] have demonstrated >35% OOIP oil recovery with another anionic surfactant. This indicates that the anionic surfactants can perform very well in the laboratory-scale. Oil was seen to leave mostly from the top of the core in the case of Alf-68, whereas it left from all sides of the core in the cases of Alf-35 and 38 (at least in the beginning of imbibition).

A photograph of the imbibition cell is shown in Fig. 23. Since the IFT of the system is low, not all the oil that leaves the core, collects on the top of the cell immediately. Some of the oil remains in the aqueous phase as a macro-emulsion, as shown in Fig. 23 (b). The data that was noted in Fig. 24 did not include the oil trapped in the aqueous macro-emulsion phase. During the initial period of experiments, until about 10 days, the solution surrounding the cores were clear

and not much of the oil recovered was trapped in the macro-emulsion form. During the intermediate time, between 10-100 days, the aqueous phase surrounding the cores was found to be brown in nature, with oil trapped in the macro-emulsion form. This amount was later calculated from CT-scan experiments to be about 1-2 ml. After 100 days, there was not much oil recovery from the cores and the settling time for macro-emulsion was shorter than the time-scale of oil recovery, hence the solution started clearing up. At the end of the experiment, most of the oil from the macro-emulsion aqueous phase had segregated to the separated oil phase at the top of the imbibition cell.

We estimate errors of our oil production volume on this basis and add that to the separated oil volume as shown in Fig. 25 for the case of Alf-35 surfactant brine solution. Other anionic surfactants in Fig. 24 show similar error bars. In case of DTAB, there is not much of oil trapped in macro-emulsion phase. Fig. 24 shows that the final oil recovery with surfactant Alf-38 and Alf-35 is around 61% and DTAB gives a recovery of 37%. Final oil recovery from Alf-68 is lower at about 41%. Most of the oil (90% of final recovery) was recovered within 100 days of imbibition, and 50% of the final recovery was produced within 30 days of imbibition.

At the end of the imbibition experiment (with Alf-35 surfactant brine solution), the core was taken and cleaved along the principal directions to visually observe the remaining oil distribution. The image of the cleaved core is shown in Fig. 26, which shows that oil saturation at the top of the core is more than that at the bottom, and the center-saturation is more than the sides. This indicates a possible combination of both gravity-driven and capillarity-driven imbibition process.

Fig. 27 shows the theoretical plot of oil recovery for an entirely gravity-driven process along with the experimentally observed data. $\overline{S}_o$, the average saturation in the core is taken as the remaining oil saturation in the core. S_{or}, residual oil saturation in the core is taken as the oil

saturation in the core at the end of the imbibition experiment (adding about 0.5 ml to the recovered oil for the oil that would have recovered had the imbibition experiment been conducted for infinite amount of time). Fig. 27 shows that there is a mismatch between the theoretical and experimentally observed curves during the initial phase of the experiment. This indicates that the process for oil recovery during early times is not entirely gravity-driven. Fig. 27 also shows that for later times, there is a match between the experimental recoveries and the theoretical curve indicating that the process may be gravity-driven for later times.

For the case of very strongly water-wet media, oil-recovery is driven by counter-current imbibition. The dimensionless group derived by Ma et al.[15] is used for estimation of dimensionless time for the experimental data observed in Fig. 25. The experimental data obtained by Ma et al.[15] fitted into a very strongly water-wet (VSWW) curve, which is shown in Fig. 28 for reference. The dimensionless time is a function of the IFT of the system. In case of surfactant brine imbibition, the IFT of the system is a function of surfactant and salt concentrations, which vary with time. For Alf-35 surfactant brine solution IFT of the system changes from an initial value of 30 mN/m to a final value of 0.001 mN/m. Fig. 28 shows plots of oil recovery observed in Fig. 3 with respect to the dimensionless time assuming different IFT's for the system. There is a mismatch between the experimental curve and the VSWW curve for both initial and final IFT of the system. However, there exists an IFT value of 0.01 mN/m for which the experimental curve matches with the VSWW case. It is not clear, how one can anticipate this IFT.

For our parametric study, Alf-38 system with 0.3 M Na_2CO_3 was taken as the base case. Table 4 lists the different imbibition experiments conducted for parametric study. To see the uniformity of wettability alteration, one of the cores (Core 7 in Table 4) was cleaved vertically to expose the inside surface. This cleaved core was immersed in a brine solution to monitor rate of

oil recovery. In another experiment, an oil-wet core (Core 6 in Table 4) was immersed in 0.05 wt% Alf-38 with 0.3 M Na_2CO_3 at 10:1 water-oil ratio (WOR). This was to study the repeatability of the results obtained in our previous work.[14] Using 0.2 M Na_2CO_3 would lead to generation of in-situ surfactants and as reported in previous work lead to reduction of IFT to a value of 10^{-1} mN/m. An oil-wet core (Core 5 in Table 2) was surrounded by 0.2 M Na_2CO_3 solution to study the amount of oil recovery from an alkaline 0.2 M Na_2CO_3 solution without any surfactant. Fig. 29 shows imbibition results for these set of experiments. In all the results that are shown, the oil recovery includes the oil phase separated and collected at the top of the imbibition cell, i.e., the recovered oil excluding the amount trapped in the macro-emulsion phase, as described in previous paragraph. Fig. 29 shows that oil recovery from the Alf-38 system with 0.3 M Na_2CO_3 is repeatable and gives about 42 % OOIP recovery in 50 days of imbibition, about 60% in 200 days. About half-of the recoverable oil is produced in less than 30 days. Fig. 29 also shows that little oil (<5% OOIP) is recovered from the cleaved core by brine indicating that the oil aging method (and time used for aging cores) leads to uniform wettability alteration to oil-wet regime throughout the core. Since 0.2 M Na_2CO_3 leads to reduction of IFT to 0.1 mN/m, it mobilizes some of the oil and leads to a recovery of 9 % OOIP, as seen in Fig. 29.

Surfactant concentration and WOR are two other parameters that can play an important role in oil-recovery by surfactant brine imbibition. Increasing surfactant concentration increases the rate of surfactant diffusion into the core. It was seen in previous studies[14, 15] that WOR plays a critical role in determining the optimal salinity of the system. Hence, to study the effect of WOR, an oil-wet core (Core 1 in Table 4) was immersed in a surfactant solution with WOR of 3:1, as compared to previous work where the WOR was kept at 10:1. In another core (Core 2 in Table 4), the imbibing solution was 0.2 wt% Alf-38 surfactant in 0.3 M Na_2CO_3. The imbibition results are shown in Fig. 30. Fig. 30 shows that increasing the surfactant concentration increases the

initial rate of oil recovery slightly, but does not affect the long term recovery at the lab-scale. Based on our previous work,[33] the rate of oil recovery by surfactant brine imbibition process is a gravity driven process, but initially is diffusion limited. Hence, increasing the surfactant concentration enhances the initial rate of recovery for the same change in IFT, but it does not enhance the final rates of recovery. The salinity used was optimal for 0.05 wt% surfactant and may not be the optimal salinity for the higher concentration. Both the contact angle and interfacial tension for this concentration are needed before this result can be explained. Fig. 30 also shows that the oil recovery decreases with the WOR. WOR plays a critical role in determining the optimal salinity of the system, and thus affects the IFT and the contact angle of the system.

In the target reservoirs, after primary production, there is always some gas present. This would affect the performance of the surfactant-brine process and was tested by imbibition experiments. An oil-wet core at residual water saturation (Core 3 in Table 4) was flooded by N_2 gas until residual oil saturation was achieved at a pressure drop of 40 psi/ft. The core was then flooded again by crude oil to reach residual gas saturation. The residual gas saturation thus obtained was 9%, as listed in Table 2, core 3. This core was immersed in the base case surfactant solution. Fig. 31 shows that the presence of a small amount of initial gas ($S_g < 0.1$) does not affect the rate of oil recovery drastically. In another core (Core 4 in Table 4), the oil-saturated core (at residual brine) was flooded by N_2 gas and then directly used for imbibition studies. In this case, the initial gas saturation was measured to be 24%. The oil recovery rate for surfactant brine imbibition for this system is much lower, as shown in Fig. 31. The presence of initial gas in the core affects the rate of recovery due to a significant decrease in oil relative permeability.

Other surfactants, which gave favorable wettability alteration (final contact angle < 90^o, towards water-wet regime) and low IFT were also tested for oil recovery. Fig. 32 shows recovery

rates for different surfactants at 0.05 wt% and their optimal salinity. The cores used for these experiments are listed in Table 4 as cores 6, 8-11. The salinity of Na_2CO_3 used is also listed in Table 4 and it corresponds to their optimal salinity. Fig. 32 shows that recovery rates for Alf-38, B-330 and CS-230 are almost identical, in line with their almost identical behavior in phase behavior, IFT and wettability alteration studies. AOS, is a surfactant for application in high temperature reservoirs, and it gives a final recovery of 21% OOIP after 50 days of imbibition. Surfactant 5166 gives low IFT ~ 10^{-3} mN/m, but does not alter the wettability to water-wet regime. Fig. 32 shows that it gives a final recovery of 19% OOIP after 50 days of imbibition.

An oil-wet core (Core 12 in Table 4) was immersed in the base case surfactant solution to study the rate of recovery for a 7 mD core. Fig. 33 shows the rate of recovery for the 7 mD core. It can be seen that about 12 % OOIP is recovered in period of 120 days. As the matrix permeability decreases, so does the oil recovery by imbibition. The oil recovery for a 150 mD core is then estimated from the results of the 7 mD core using capillary and gravity scaling groups. Fig. 14 shows that the 150 mD core recoveries are much higher than those estimated with capillarity scaling (Eq. 1). Scaling the imbibition time using Eq. 3, as a gravity-dominated process, gives recovery estimates that match the 150 mD, 22% porosity core results, as shown in Fig. 33. This indicates that the surfactant brine imbibition process is gravity-dominated.

The dimensionless time for a gravity-driven process (as given by Eq. 3) can be increased by decreasing the length of the core which can lead to higher oil recovery rate. An oil-wet core was cut into half-horizontally (Core 14 in Table 4). In another experiment, an oil-wet core was cleaved into half-vertically (Core 15 in Table 4) for imbibition experiments. It was supposed to lower the effective diffusion length for the surfactant and enhance the rate of recovery. The oil recovery for these experiments is plotted in Fig. 34. Decreasing the fracture length and decreasing the effective diffusion length increases the rate of oil recovery. Hence, in an oil-wet

naturally fractured reservoir, smaller fracture spacing and height would lead to an increase in the rate of oil recovery by surfactant brine imbibition process.

Mechanistic Numerical Simulation. In order to better understand the process of oil recovery from an oil-wet matrix block using surfactants, a 3-D simulator using the numerical models discussed earlier is developed. It is used to simulate the laboratory experiments.

A primary drainage mercury capillary pressure curve was measured for the cores used in the study. The capillary pressure was converted for the gas/water system and is shown in Fig. 35. It could be seen that the carbonate core has a bimodal pore throat size distribution. This capillary pressure curve was further modified for oil-water system using appropriate IFT and contact angles. The end point relative permeabilities were calculated before and after aging for a sample core. These parameters were used in Eqs. (7) – (10) for estimation of relative permeabilities. The exponents for relative permeabilities were used as simulation parameters. The final values used for simulation are given in Table 5.

The partition of each component between aqueous and oil phases was modeled independent of component concentrations. The IFT of the system depends on the surfactant and salt concentrations. This dependence was obtained by fitting a smooth curve through the experimental IFT data obtained by varying the surfactant concentration at 0.3 M Na_2CO_3 solution for water-oil system. The water-oil ratio (WOR) used in this study was fixed at 1:1. The experimental fit is shown in Fig. 36. The IFT is divided into three fits, a straight line fit for low surfactant concentration (<0.01 wt%), where the IFT is constant at 30 mN/m, another straight line fit for high surfactant concentrations (> 0.035 wt%) where the IFT is constant at 0.001 mN/m and a third-order polynomial fit for $\ln(\sigma)$ is used for surfactant concentration lying in between the two concentrations. It was assumed that the salt diffusion is much faster compared

to the surfactant diffusion in water. Hence, the salt concentration is kept constant at 0.3 M Na_2CO_3. This results in IFT being a sole function of surfactant concentration, and the functional form is shown in Fig. 36. The salt diffusion could be taken into account in the simulator if needed. The effect of WOR on IFT was not incorporated in simulation.

Wettability, measured through contact angle, depends on the surfactant and salt concentrations. This dependence is modeled (for simplicity) similar to IFT behavior, a constant initial contact angle for low surfactant concentrations (<0.01 wt%), a constant final contact angle for high surfactant concentrations (>0.035 wt%) and a linear variation of contact angle from the initial value to the final value between the two surfactant concentrations. This is a conceptual model for lack of quantitative model based on experimental data. Experimentally, we know that the initial contact angle is 160^0-180^0. The final wettability of the core is obtained from mineral-scale experiments[3] for the surfactants used, though it is kept as a flexible parameter as the composition of the core is different from the mineral used.

The core is cylindrical in shape and it is assumed to be homogeneous with uniform permeability and porosity. Thus, radial symmetry is assumed for the system. A constant pressure boundary condition is used for the boundaries. A 2-D radial grid is constructed to represent the core as shown in Fig. 37.

Fig. 38 shows the comparison between numerical simulation and imbibition experiments for cores 6 and 12. Estimates of oil in the aqueous phase emulsion are shown as vertical bars in these plots. If this emulsion oil is included, then the simulation results match the experimental data closely. The relative permeability parameters in the numerical model were adjusted to get this match. The number of grid blocks used for this simulation is 10 X 40 (10 in radial direction and 40 in the vertical direction). The effect of grid blocks was tested by increasing the number of grid blocks to 50 X 100 and 100 X 100. There was no appreciable difference between the results

from 10 X 40 and 100 X 100 grid block simulations. Hence for further analysis the grid blocks used were kept at 50 X 100. The simulation of the oil production also generates in situ distribution of many properties, e.g., the oil-saturation, capillary pressure, IFT, Contact angle, surfactant concentration, etc., with time.

Snap shots of the oil saturation at various times are shown in Fig. 39. At each time, the oil saturation is plotted as contour, the distance from center of the core as X-axis and the distance from bottom of the core as Y-axis. Since the core is symmetric along the radial direction, profiles along the center of the core to the boundary are plotted. Fig. 39 shows that in the first snap shot, the oil saturation decreases almost uniformly from top to bottom of the core along the sides of the core. This is an indication of counter-current like imbibition. This process is present until the sixth snap shot (t ~21 days). At the end of 21 days Fig. 39 shows a gradient in the oil saturation, with oil saturation being higher at the top of the core than at the bottom. This indicates that the gravitational forces are starting to dominate the process. This saturation distribution is consistent with the experimental image of Fig. 26.

Similar snap shots of the capillary pressure, P_c at various times are shown in Fig. 40. At each snap shot the P_c (psi) is plotted as the contour. Fig. 40 shows that in the first snap shot, the capillary pressure is negative, indicating that the core is oil-wet in nature initially. As surfactant diffuses through the boundary, it alters both IFT and the wettability, thereby changing the capillary pressure, as given by Eq. (16). Fig. 40 shows that P_c reaches a steady value by the end of 15 days. This time also corresponds with the end of counter-current imbibition shown in Fig. 40. By this period of time, P_c is nearly zero.

Fig. 41 shows snap shots of IFT at the same times as in Fig. 28. The IFT (N/m) is plotted on the contours. Similar to Fig. 40, the IFT reaches a steady value by the end of 18 days, which by Eq. 21 results in near-zero P_c shown in Fig. 41. IFT is reduced to a low value by surfactant

diffusion, and IFT reduction with surfactant concentration is given in Fig. 36. Fig. 42 shows the change in wettability as measured by contact angle at various times. Wettability is completely altered to water-wet everywhere by the end of 21 days. The contact angle after 21 days of imbibition is 75^o throughout the core, in this example.

The reduction of IFT and change of wettability is caused by an increase in surfactant concentration by diffusion and convection. Fig. 43 shows the surfactant concentration at the same times as in Figs. 40-42. Here, surfactant concentration (as weight fraction in aqueous phase) is plotted as the contour. Fig. 43 shows that the surfactant concentration plateaus after 24 days, hence resulting in the plateaus for wettability, IFT, P_c observed in Figs. 40-42.

Because the wettability changes with surfactant concentration, the relative permeability function changes. Fig. 44 shows the oil relative permeability as function of position (radial distance from the center, r) and time. Oil relative permeability is a function of both wettability and oil saturation. At the beginning oil saturation is high, but the medium is oil-wet. Therefore the oil relative permeability is low. As regions become more water-wet, relative permeability increases. But as the oil saturation decreases the oil relative permeability decreases. At 15 days, the oil permeability is low at large radii, because the oil saturation is low. It is low near the center of the core because it is still oil-wet. In the middle, the oil relative permeability is high because it is water-wet and oil saturation is high. Higher oil permeability aids in the gravity drainage of oil.

Fig. 45 shows the water phase velocity field. In the beginning the water velocity is very low. Water comes in from the sides, especially the bottom part of the sides. With time, invasion of water comes from the higher part of the sides. The water flow field is primarily horizontal. Fig. 46 shows the oil phase velocity field. It is predominantly vertical indicating that water comes in from the sides and the oil leaves from the top. Oil velocity is high in the region the oil relative

permeability is high. This indicates that wettability alteration increases oil relative permeability which helps gravity to pull out the oil by gravity drainage.

When the oil-wet cores are initially immersed in an imbibition cell and surrounded by a brine solution, the brine does not go in immediately because the entry capillary pressure with the connate brine exceeds the gravitational force, i.e., the macroscopic bond number, N_B^{-1} (given by Eq. 1) is greater than 1. As the surfactant diffuses into the core, the IFT and the wettability of the core change. As the IFT is lowered, capillary pressure falls, and N_B^{-1} decreases. When it becomes less than 1, water starts invading the core from the bottom and the side of the core. Also, as the wettability is altered the capillary pressure changes from negative to positive, but it leads to little counter current imbibition because the magnitude of capillary pressure is low. As the wettability is altered, the relative permeability of the oil phase increases and it enhances the rate of oil recovery by gravity drainage.

The effect of wettability alteration on oil recovery rate was studied by changing the contact angle from the initial value of 180^0 to final values of 180^0 (no wettability alteration), 90^0 (intermediate-wet), 75^0 (actual wettability for Alf-38), and 0^0 (strongly water-wet). IFT was the same in all these cases. By increasing the extent of wettability alteration, it was observed that the oil recovery rate increased, as shown in Fig. 44. Since the process is mostly gravity driven, Eq. 3 suggests that as the oil permeability increases, dimensionless time increases, which results in an increase in oil recovery. Hence, for the same time as the block becomes more water-wet, oil relative permeability increases and thus, the oil recovery increases. Oil is recovered in all the cases because of low tension, but increasing the extent of wettability alteration increases the rate of oil recovery.

Field-Scale Simulation. Oil recovery from bigger (field-scale) fracture blocks of 1 m wide X 1 m high to 10 m wide X 10 m high were simulated with parameters that matched lab-scale experimental data. The expected recovery from such systems is shown in Fig. 48. All the fracture blocks here are taken to be of the same properties as the core under which experiments were carried out. Fig. 45 shows that 60% recovery takes 30 days in the lab-scale core, 10 years for 1 m X 1 m block and 100 years for a 10 m X 10 m block. The recovery of oil from these cores is controlled by surfactant diffusion. Fig. 17 also shows that the recovery is almost the same for a 10 m wide X 1 m high and 1 m wide X 10 m high matrix blocks for the first 800 days. Plots of surfactant concentration for these cases also show that by 800 days surfactant reaches a steady value of 0.05 wt% for both these cases. After surfactant has reached a steady value, the mechanism for oil recovery is through gravitational forces. According to Eq. (3), for the same time, as L increases t_{Dg} decreases; this results in lower recovery, E_R. Hence, a smaller block length should have more recovery for the same time. Fig. 48 shows the same, i.e., higher recovery rates for the 10 m wide X 1 m high matrix block compared to 1 m wide X 10 m high matrix block.

The simulator with parameters that matched laboratory-scale data was used to estimate oil production in reservoir-scale matrix blocks (in a Wyoming reservoir). The reservoir dimensions used were 1000m length, 300m width with a 10m height of fractures (sketched in Fig. 49). The fracture spacing along the length was varied from 1m to 10 m. It was assumed that the matrix is homogeneous. The surfactant water was injected through a horizontal injector well at the bottom of the reservoir and similarly, a horizontal producer well at the top of the reservoir was used to collect the oil recovered. These two horizontal wells were assumed to be connected to all the fractures, which were perpendicular to the wells. In the simulations, the fractures were assumed to be of infinite permeability and were always filled with the surfactant solution. This is an ideal

case, but can indicate the scale-up of the laboratory results. The properties of the reservoir were assumed to be 150 mD permeability, 15% porosity, 5 cP oil viscosity, and 0.85 g/ml oil density. Initial oil saturation inside the reservoir was 0.72 and total oil recoverable by secondary production (corresponding to Soi-Sor) was about 1.4 MMBbl. The simulation was carried for 30 years of production. Fig. 50 shows the oil production rate by the surfactant brine process for fracture spacing of 1 m and 10 m along with the cumulative oil production. For a fracture spacing of 1 m, more than 500 Bbl of oil is produced per day for 3 years and the production declines after that. In a period of 3 years about 50% of the recoverable oil is recovered. Increasing the fracture spacing increases the time for diffusion and the recovery rates. For fracture spacing of 10m in the same reservoir, the oil production decreases to 200-300 Bbl of oil produced per day for the first 3 years and by end of which, about 25 % of the recoverable oil is recovered. Waterflooding would produce no oil from such a fractured oil-wet reservoir. Surfactant aided gravity drainage can recover a large fraction of the oil in less than 30 years if the fracture spacing is small. Further investigation is needed to evaluate the effectiveness of this process in realistic heterogeneous naturally fractured reservoirs.

Cost of Chemicals. In the surfactant brine imbibition process, surfactant brine imbibes into the oil-wet matrix and displaces the oil for recovery. In the cost analysis, we can assume that for every single barrel of oil produced, we would require a single barrel of the chemicals. In our study, for every single barrel of chemicals we have 0.05 wt% of anionic surfactant solution and alkaline solution at optimal salinity. If cationic surfactants are to be used, then 1 wt% of cationic surfactant for every barrel of chemical is used to displace oil. It is assumed from literature survey that cationic surfactants cost 4 $/kg (on active basis), whereas the anionic surfactants we are evaluating would cost 2 $/kg (on active basis). The other chemicals cost are: Na_2CO_3 – 100

$/ton, NaCl – 30 $/ton. Hence, the chemical cost for 1 wt% cationic surfactant brine imbibition process for oil recovery would cost, 6.8 $/Bbl of oil recovered. For anionic surfactants at 0.05 wt% and optimal salinity of 0.3 M Na_2CO_3, the chemical cost would be 0.64 $/Bbl of oil. From imbibition experiments it was observed that 0.05 M Na_2CO_3 is sufficient to negate surfactant adsorption and remaining salinity can be achieved by using cheaper chemical NaCl. In that case, using 0.05 wt% anionic surfactant with 0.05 M Na_2CO_3 and 0.5 M NaCl, we get chemical cost as 0.38 $/Bbl of oil recovered. In either case, the chemical cost associated with dilute alkaline anionic surfactant process for enhanced oil recovery from fractured oil-wet carbonate reservoirs could be estimated to be less than 1$/Bbl of oil recovered, significantly lower than using cationic surfactants at 6.8 $/Bbl of oil recovered. Traditional tertiary surfactant flooding chemical costs are about 10 $/Bbl of oil recovered. Oil industry has traditionally considered the surfactant process to be an expensive process. The dilute surfactant process developed in this study is not an expensive process (chemical cost is less than 1 $/Bbl).

Technology Transfer

We have written and presented in professional society meetings the following papers:

1. Adibhatla, B. & Mohanty, K. K., "Oil Recovery from Fractured Carbonates by Surfactant–Aided Gravity Drainage: Laboratory Experiments and Mechanistic Simulation," SPE 99773, Proceedings of SPE/DOE 15th Symposium on Improved Oil Recovery, Tulsa, April 22-26, 2006.
2. Adibhatla, B., Sun, X., & Mohanty, K. K., "Numerical Studies of Oil Production from Initially Oil-Wet Fracture Blocks by Surfactant Brine Imbibition," SPE 97687, Proceedings of SPE International Improved Oil Recovery Conference, Kuala Lumpur, Malaysia. 4–6 December, 2005.

3. Kumar, K., Dao, E. & Mohanty, K. K., "Atomic Force Microscopy Study of Wettability Alteration," SPE 93009, Proceedings of SPE Intl. Symp. on Oil Field Chemistry, Woodlands, Feb. 2-5, 2005.
4. Seethepalli, A., Adibhatla, B. & Mohanty, K. K., "Physicochemical Interactions During Surfactant Flooding of Carbonate Reservoirs," *SPE J.*, 9 (4), 411-418 (December, 2004).
5. Adibhatla, B., Mohanty, K. K., Berger, P. & Lee, C. "Effect of Surfactants on Wettability of Near-Wellbore Regions of Gas Reservoirs," Proceedings of 8th International Symposium on Reservoir Wettability, Houston, May 16-18, 2004.
6. Seethepalli, A., Adibhatla, B. & Mohanty, K. K., "Wettability Alteration During Surfactant Flooding of Carbonate Reservoirs," SPE 89423, Proceedings of SPE/DOE 14th Symposium on Improved Oil Recovery, Tulsa, April 17-21, 2004.

We have held annual industrial reviews of our projects at the UH Institute for Improved Oil Recovery and the following companies have attended our meetings: BP, Chevron, Conoco-Phillips, Corelabs, ExxonMobil, Landmark, Marathon, Oil Chem, Schlumberger, Sasol, Shell, Stepan, and Westport.

Conclusions

The process of using dilute anionic surfactants in alkaline solutions has been investigated for oil recovery from fractured oil-wet carbonate reservoirs both experimentally and numerically. This is a surfactant-aided gravity drainage process where surfactant diffuses into the matrix, lowers IFT and contact angle, which decrease capillary pressure and increase oil relative permeability enabling gravity to drain the oil up. Based on this study, the following can be concluded:

- Anionic surfactants have been identified which at dilute concentration of 0.05 wt% and optimal salinity can lower the interfacial tension with the crude oil to very low values ($<10^{-2}$ mN/m).
- Anionic surfactants have also been identified which, at 0.05 wt%, can change the wettability of the calcite surface to intermediate/water-wet condition as well or better than the cationic surfactant DTAB with a West Texas crude oil in the presence of Na_2CO_3.
- All the carbonate surfaces (Lithographic Limestone, Marble, Dolomite and Calcite) show similar behavior with respect to wettability alteration with surfactant 4-22, and calcite was used as the base mineral for wettability alteration studies for remaining surfactants.
- The force of adhesion in AFM of oil-wet regions changes after anionic surfactant treatment to values similar to those of water-wet regions. This was not observed for the cationic surfactant.
- The AFM topography images showed that the oil-wetting material was removed from the surface by the anionic surfactant treatment.
- Adsorption studies indicate that extent of adsorption for anionic surfactants on calcite minerals decreases with increase in pH and with decrease in salinity. Hence, in the presence of Na_2CO_3 (concentration > 0.05 M) surfactant adsorption is reduced significantly on the calcite surface.

- Adsorption of the surfactant solutions on calcite minerals can increase or decrease with increase in temperature depending on whether adsorption is enthalpy driven or entropy driven.
- Laboratory-scale surfactant brine imbibition experiments give high oil recovery (20-42% OOIP in 50 days; up to 60% in 200 days) for initially oil-wet cores through wettability alteration and IFT reduction. The experimental results are reproducible.
- Limestone cores are rendered oil-wet uniformly by the current oil-aging process.
- IFT and wettability alterations are not linear functions of surfactant concentration. Hence, higher surfactant concentration need not translate into enhanced rate of oil recovery.
- It was also found that small (<10%) initial gas saturation does not affect significantly the rate of oil recovery in the imbibition process, but larger gas saturation decreases the oil recovery rate.
- As the core permeability decreases, the rate of oil recovery reduces, and this reduction can be scaled by the gravitational dimensionless time. This also indicates that the process of oil recovery by surfactant brine imbibition is gravity-driven.
- Mechanistic simulation of core-scale surfactant brine imbibition matches the experimental data.
- Simulations indicate that surfactant diffusion is the rate determining step at larger scale.
- The capillary pressure needed for counter-current imbibition goes to near zero because of low interfacial tension before less than 30% oil recoverable is recovered (in the laboratory cores). Most of the oil is recovered through gravitational forces.
- Oil left behind at the end of this process is at its residual oil saturation. The capillary and Bond numbers are not large enough to affect the residual oil saturation.

- At the field-scale, 50% of the recoverable oil is recovered in about 3 years if the fracture spacing is 1 m and 25% if 10 m, in the example simulated.
- Decreasing fracture spacing and height, increasing permeability, and increasing the extent of wettability alteration increase the rate of oil recovery from surfactant-aided gravity drainage.
- This dilute surfactant aided gravity-drainage process is relatively cheap. The chemical cost for a barrel of oil produced is expected to be less than $1.

References

1. Akbar, M., Vissapragada, B., AlghamDi, A.H., Allen, D., Herron, M., Carnegie, A., Dutta, D., Olesen, J-R.,Chourasiya, R.D., Logan, D., Stief, D., Netherwood, R., Russel, S.D., and Saxena, K.: "A Snapshot of Carbonate Reservoir Evaluation," *Oilfield Review* **12**, no. 4 (Winter 2000/2001): 20-21
2. Allan, J. and Sun, S.Q.: "Controls on Recovery Factor in Fractured Reservoirs: Lessons Learned from 100 Fractured Fields," paper SPE 84590 presented at the 2003 SPE Annual Technical Conference and Exhibition, Denver, 5–8 October, 2003.
3. Downs, H.H. and Hoover, P.D., "Oil Field Chemistry: Enhanced Recovery and Production Stimulation," J. K. Borchardt & T. F. Yen, editors, ACS Symposium series 396, Washington, DC: American Chemical Society, 1989.
4. Buckley, J.S., Takamura, K., and Morrow, N.R, "Influence of Electrical Surface Charges on the Wetting Properties of Crude Oils," SPE 16964 presented at 62nd Annual Technical Conference and Exhibition of the Society of Petroleum Engineers held in Dallas, TX, September 27-30, 1987.
5. Freer, E.M., Svitova, T.and Radke, C.J., "The Role of Interfacial Rheology in Reservoir Mixed Wettability," *J. Petroleum Science and Engineering* (2003) **39**, 137-158.
6. Salathiel, R.A., "Oil Recovery by Surface Film Drainage in Mixed Wettability Reservoir Rocks," *JPT* (1973) **25**, 1216-1224.
7. Yang, H. D. and Wadleigh, E. E., "Dilute Surfactant IOR – Design Improvement for Massive, Fractured Carbonate Applications," paper SPE 59009 presented at SPE International Petroleum Conference and Exhibition in Mexico held in Villahermosa, Mexico, 1-3 February, 2000.

8. Kalpakci, B., Arf, T. G., Barker, J. W., Krupa, A. S., Morgan, J. C., and Neira, R. D., "The Low Tension Polymer Flood Approach to Cost Effective Chemical EOR," SPE/DOE 20220, SPE/DOE Symposium on EOR, Tulsa, April 22-25, 1990.
9. Reppert, T.R., Bragg, J.R., Wilkinson, J.R., Snow, T.M., Maer Jr., N.K. and Gale, W.W.," Second Ripley Surfactant Flood Pilot Test", paper SPE 20219, SPE/DOE Enhanced Oil Recovery Symposium, 22-25 April, Tulsa, Oklahoma
10. Ferrell, H.H, King, D.W and Sheely, Jr., C.Q.," Analysis of the Low-Tension Pilot at Big Muddy Field, Wyoming", *SPE Formation Evaluation* (1988) p.p., 315-321
11. Pope, G.A, Wang,B., Kerming, T.," A Sensitivity Study of Micellar/Polymer Flooding", *SPEJ* (1979), December, 357-368
12. Glover, C.J Puerto, M.C., Maerker, J.M., and Sandvik, E.L., "Surfactant Phase Behavior and Retention in Porous Media", *SPEJ* (1979), June, 183-193.
13. Salter, S. J. and Mohanty, K. K., "Multiphase Flow in Porous Media: I. Macroscopic Observations and Modeling", paper SPE 11017, SPE Annual Technical Conference and Exhibition, 26-29 September, New Orleans, Louisiana
14. Gupta, S. P., "Dispersive Mixing Effects on the Sloss Field Micellar System", *SPEJ* (1982), August, 481-492.
15. Giordano, R.M.," Estimating Field-Scale Micellar/Polymer Performance", paper SPE 16731, SPE Annual Technical Conference and Exhibition, 27-30 September, Dallas, Texas
16. Gogarty, W.B.," Enhanced Oil Recovery Through the Use of Chemicals-Part I", *JPT* (1983), September, 1581-1590
17. Gogarty, W.B.," Enhanced Oil Recovery Through the Use of Chemicals-Part II", *JPT* (1983), October, 1767-1775

18. Austad, T. and Milter, J.: "Spontaneous Imbibition of Water Into Low Permeable Chalk at Different Wettabilities Using Surfactants," paper SPE 37236 presented at the 1997 SPE International Symposium on Oilfield Chemistry, Houston, 18–21 February, 1997.
19. Standnes, D.C. and Austad, T.: "Wettability Alteration in Chalk 1. Preparation of Core Material and Oil Properties," *JPSE*, **28**, 111 (2000).
20. Standnes, D.C. and Austad, T.: "Wettability Alteration in Chalk 2. Mechanism for Wettability Alteration from Oil-Wet to Water-Wet Using Surfactants," *JPSE*, **28**, 123 (2000).
21. Standnes, D.C. and Austad, T.: "Wettability Alteration In Carbonates: Interaction Between Cationic-Surfactant and Carboxylates as a Key Factor in Wettability Alteration from Oil-Wet to Water-Wet Conditions," *Colloids and Surfaces A: Physicochemical Engineering Aspects,* 216, 243 (2003).
22. Standnes, D.C. and Austad, T.: "Wettability Alteration in Carbonates: Low-cost Ammonium Surfactants Based on Bio-derivatives from the Coconut Palm as Active Chemicals to Change the Wettability from Oil-wet to Water-wet Conditions," *Colloids and Surfaces A: Physicochemical Engineering Aspects,* **218**, 161 (2003).
23. Standnes, D.C. and Austad, T.: "Nontoxic Low-cost Amines as Wettability Alteration Chemicals in Carbonates," *J. Petroleum Science and Engineering,* **39**, 431 (2003).
24. Strand, S., Standnes, D.C., and Austad, T.: "Spontaneous Imbibition of Aqueous Surfactant Solutions Into Neutral to Oil-Wet Carbonate Cores: Effects of Brine Salinity and Composition," *Energy and Fuels* **17**, 1133 (2003).
25. Seethepalli, A., Adibhatla, B., and Mohanty, K.K.:" Physicochemical Interactions During Surfactant Flooding of Fractured Carbonate Reservoirs". *SPEJ*, **9**(4), 411-418 (December, 2004).

26. Hirasaki, G. and Zhang, D.L.: "Surface Chemistry of Oil Recovery from Fractured, Oil-Wet, Carbonate Formation," *SPEJ*, **9**(2), 151-162 (June 2004).

27. Chen, H.L., Lucas, L.R., Nogaret, L.A.D., Yang, H.D., and Kenyon, D.E, "Laboratory Monitoring of Surfactant Imbibition using Computerized Tomography," *SPEREE* (2001) **4**, 16-25.

28. Schechter, D.S., Zhou, D. and Orr, F. M., "Low IFT Drainage and Imbibition," *J. Petroleum Science and Engineering* (1994) **11**, 283-300.

29. Spinler, E.A., Zones, D.R., Tobola, D.P., and Moradi-Araghi, A, "Enhancement of Oil Recovery Using a Low Concentration of Surfactant to Improve Spontaneous and Forced Imbibition in Chalk," SPE 59290 presented at the SPE/DOE Improved Oil Recovery Symposium held in Tulsa, Oklahoma, 3-5 April, 2000.

30. Zhou, X., Morrow, N.R. and Ma, S.: "Interrelationship of Wettability, Initial Water Saturation, Aging Time, and Oil Recovery by Spontaneous Imbibition and Waterflooding," paper SPE 35436, presented at the SPE/DOE Improved Oil Recovery Symposium, Tulsa, OK., 21–24 April, 1996.

31. Morrow, N.R. and Mason, G.: "Recovery of Oil by Spontaneous Imbibition," *Current opinion in colloid and interface science* **6**, 321-337 (2001).

32. Mattax, C.C. and Kyte, J.R.: "Imbibition Oil Recovery from Fractured, Water-Driven Reservoir," *SPEJ*, **2**, 177-184 (June, 1962).

33. Ma, S., Zhang, X., and Morrow, N.R.: "Influence of Fluid Viscosity on Mass Transfer between Rock Matrix and Fractures," J. *Can. Pet. Tech.*, **38**, 25-30 (1999).

34. Cuiec, L.E., Bourbiaux, B. and Kalaydjian, F.: "Imbibition in Low-Permeability Porous Media: Understanding and Improvement of Oil Recovery," SPE 20259, presented at 1990 7th Annual. Symposium. EOR, Tulsa, OK, 1990.

35. DuPrey, L.: "Gravity and Capillary Effects during Imbibition," *SPEJ*, 18(6), 927 -935 (1978)

36. Hagoort, J.: "Oil Recovery by Gravity Drainage" *SPEJ*, **20**, 139-150 (June, 1980).

37. Morrow, N.R. and Songkran, B.: "Effect Of Viscous and Buoyancy Forces on Nonwetting Phase Trapping in Porous Media," in D. Shah (Editor), *Surface Phenomena in EOR*. Plenum Press, New York, N.Y., pp. 387-411, 1982

38. Li, K. and Horne, R.N.: "A General Scaling Method for Spontaneous Imbibition," SPE 77544, presented at SPE ATCE San Antonio, TX, 29 September–2 October, 2002.

39. John, A., Han, C., Delshad, M., Pope, G. A. and Sepehrnoori, K.: "A New Generation Chemical Flooding Simulator," SPE 89436, Proceedings of the SPE/DOE 14th Symposium on Improved Oil Recovery, Tulsa, OK,17–21 April, 2004.

40. Shutang, G., Huabin, L., Zhenyu, Y., Pitts, M.J., Surkalo, H., and Wyatt K.: "Alkaline-Surfactant-Polymer Pilot Performance of the West Central Saertu, Daqing Oil Field," paper SPE/DOE 35383 at the 1996 SPE/DOE tenth symposium on IOR, Tulsa, OK, April 1996.

41. Van der Vegte, E. W. and Hadziioannou, G.: "Scanning Force Microscopy with Chemical Specificity: AN Extensive study of Chemically Specific Tip-Surface Interactions and the Chemical Imaging of Surface Functional Groups," *Langmuir* (1997), **13**, 4375-4368.

42. Schneider, J.; Barger, W. and Lee, G. U.: "Nanometer Scale Properties of Supported Lipid Bilayers Measured with Hydrophobic and Hydrophilic Atomic Force Probes," *Langmuir* (2003), **19**(5), 1899-1907.

43. Capella, B. and Dietler, G.:"Force-Distance Curves by Atomic Force Microscopy," *Surface Science Reports* (1999), **34**, 1-104.

44. Lake, L. W.: *Enhanced Oil Recovery*, Prentice-Hall Inc. Upper Saddle River, NJ. (1989).

45. Pruess, K. and Moridis, G. TOUGH2 User's Guide, Version 2.0. LBNL-43134. Lawrence Berkley National Laboratory, University of California, Berkley, California 94720, 1999.

46. Pope, G. A., Wu, W., Narayanaswamy, G., Delshad, M., Sharma, M. M. and Wang, P.: "Modeling Relative Permeability Effects in Gas-Condensate Reservoirs with a New Trapping Model," *SPE Reservoir Eval. & Eng.,* **3** (2), 171-178 (2000).
47. Anderson, A. G.: "Wettability Literature Survey-Part 5: The Effects of Wettability on Relative Permeability," *J. Petroleum Technology,* 1453-1468 (November, 1987).
48. Fulcher Jr, R. A., Ertekin, T. and Stahl, C. D.: "Effect Of Capillary Number and Its Constituents on Two-Phase Relative Permeability Curves," *J. Petroleum Technology,* 249-260 (Feb., 1985).
49. Masalmesh, S. K.: "The Effect of Wettability on Saturation Functions and Impact on Carbonate Reservoirs in the Middle East," Proceedings of the 10th International Petroleum Exhibition and Conference. SPE 78515, 13-16 October, Abu Dhabi, 2002.
50. Tang, G. and Firoozabadi, A.: "Relative Permeability Modification in Gas/Liquid Systems through Wettability Alteration to Intermediate Gas Wetting," *SPE Reservoir Eval. & Eng.,* **5**, 427-436 (2002).
51. Bardon, C. and Longeron, D. G.: "Influence of Very Low Interfacial Tensions on Relative Permeability," *SPEJ,* **20**, 391-401 (October, 1980).
52. Helnemann, Z. E., Brand, C. W., Munka, M. and Chen, Y. M.: "Modeling Reservoir Geometry with Irregular Grids," SPE 18412, Proceedings of the SPE symposium on reservoir simulation, Houston, TX, 6-8 February, 1989.
53. Moridis, G. J. and Pruess, K.: "T2SOLV: An enhanced package of solvers for the TOUGH2 family of reservoir simulation codes," *Geothermics*, **27** (4), 415-444, 1998.
54. Press, W. H., Teukolsky, S. A., Vetterling, W. T. and Flannery, B. P.: Numerical Recipes in Fortran 77: the Art of Scientific Computing. 2nd Ed. Cambridge University, Cambridge, UK.

Table 1: Surfactants evaluated in this study

Trade name	Structural name	Active %	Molecular Wt.	CMC in water (g/l)
Anionic Surfactants				
Sulfonates				
4-22	Alkyl aryl ethoxylated sulfonated phenol	50%	-	0.001
5-166	Alkyl aryl sulfonate	50%	-	0.001
SS-6566	Alkyl aryl ethoxylated sulfonate	50%	-	0.002
Propoxylated sulfates, sodium salt				
Alf-33	Propoxylated sulfates -3PO	28.1%	485	0.01
Alf-35	Propoxylated sulfates -5PO	28.0%	588	0.006
Alf-38	Propoxylated sulfates -8PO	26.0%	715	0.005
Alf-63	Propoxylated sulfates -3PO	30.0%	467	0.025
Alf-65	Propoxylated sulfates- 5PO	31.6%	561	0.018
Alf-68	Propoxylated sulfates -8PO	30.6%	667	0.014
Ethoxylated sulfates				
CS-130	Sodium lauryl ether sulfate-1EO	25.3%	346	0.167
CS-230	Sodium lauryl ether sulfate-2EO	25.5%	382	0.119
B-330S	Sodium lauryl ether sulfate-3EO	27.7%	422	0.091
B-27	Sodium nonyl phenol ethoxylated sulfate – 4EO	29.9%		0.175
AOS	C-20-22 Alpha Olefin Sulfonate	30%		
Cationic Surfactant				
DTAB	Dodecyltrimethylammonium bromide		308.3	4.625

Table 2: Brine composition

Composition of reformulated brine

Salt	gm/l
$CaCl_2.2H2O$	2.942
$MgCl_2.6H2O$	2.032
NaCl	5.815
$Fe(NH_4)_2(SO_4)_2.6H2O$	0.007
Na_2SO_4	0.237

Table 3: Contact angles on different minerals with surfactant 4-22

	Marble	**Limestone**	**Dolomite**	**Calcite**
Before ageing with oil				
Receding Angle	$44\text{-}45^0$	$160\text{-}163^0$	43^0	$55\text{-}56^0$
Advancing Angle	$126\text{-}137^0$	$165\text{-}168^0$	$110\text{-}125^0$	$110\text{-}116^0$
After ageing the mineral plate with oil at 80^0 C				
1. Contact with Brine -after 60 mins	132^0	180^0	160^0	$>170^0$
2. Contact with surfactant				
-after 1 hour	121^0	161^0	156^0	145^0
-after 48 hours	146^0	163^0	141^0	140^0

Table 4: Imbibition experiment conditions					
Number	**Surfactant**	**Na_2CO_3 (M)**	**Length (cm)**	**S_{oi}**	**WOR**
1	Alf-38	0.3	12.96	74.73	3:1
2	Alf-38-0.2 wt%	0.3	12.38	69.62	10:1
3	Alf-38	0.3	13.05	63.75 (S_{gi}=8.8)	10:1
4	Alf-38	0.3	12.71	48.37 (S_{gi} =24.12)	10:1
5	-	0.2	13.35	71.05	10:1
6	Alf-38	0.3	11.9	70.97	10:1
7	-	-	9.20	68.63	1:1
8	B-330	0.8	11.53	73.02	10:1
9	AOS	1.0	10.45	73.67	10:1
10	5166	0.2	10.05	73.58	10:1
11	CS 230	1.0	14.46	73.00	1:1
12	Alf-38	0.3	14.88	66.00	5:1
13	Alf-38	0.3	14.92	66.45	10:1
14	Alf-38	0.3	3.7*2	66.02	1:1
15	Alf-38	0.3	7.4	66.00	1:1

Table 5 **Properties of the core used for imbibition**			
Length (cm)	15	S_{wr}	27.5 %
Diameter (cm)	3.85	k^0_{rwet}	0.1
Porosity	22.0 %	n_{wet}	4.5
Permeability(mD)	150	$k^0_{r.nw}$	0.9
S_{or}	25.0 %	n_{nw}	2.25

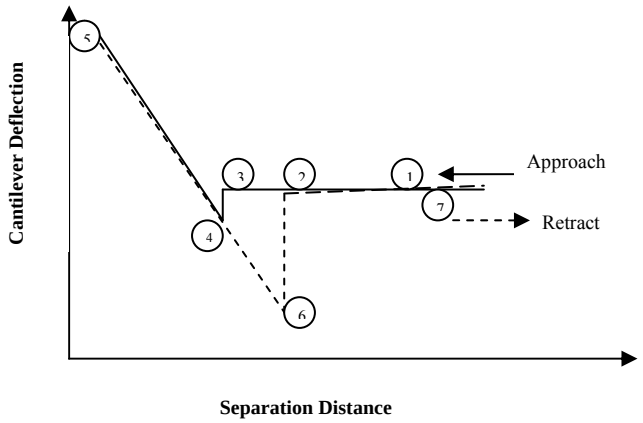

Fig. 1: A typical cantilever displacement vs. separation distance plot as obtained by AFM.

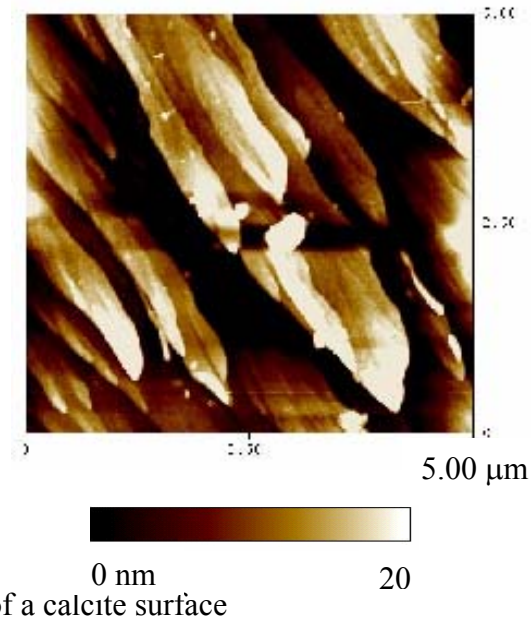

Fig. 2: A 5 µm x 5 µm scan of a calcite surface

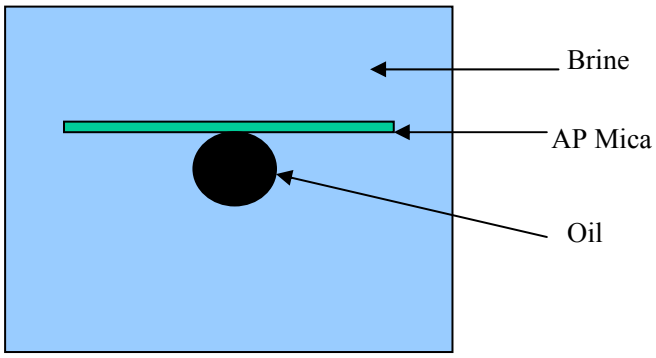

Fig. 3: A schematic diagram of AP mica being with crude B.

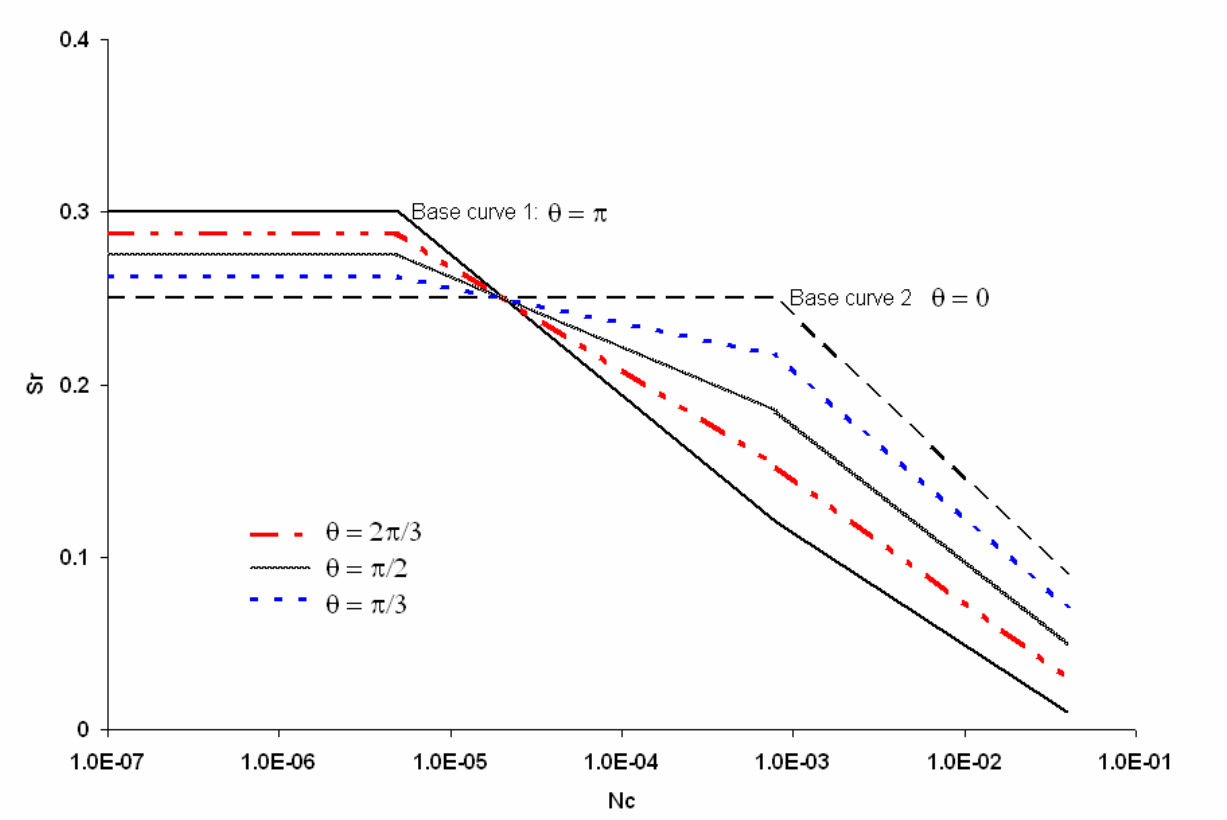

Fig. 4: Capillary desaturation curve as function of wettability

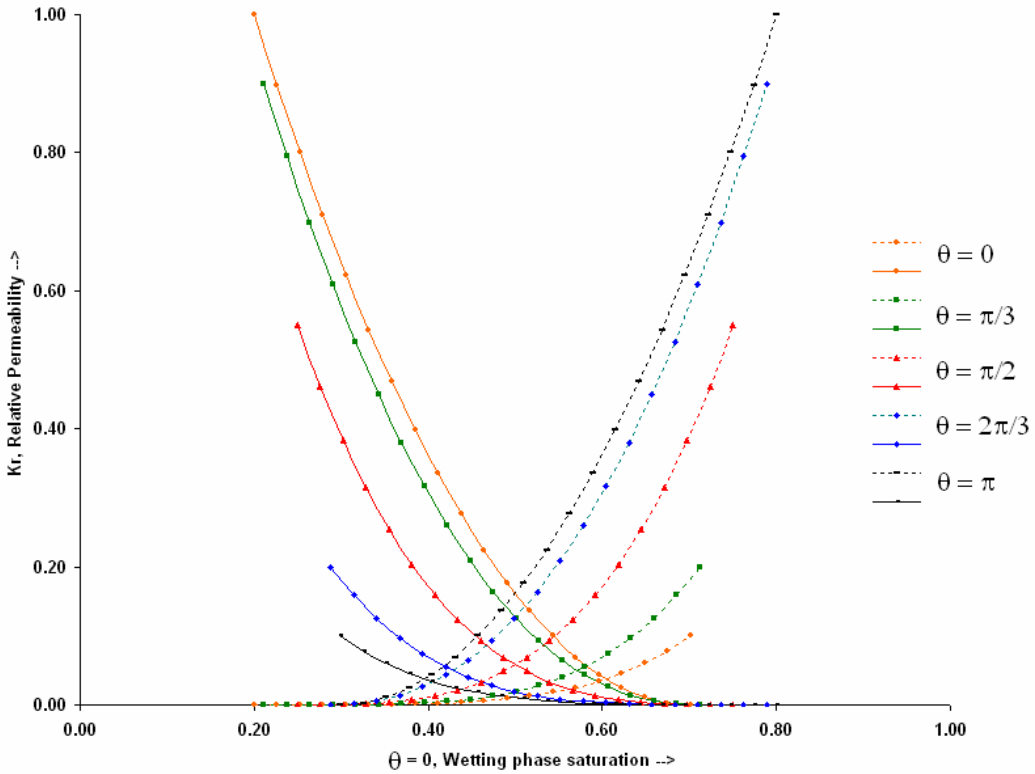

Fig. 5: Relative permeability variation as a function of contact angle

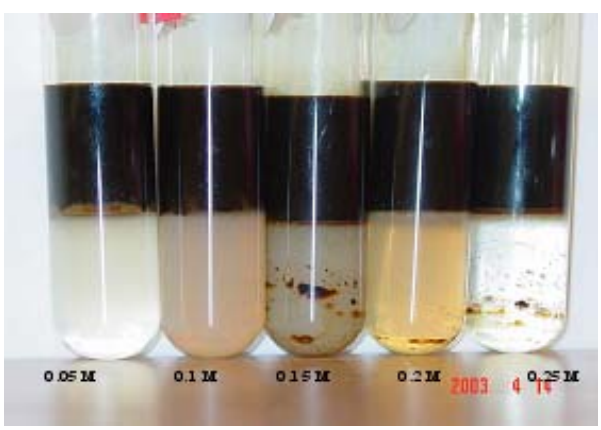

(a)

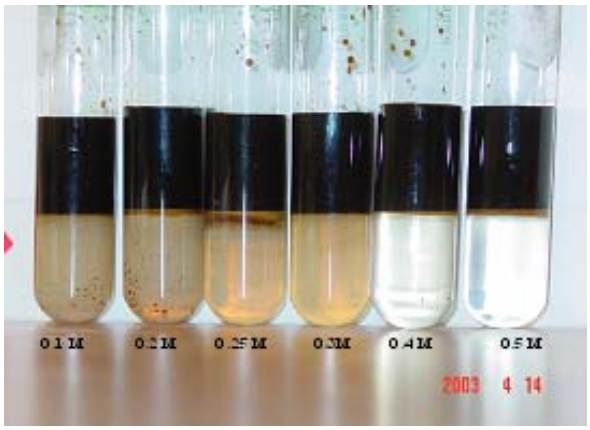

(b)

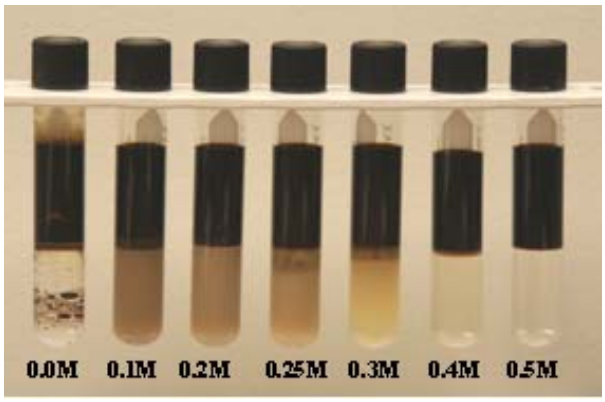

(c)

(d)

Fig. 6: Phase behavior study of surfactant with varying Na_2CO_3 concentration (a) No surfactant (b) Sulfonate surfactant, 0.05 wt% 5166 (c) Propoxylated sulfate surfactant, 0.05 wt% Alf-38 (d) Ethoxylated surfactant, 0.05 wt% B-330

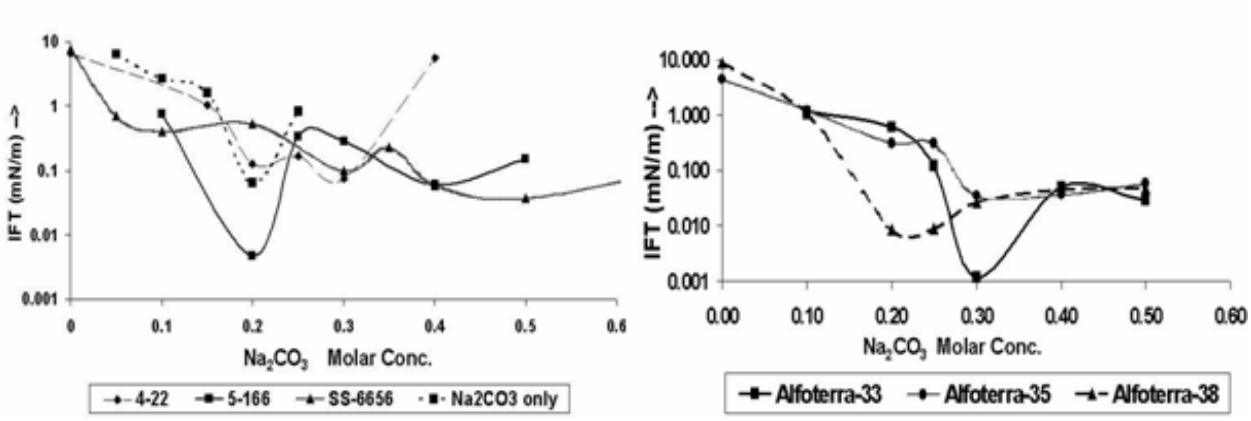

(a)

(b)

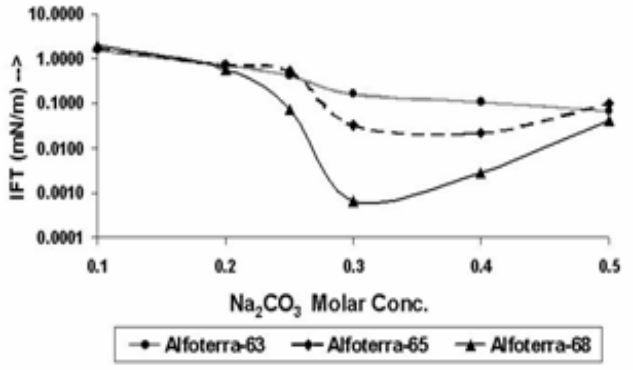

(c)

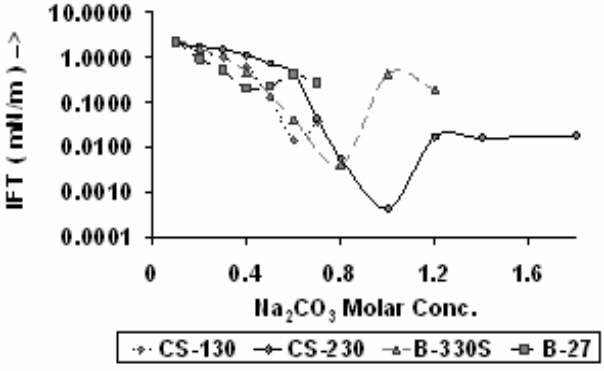

(d)

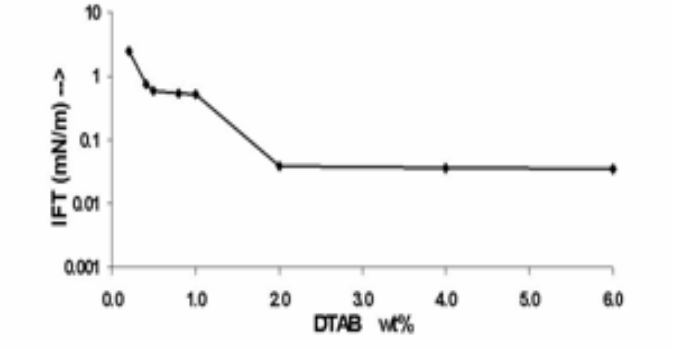

(e)

Fig. 7: IFT at optimal salinity for different surfactants at 0.05 wt% (a) Sulfonate surfactants, (b) Propoxy sulfates Alf-3n series, (c) Propoxy sulfates Alf-6n series, (d) Ethoxy sulfates, (e) Cationic surfactant DTAB at varying concentration

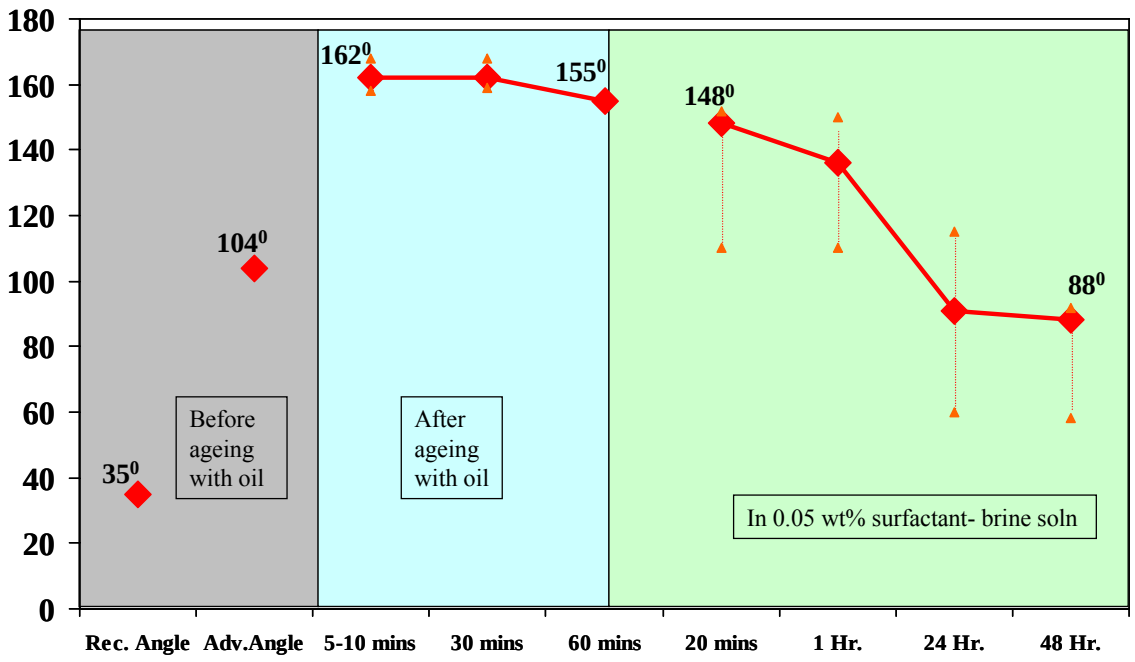

Fig. 8: Contact angle at different stages – Example of 0.05 wt% SS-6566.

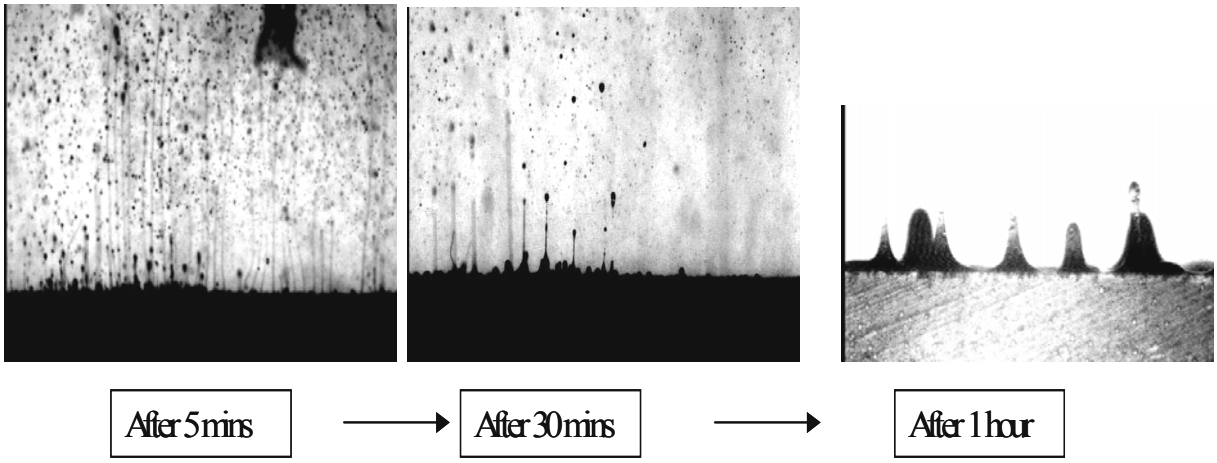

Fig. 9: Images of oil drop after the oil-wet calcite plate was contacted with 0.05 wt% 5-166 surfactant solution during the wettability experiment – 5-166 is an example of a low IFT producing surfactant.

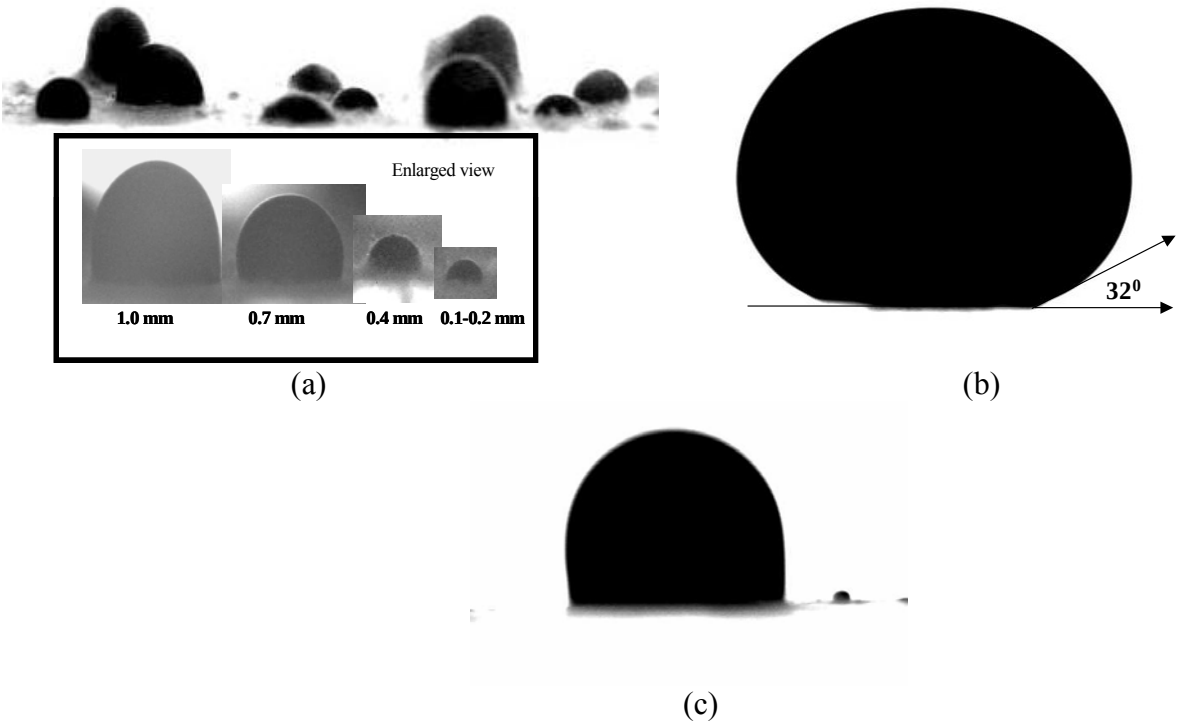

Fig. 10: (a) Different sizes of drops (1-0.1 mm) evolved when the oil-wet calcite plate was contacted with any surfactant solution. This is the image of the plate after 48 hours in SS-6566 surfactant solution (b) Post wettability test: the oil-wet calcite plate was contacted with 0.05 wt% Alf-38 surfactant solution for two days, thereafter; it was washed with brine before placing an oil-drop on it.(c) Image of an oil drop after the calcite plate was contacted with 1 wt% DTAB surfactant solution for about two days.

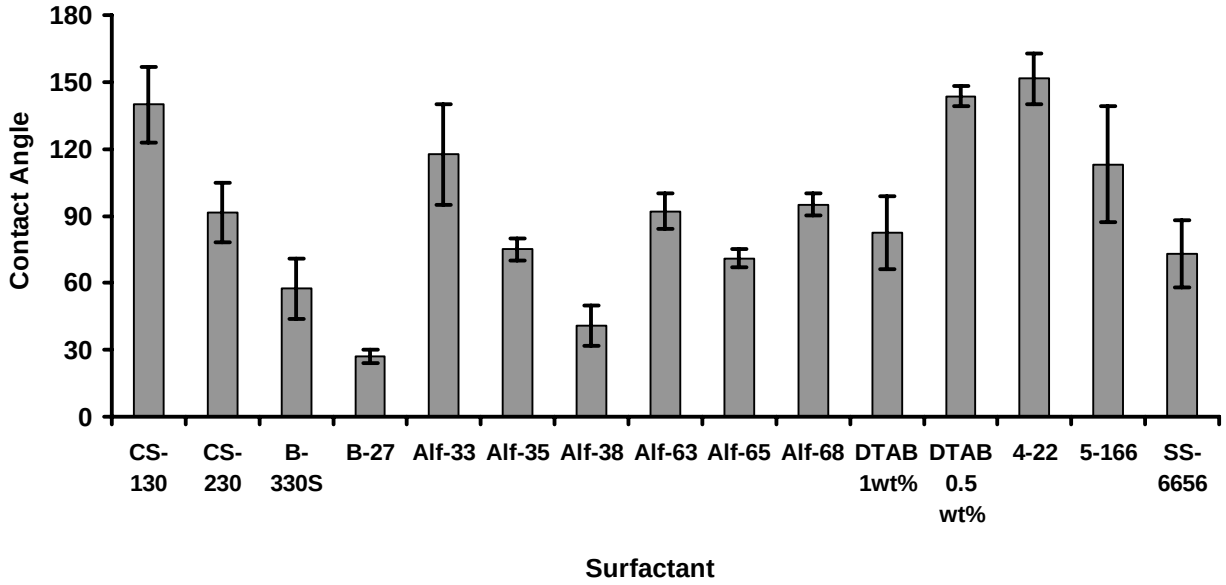

Fig. 11: Contact angles after wettability alteration using 0.05 wt% surfactants at optimal salinity (Except for DTAB)

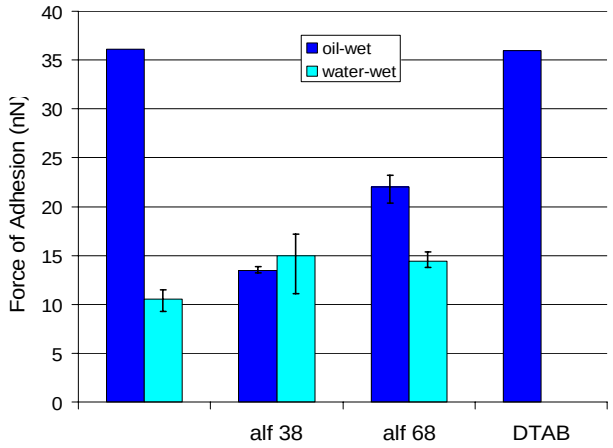

Fig. 12: Force of adhesion for oil-aged AP mica treated with and without surfactant treatment using COOH terminated tip

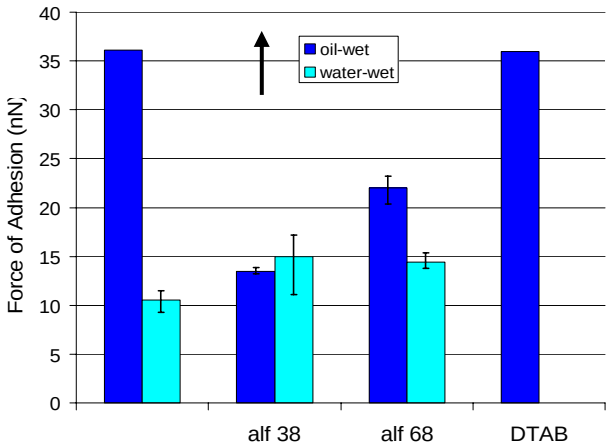

Fig. 13: Force of adhesion for oil-aged AP mica treated with and without surfactant treatment using NH_2 terminated tip

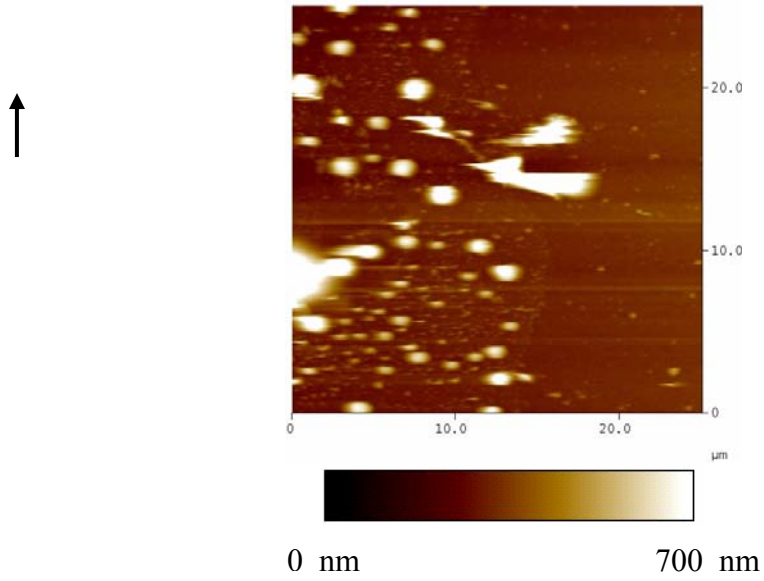

Fig. 14: Oil-wet and Water-wet Interface (25 μm x 25 μm)

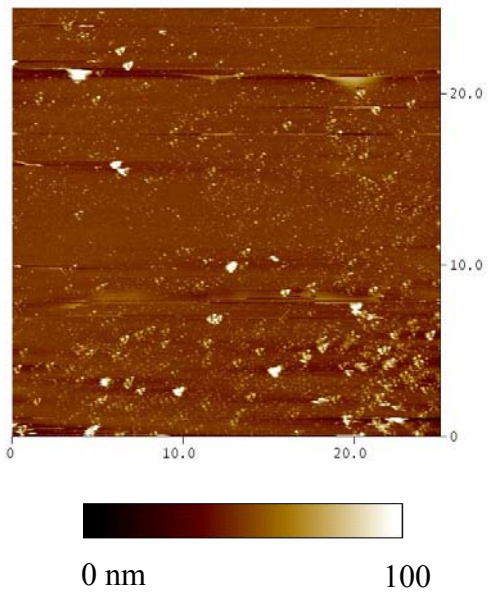

Fig. 15: Oil-wet and water-wet interface treated with Alf-38 for 15 min. (25 μm x 25 μm).

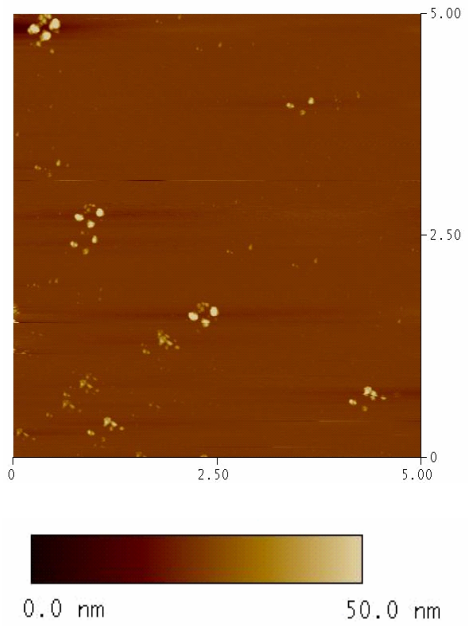

Fig. 16: Oil aged AP mica treated with Alf-38 for 1 day (5 µm x 5 µm).

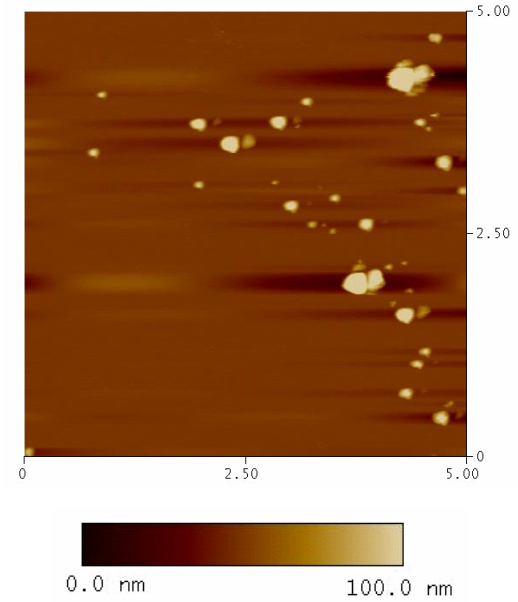

Fig. 17: Oil aged AP mica treated with Alf-68 for 1 day (5 µm x 5 µm).

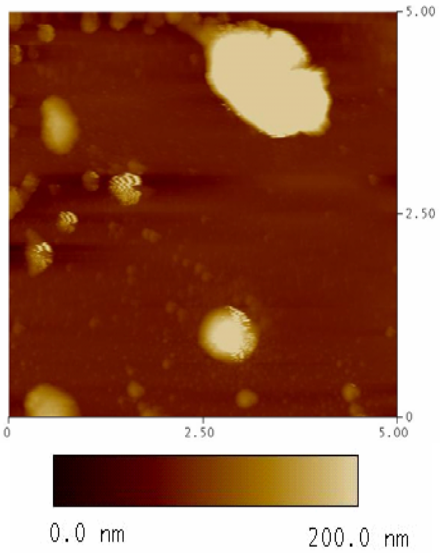

Fig. 18: Oil aged AP mica treated with DTAB for 1 day (5 µm x 5 µm).

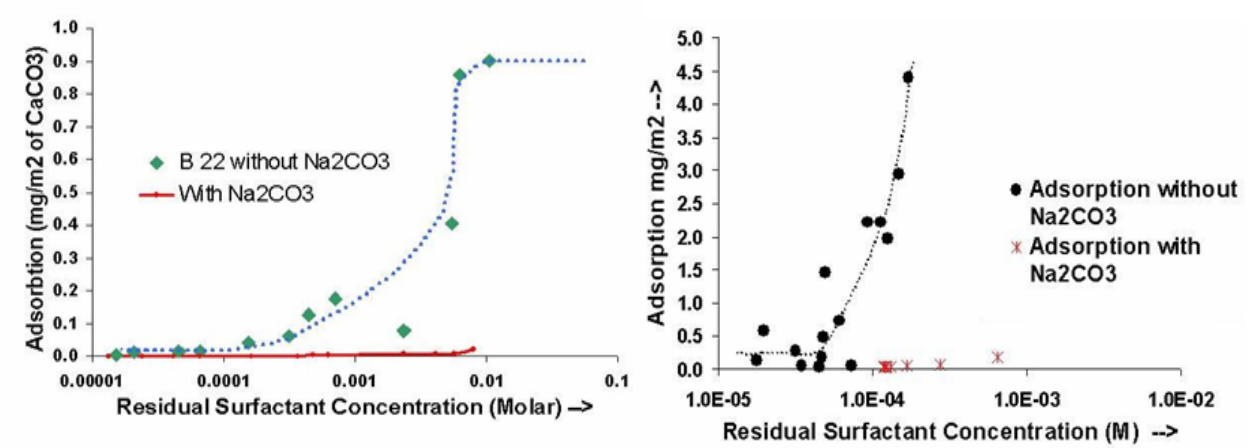

(a) (b)

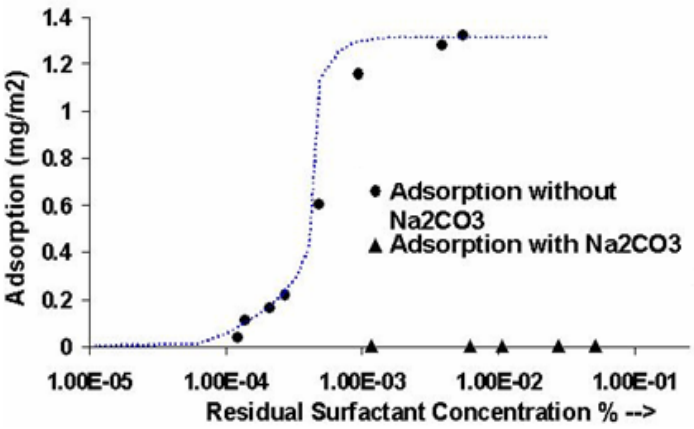

(c)

Fig. 19: Adsorption isotherms for surfactants (a) B-22 (4-22) (b) 5166 (c) 6566

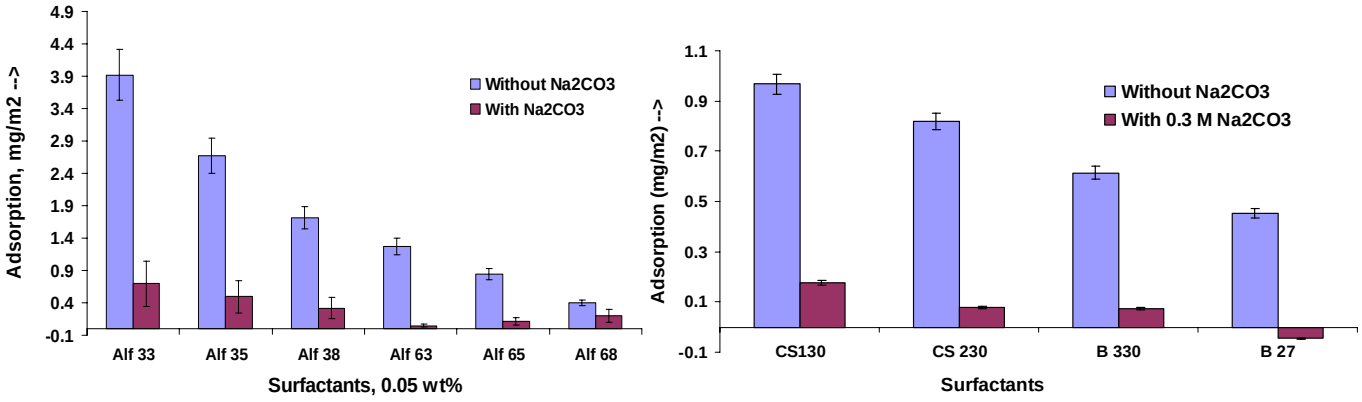

(a) (b)

Fig. 20: Plateau adsorption densities at 0.05 wt% surfactant concentration with and without the presence of 0.3 M Na_2CO_3 (a) Alkyl propoxy sulfates (b) Alkyl ethoxy sulfates

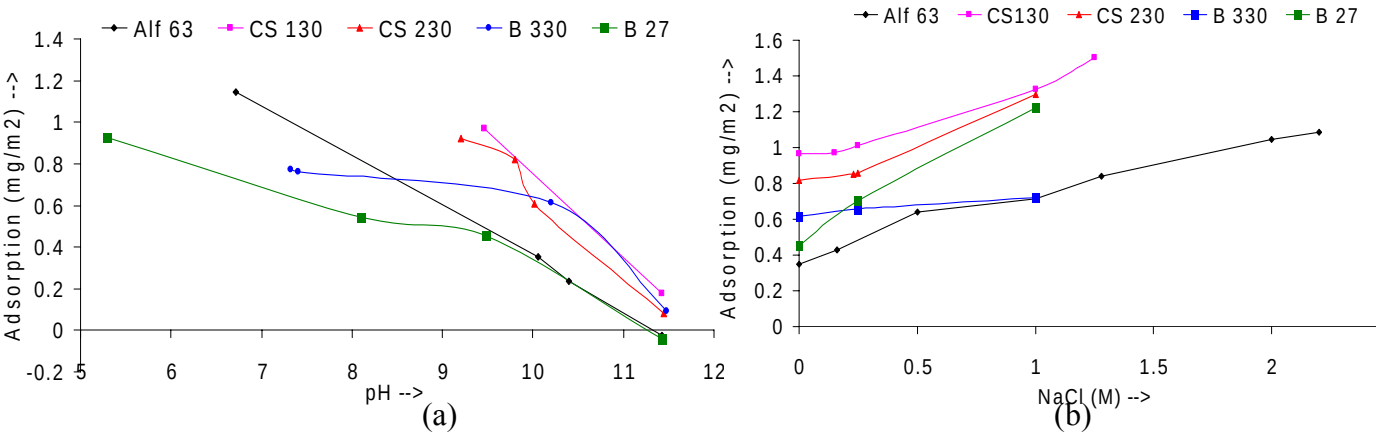

(a) (b)

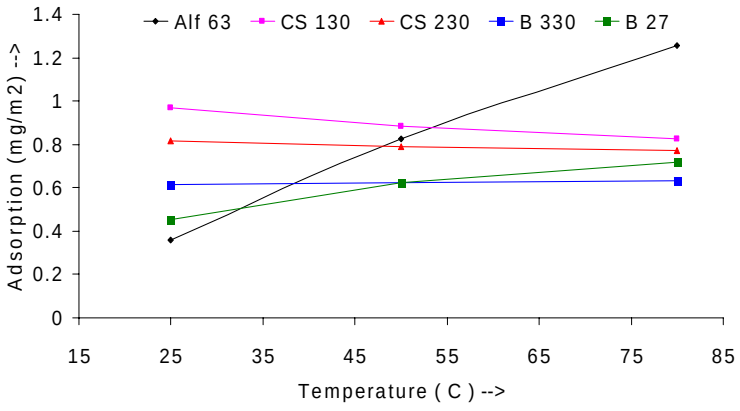

(c)

Fig. 21: Effect of different parameters on adsorption densities (a) pH (b) Salt concentration (c) Temperature

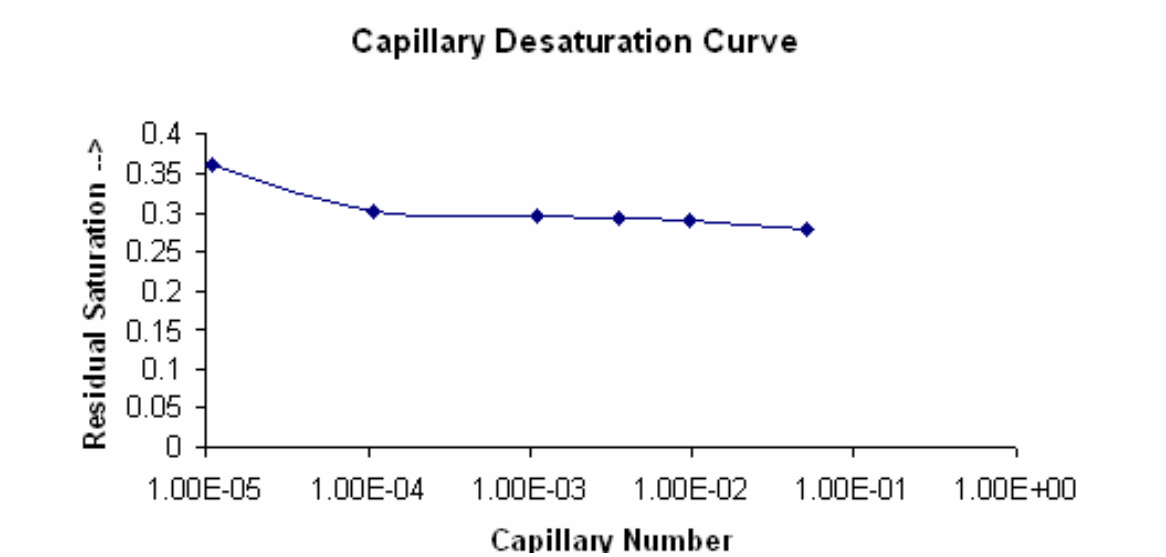

Fig. 22: Capillary desaturation curve for 150 mD carbonate outcrop.

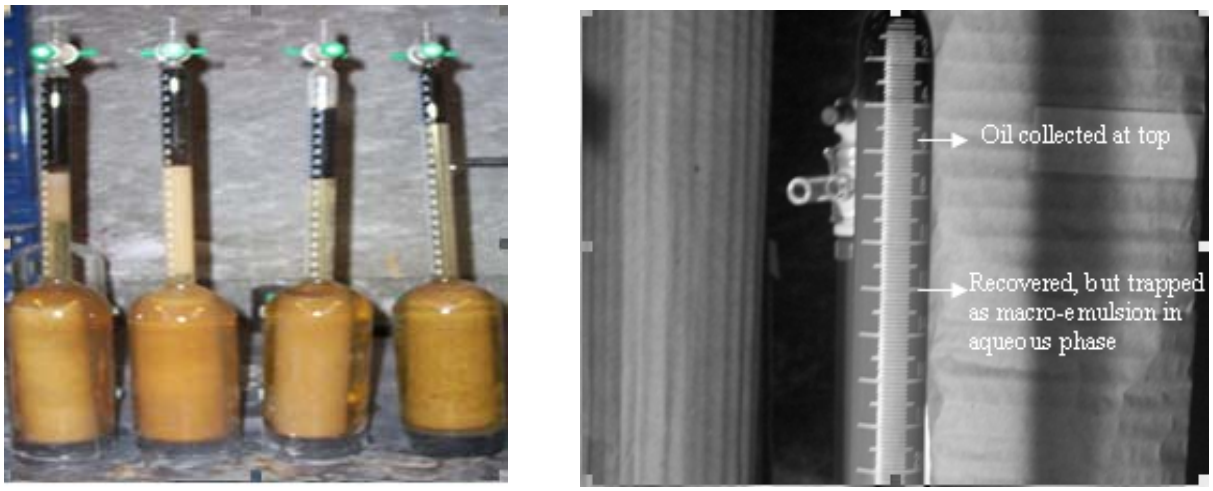

(a) (b)

Fig. 23: Imbibition set up for evaluating the surfactants in lab scale cores for oil recovery.

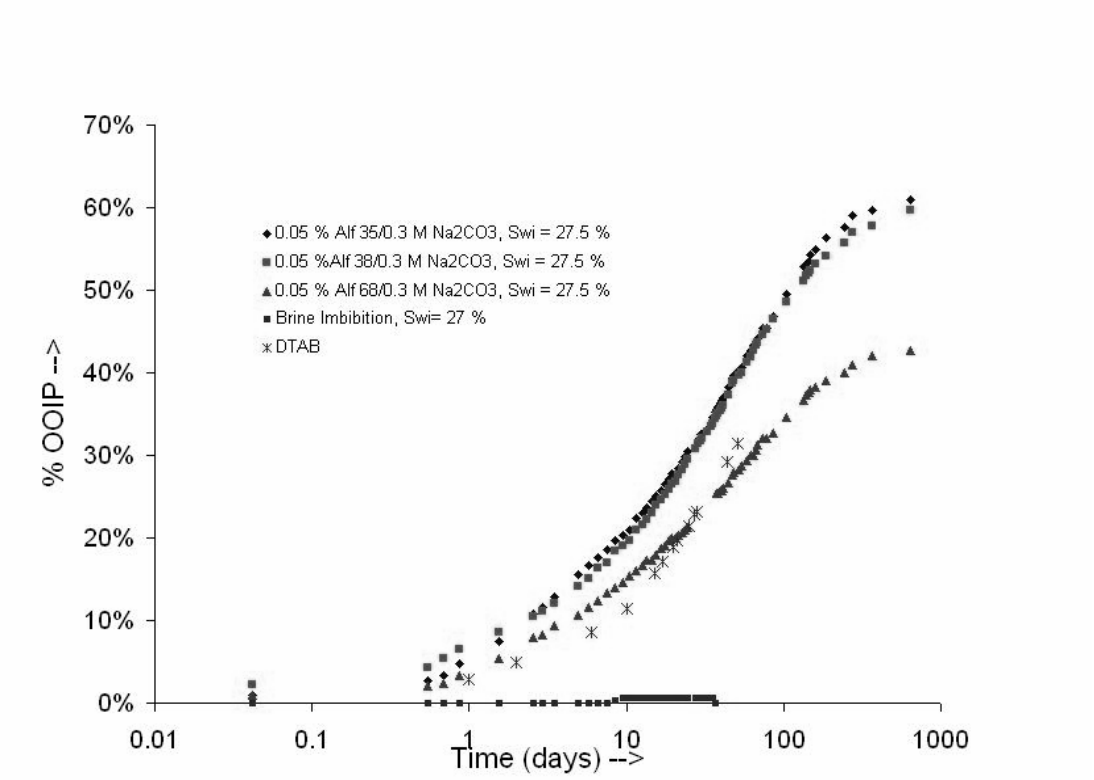

Fig. 24: Oil (separated) production for the surfactant brine imbibition in initially oil-wet cores.

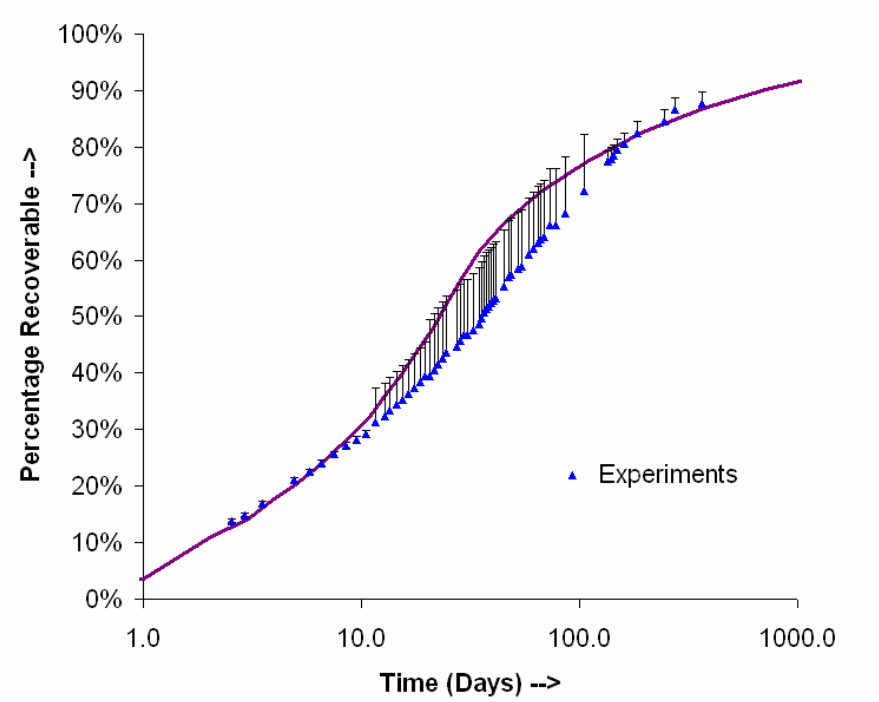

Fig. 25: Plausible experimental oil recovery curve for Alf-35 system in Fig. 24.

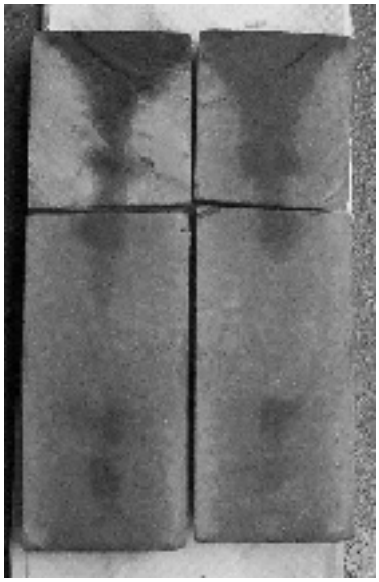

Fig. 26: Cleaved section of core at the end of imbibition

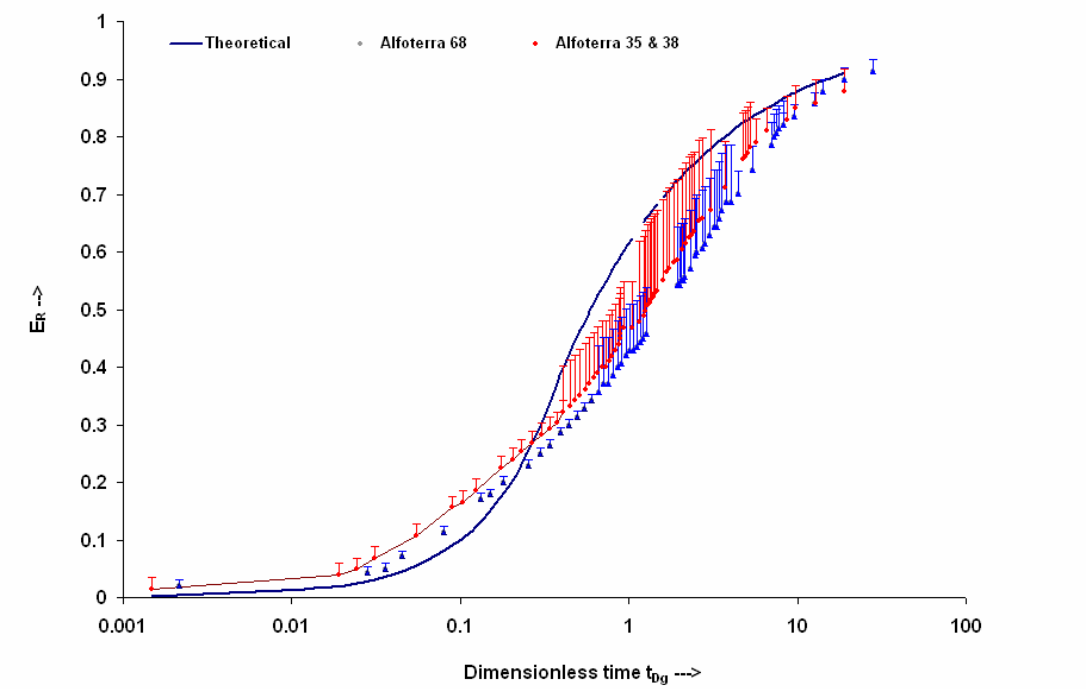

Fig. 27: Comparison of experimental results with theoretically predicted curve for gravity drainage

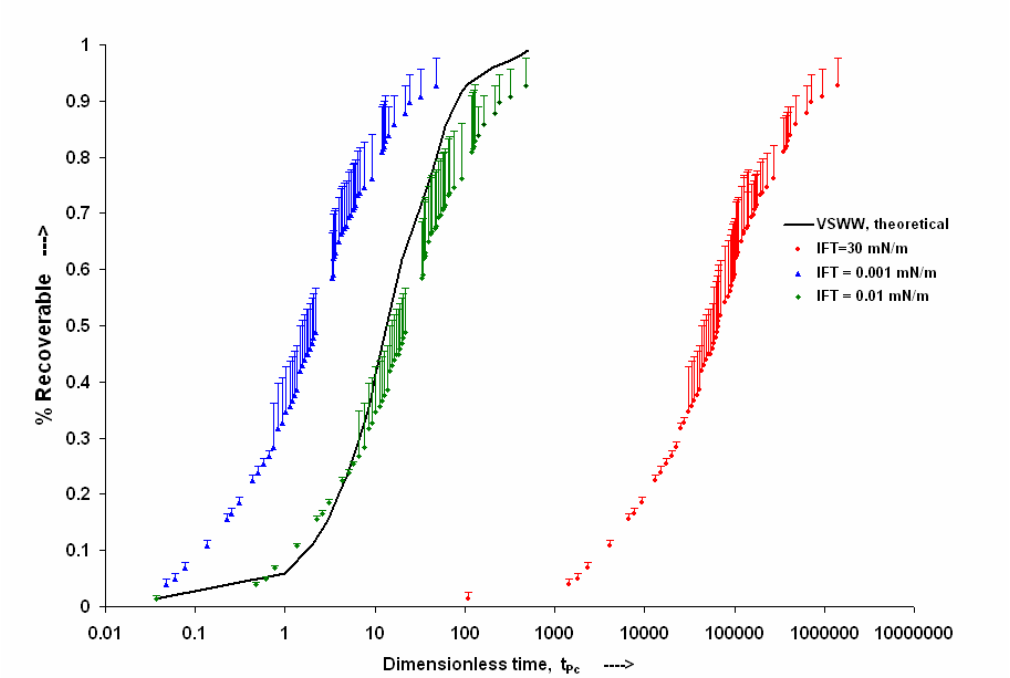

Fig. 28: Comparison of the experimental results with theoretically predicted capillarity-driven strongly water-wet curve

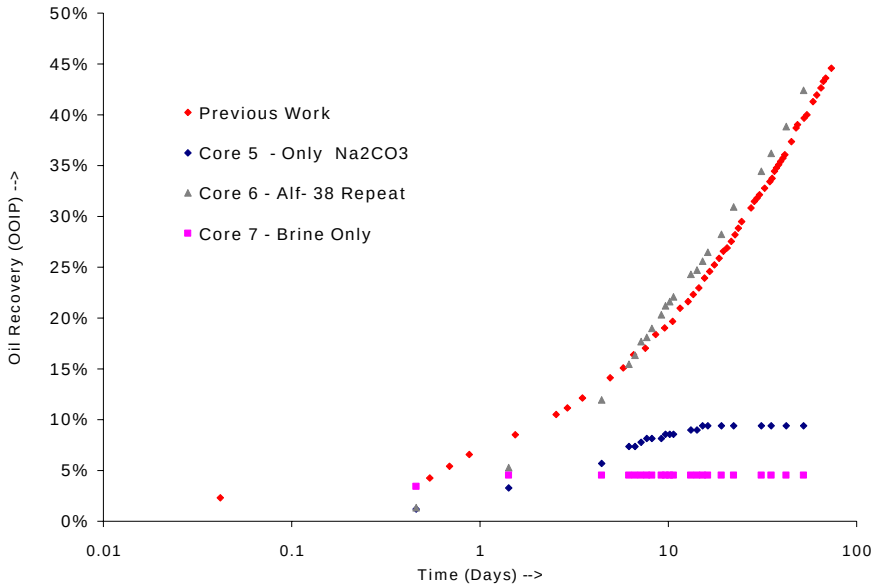

Fig. 29: Imbibition – Repeat experiment, only Na_2CO_3 and brine imbibition

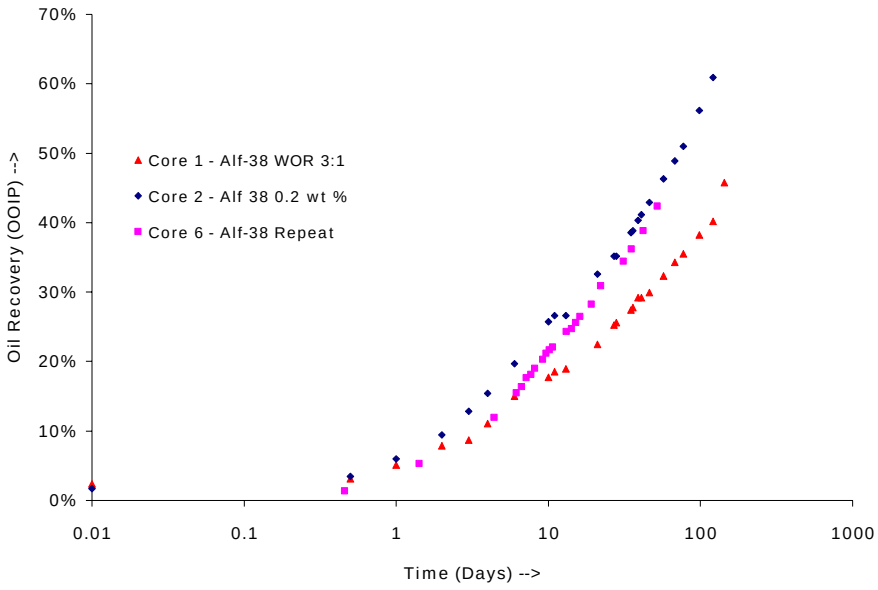

Fig. 30: Surfactant-brine imbibition: Effect of surfactant concentration and WOR.

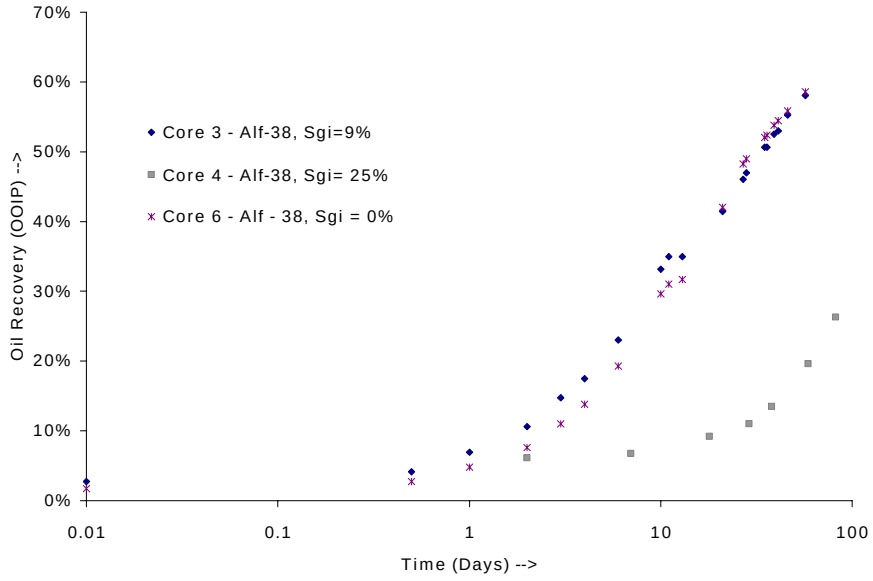

Fig. 31: Surfactant-brine imbibition: Effect of initial gas saturation

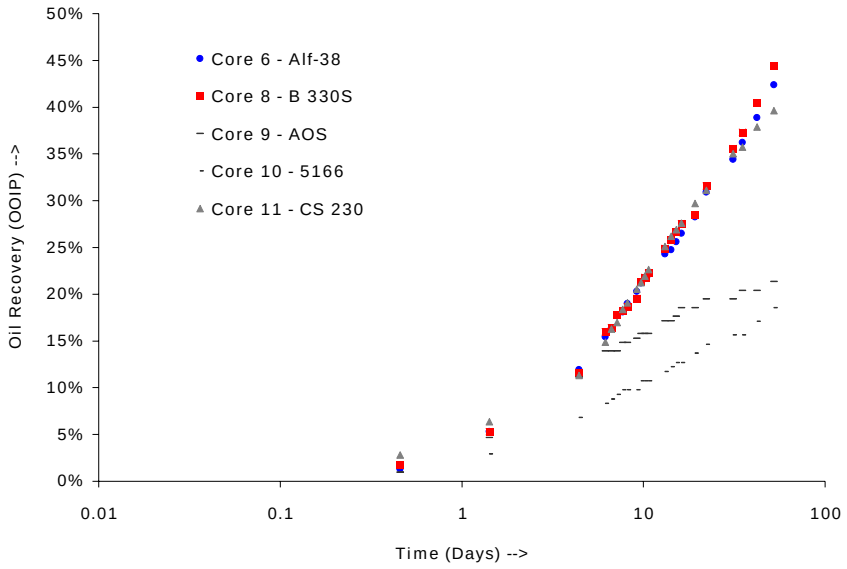

Fig. 32: Surfactant-brine imbibition: Effect of different surfactants

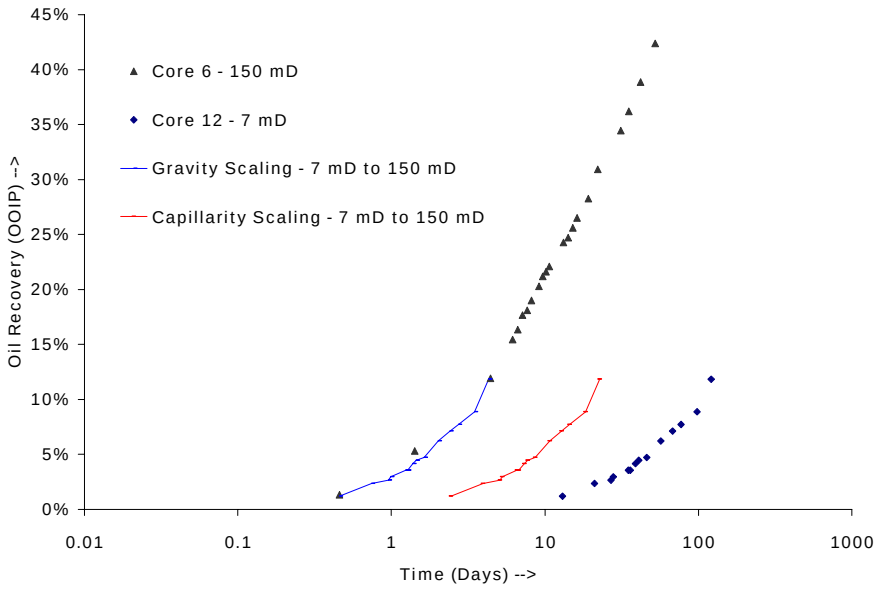

Fig. 33: Surfactant-brine imbibition: Effect of permeability, scaling with gravity and capillarity dimensionless times

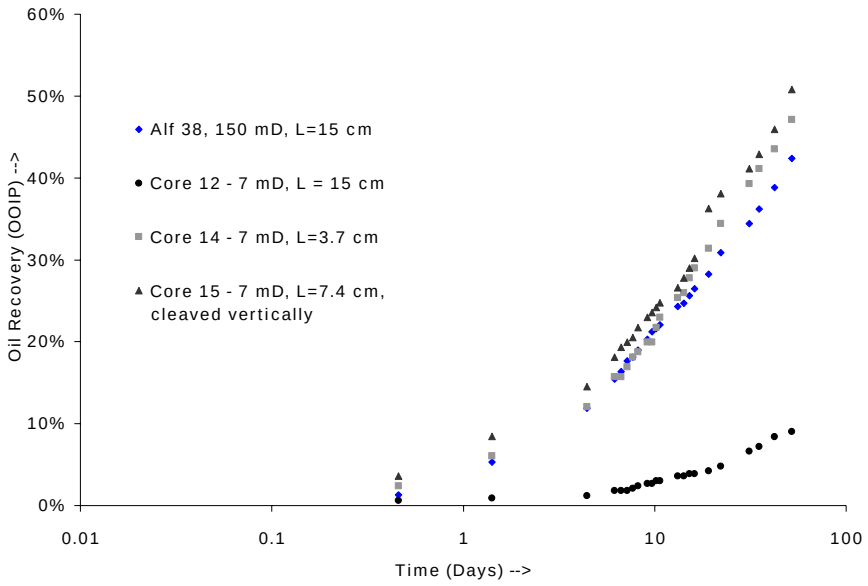

Fig. 34: Surfactant-brine imbibition: Effect of fracture length and diffusion length

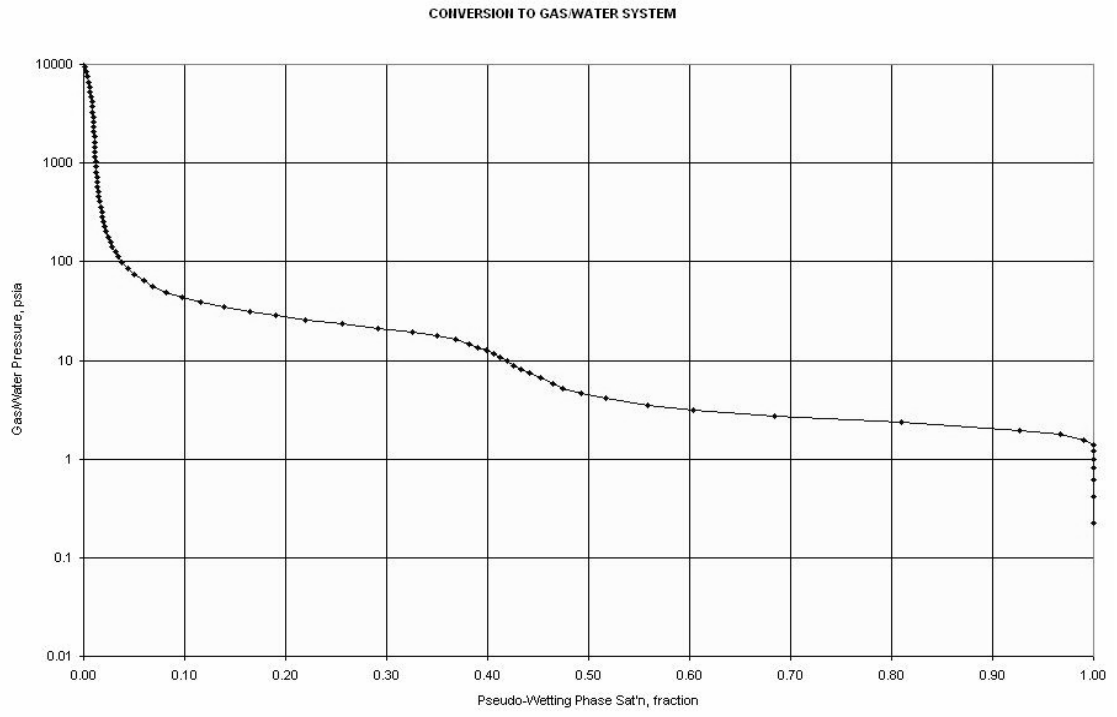

Fig. 35: Primary drainage capillary pressure curve for the cores used in the experiment.

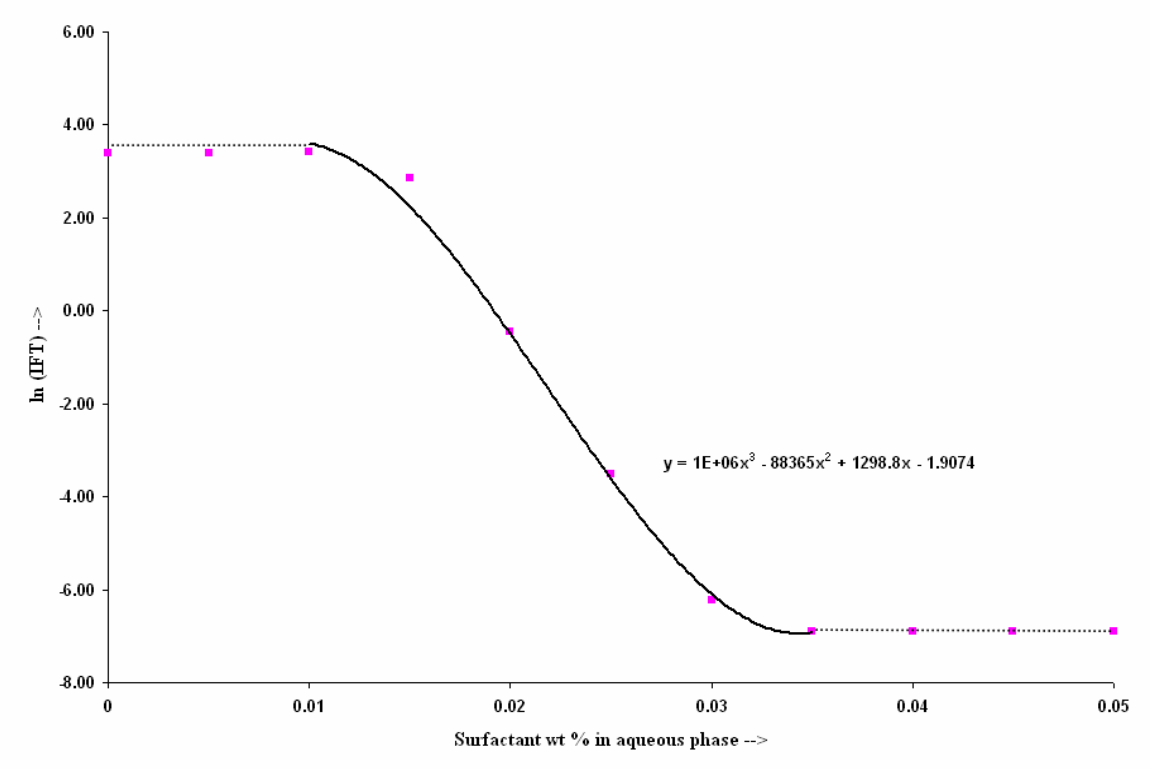

Fig. 36: IFT as function of surfactant concentration at 0.3 M Na_2CO_3 with numerical fit.

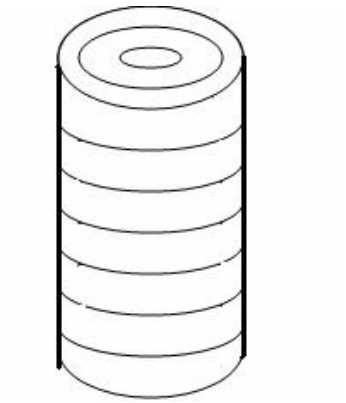

Fig. 37: Simulation grid structure for a cylindrical core

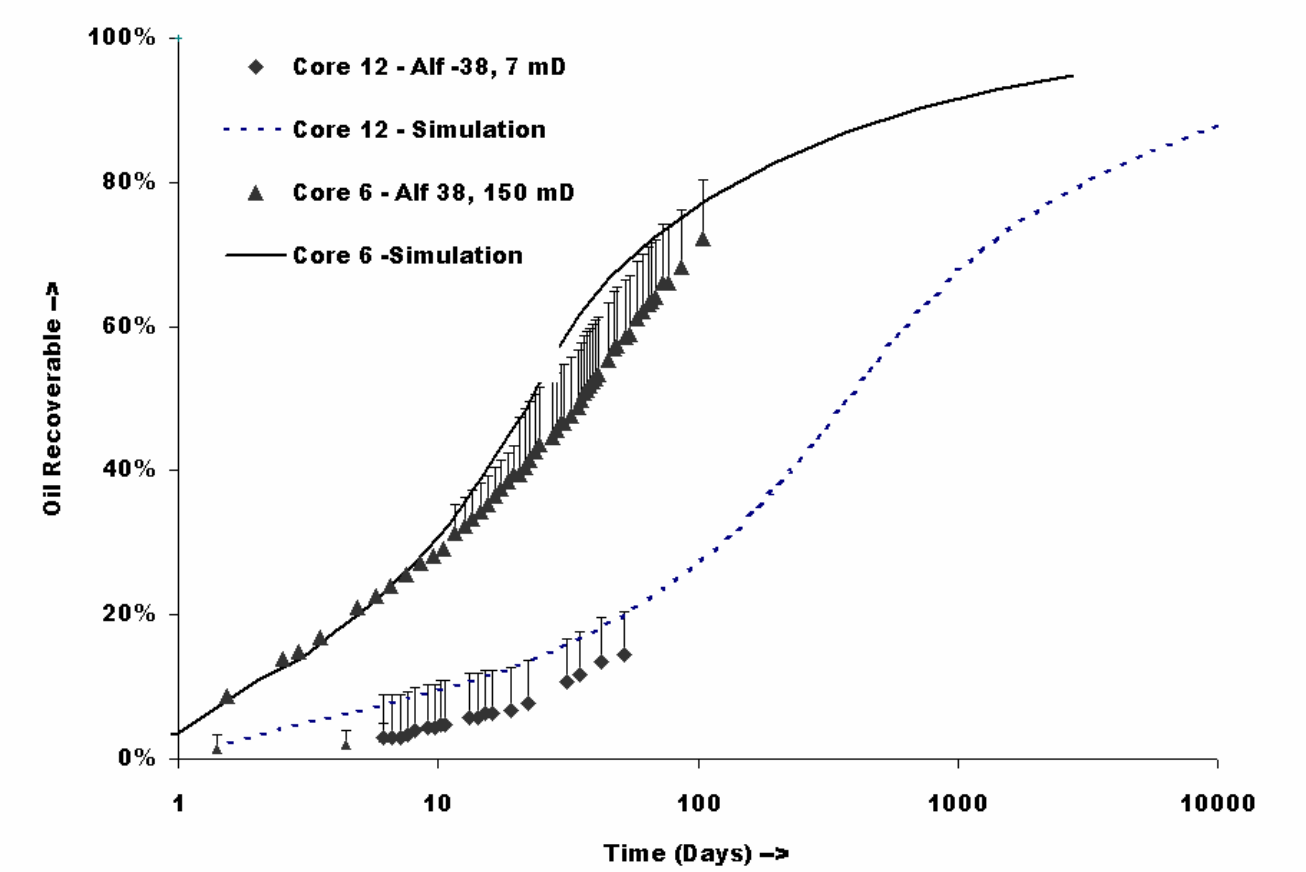

Fig. 38: Comparison of experimental and simulation results for 0.05 wt% Alf-38 system at 0.3 M Na_2CO_3 for 150 mD and 7 mD cores.

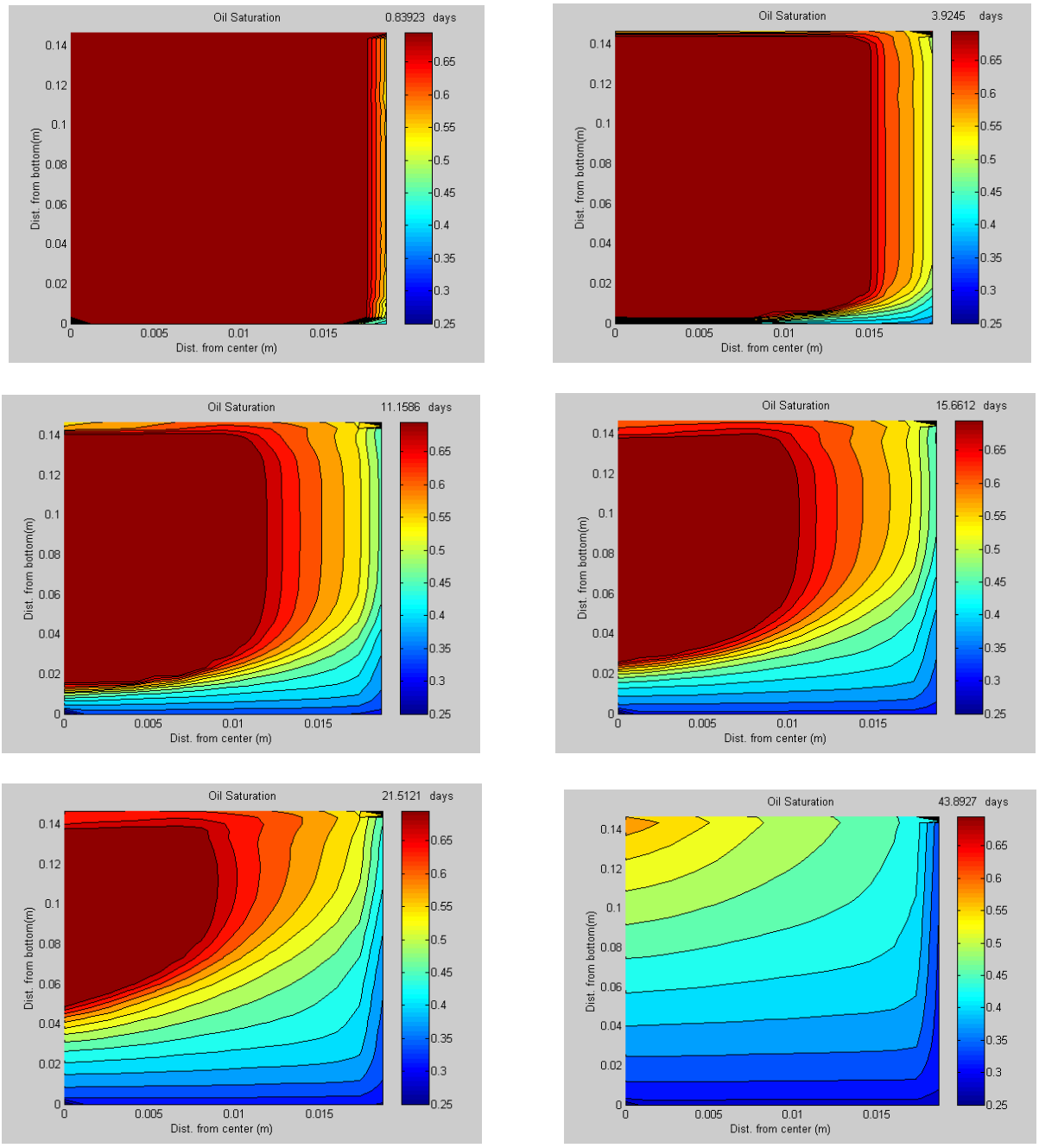

Fig. 39: Oil Saturation at various times, t=0.83, 3.9, 11.5, 15.16, 21.5, 43.8 days from top left, row-wise. X-axis is radial distance from center, Y-axis is distance from bottom. At end of 21 days, 30 % of oil recoverable is produced.

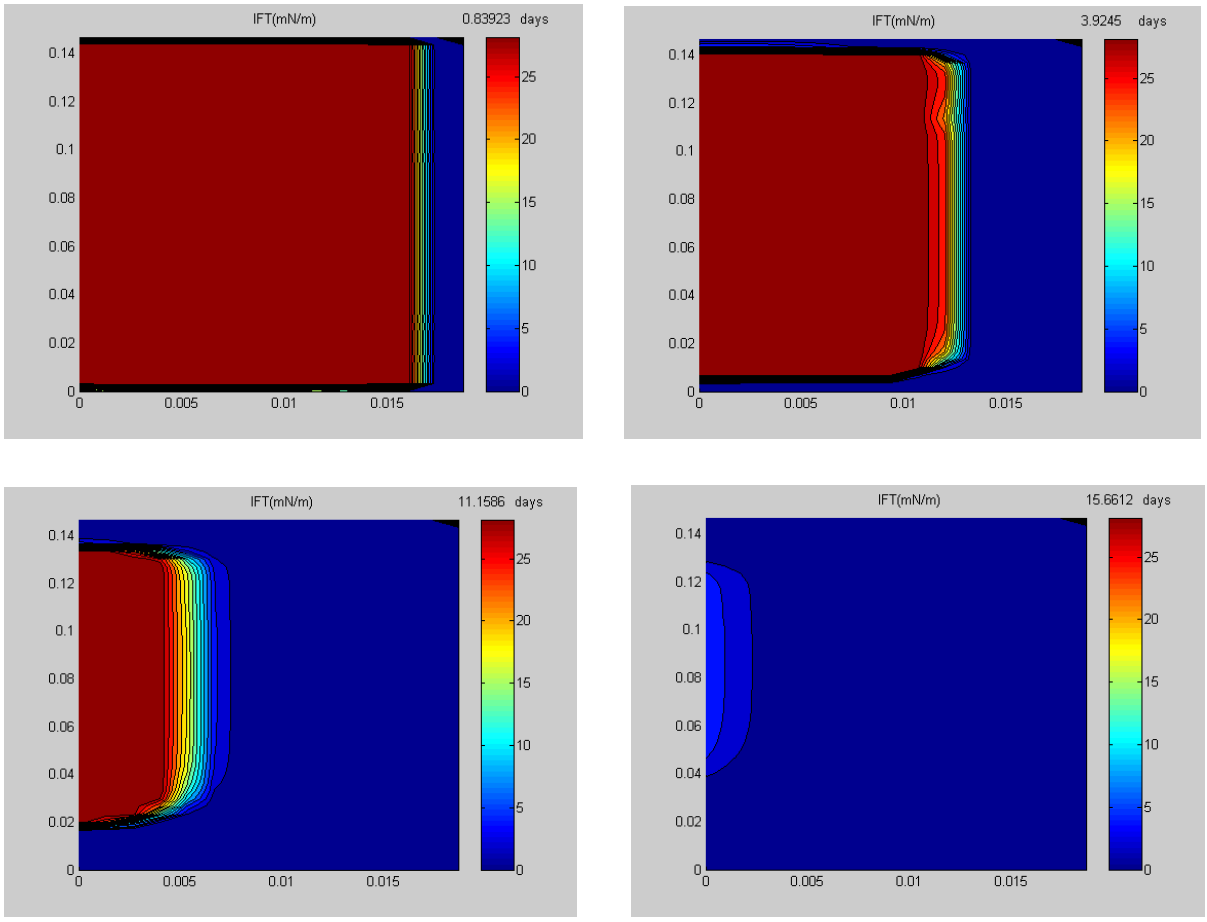

Fig. 40: IFT at various times, t = 0.83, 3.9, 11.5, 15.16 days from top left, row-wise. X-axis is radial distance from center, Y-axis is distance from bottom

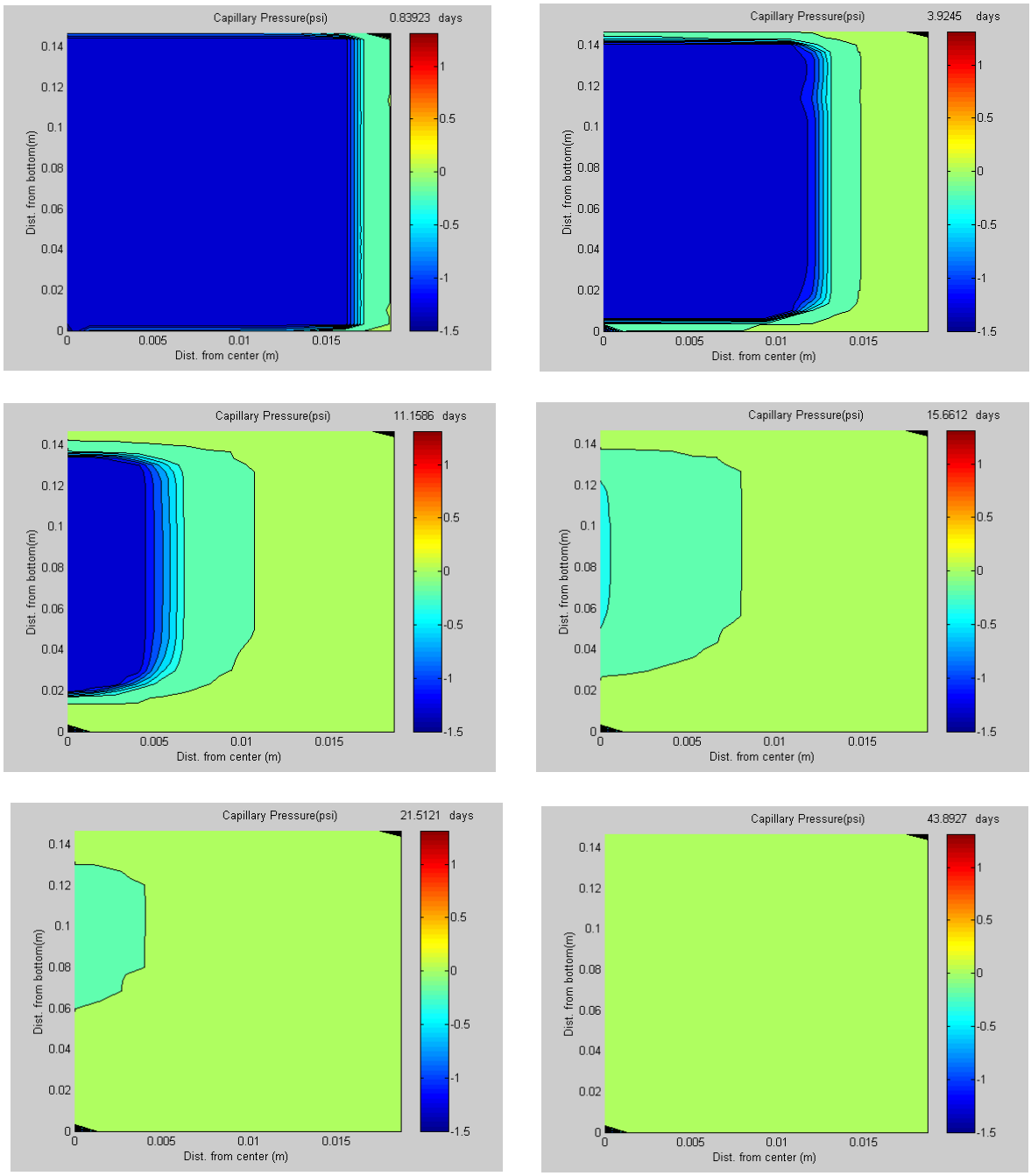

Fig.41: Pc at various times, t = 0.83, 3.9, 11.5, 15.16, 21.5, 43.9 days from top left, row-wise.

X-axis is radial distance from center, Y-axis is distance from bottom

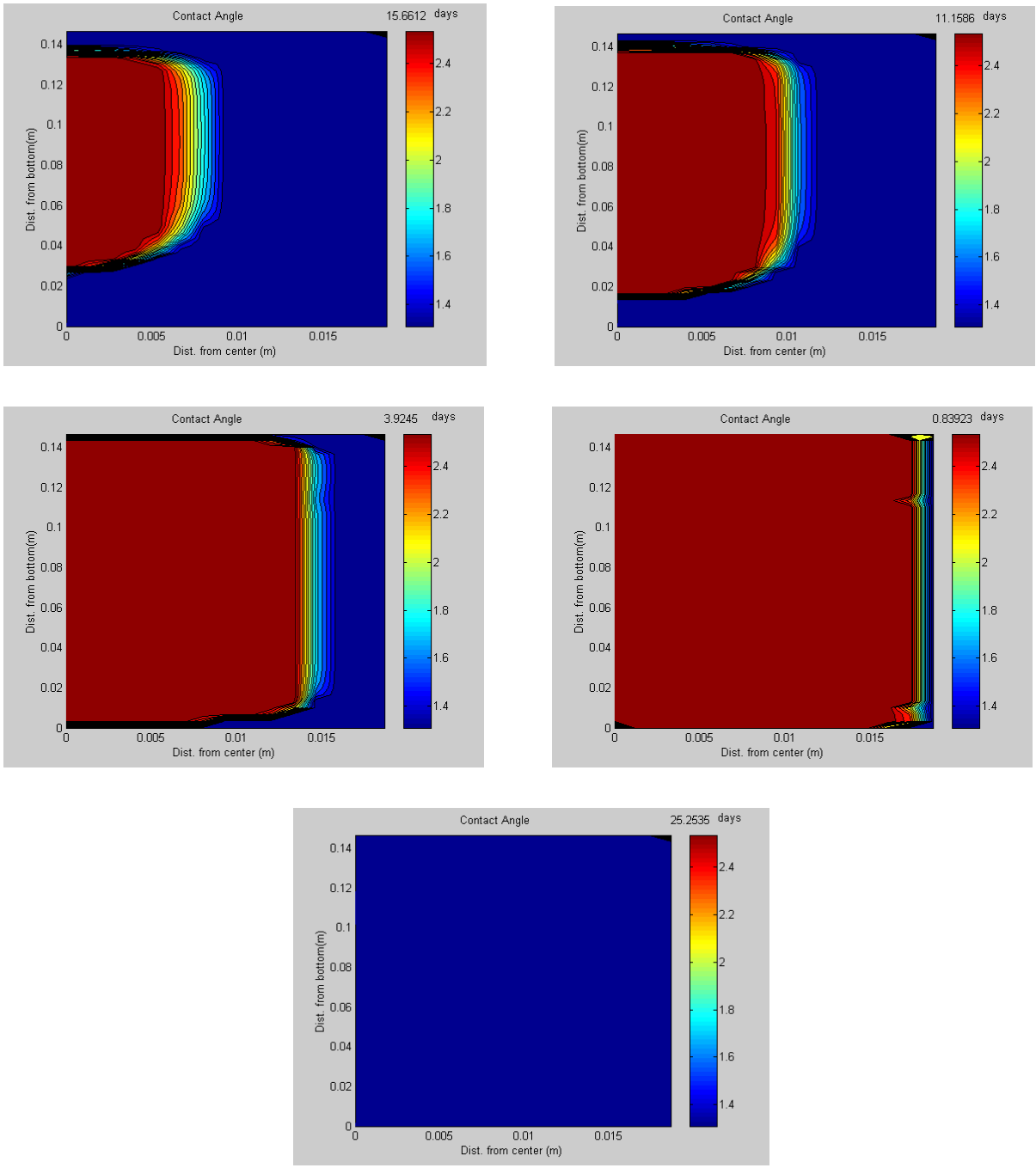

Fig. 42: Contact angle at various times, t = 0.83, 3.9, 11.5, 15.16, 25.25 days from top left, row-wise. X-axis is radial distance from center, Y-axis is distance from bottom

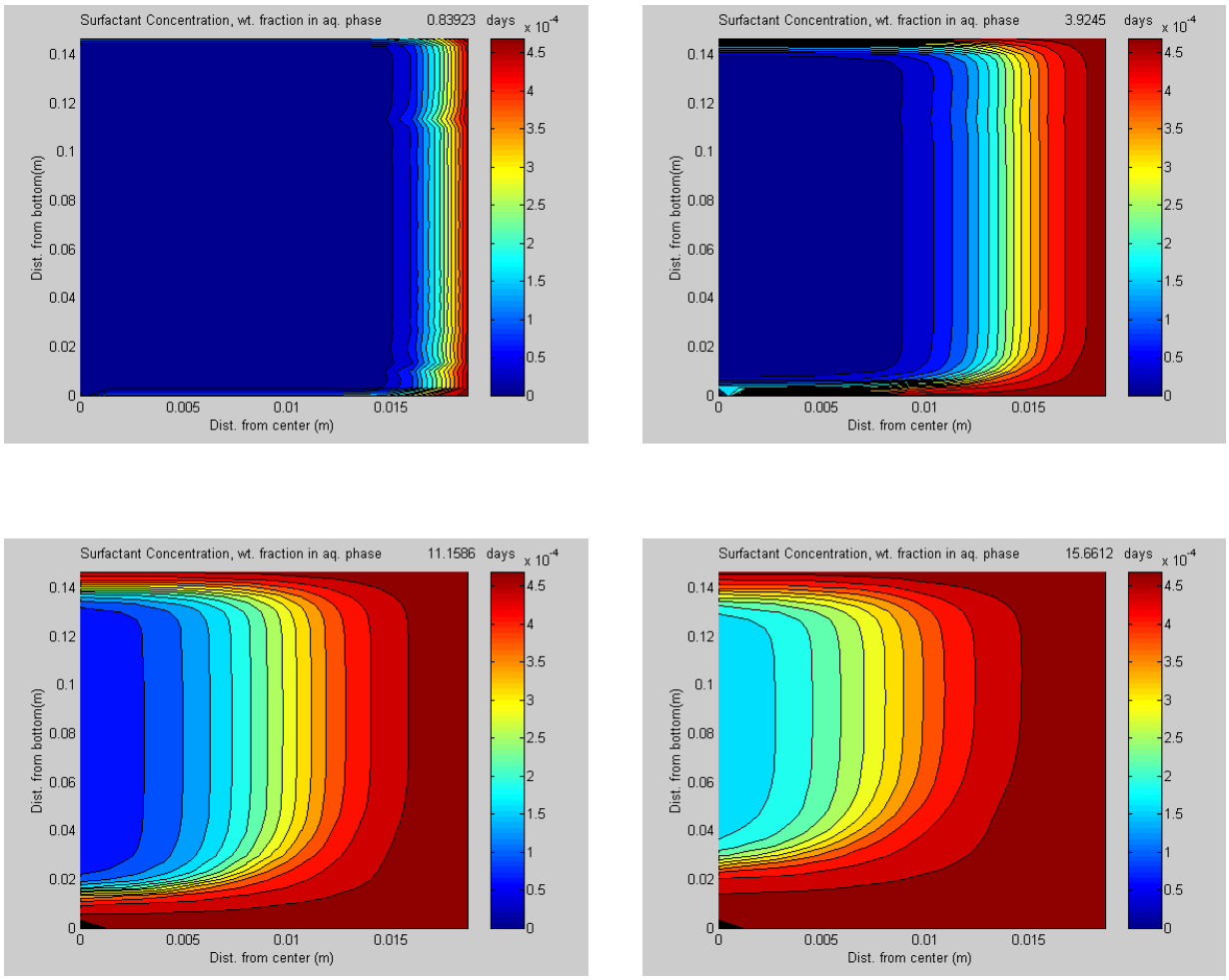

Fig. 43: $C_{surfactant}$ at various times, t = 0.83, 3.9, 11.5, 15.16 days from top left, row-wise. X-axis is radial distance from center, Y-axis is distance from bottom. System reaches steady value of 0.05 wt% in 24 days.

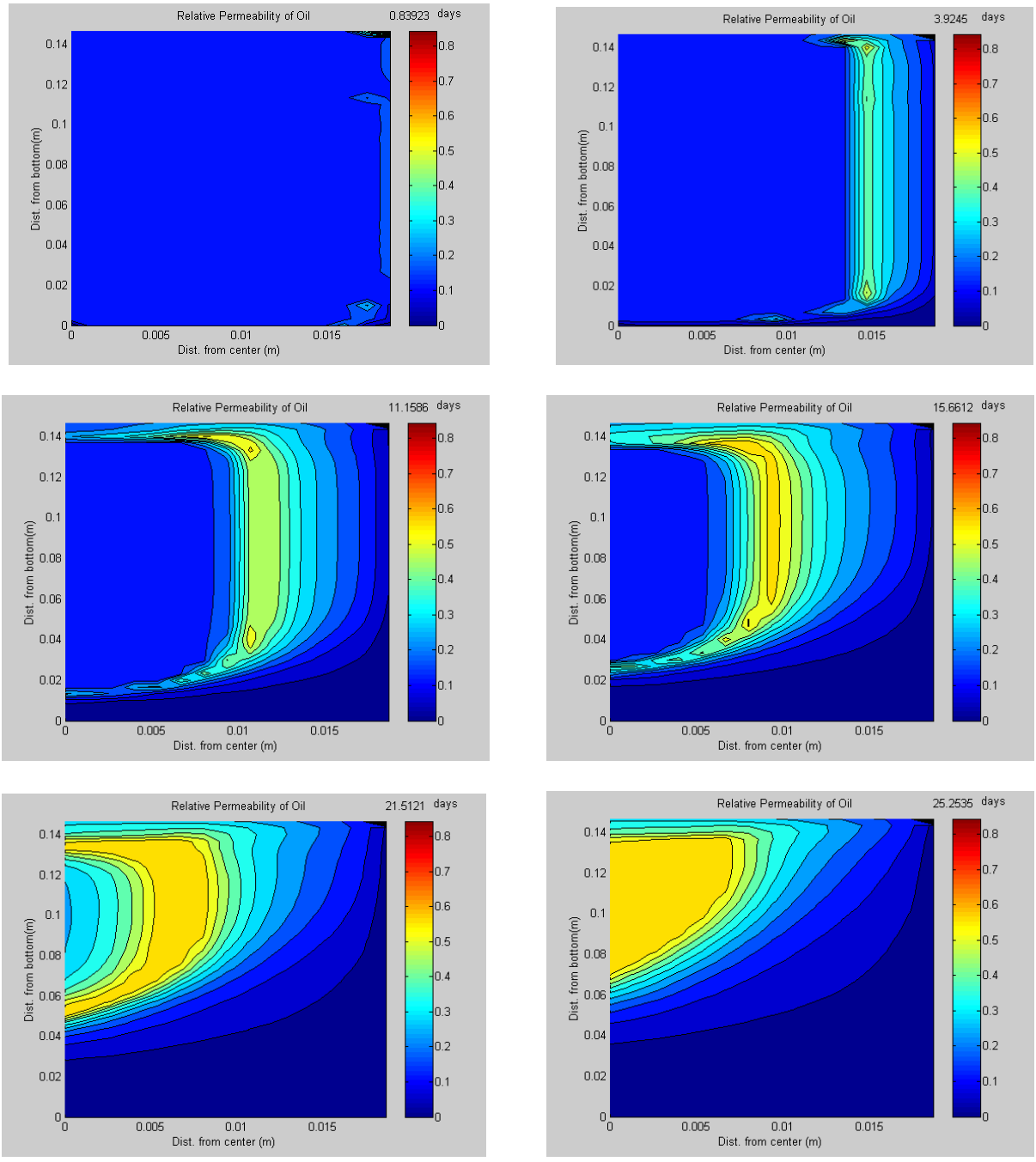

Fig. 44: Relative permeability of oil, K_{ro} at various times, t = 0.83, 3.9, 11.5, 15.16, 21.5, 25.25 days from top left, row-wise.

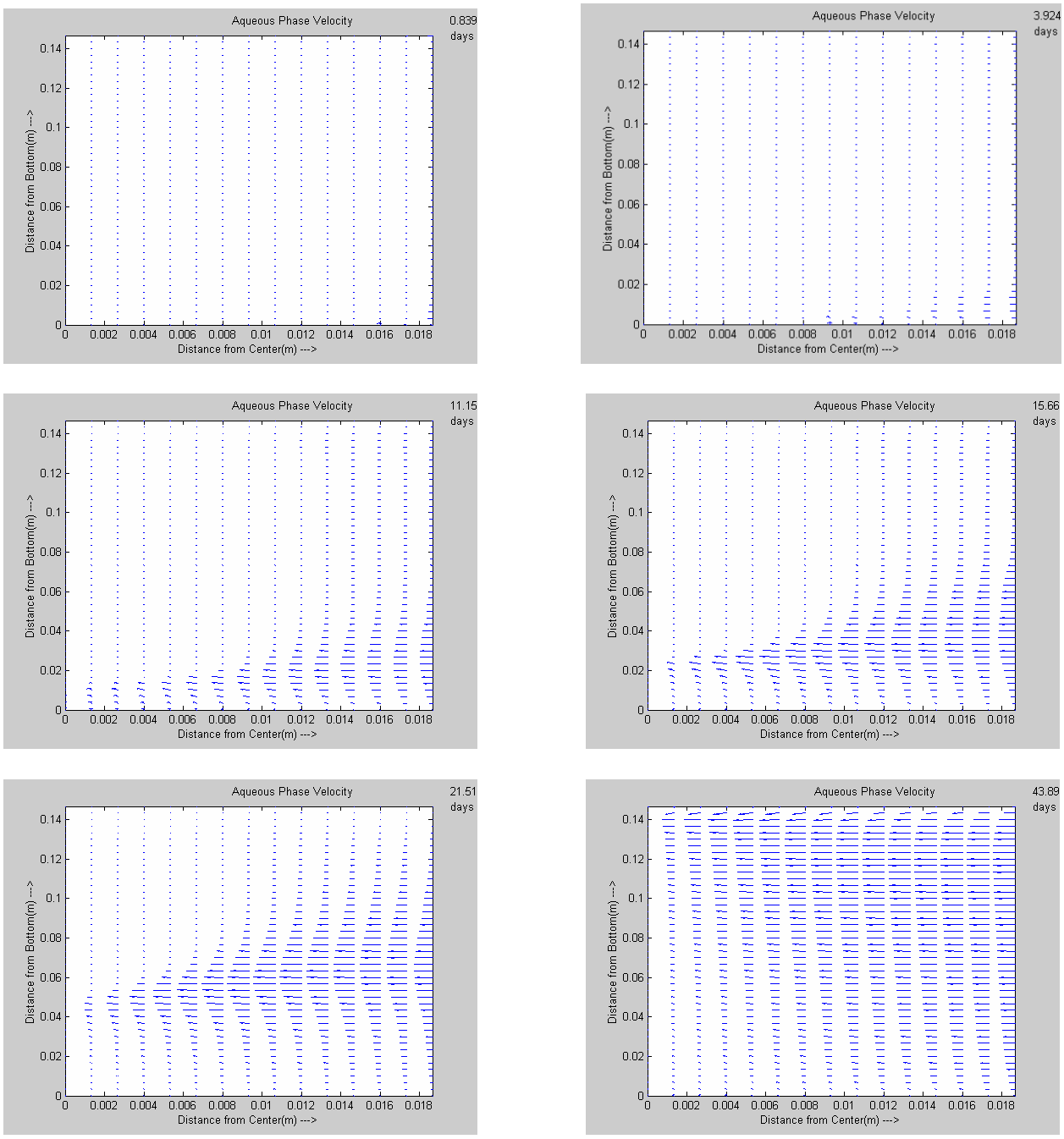

Fig. 45: Aqueous phase velocities at various times, t = 0.83, 3.9, 11.5, 15.16, 21.5, 43.89 days from top left, row-wise. Aqueous phase is seen to imbibe radially with prominent velocity streak traveling from bottom of the core to the top as time progresses.

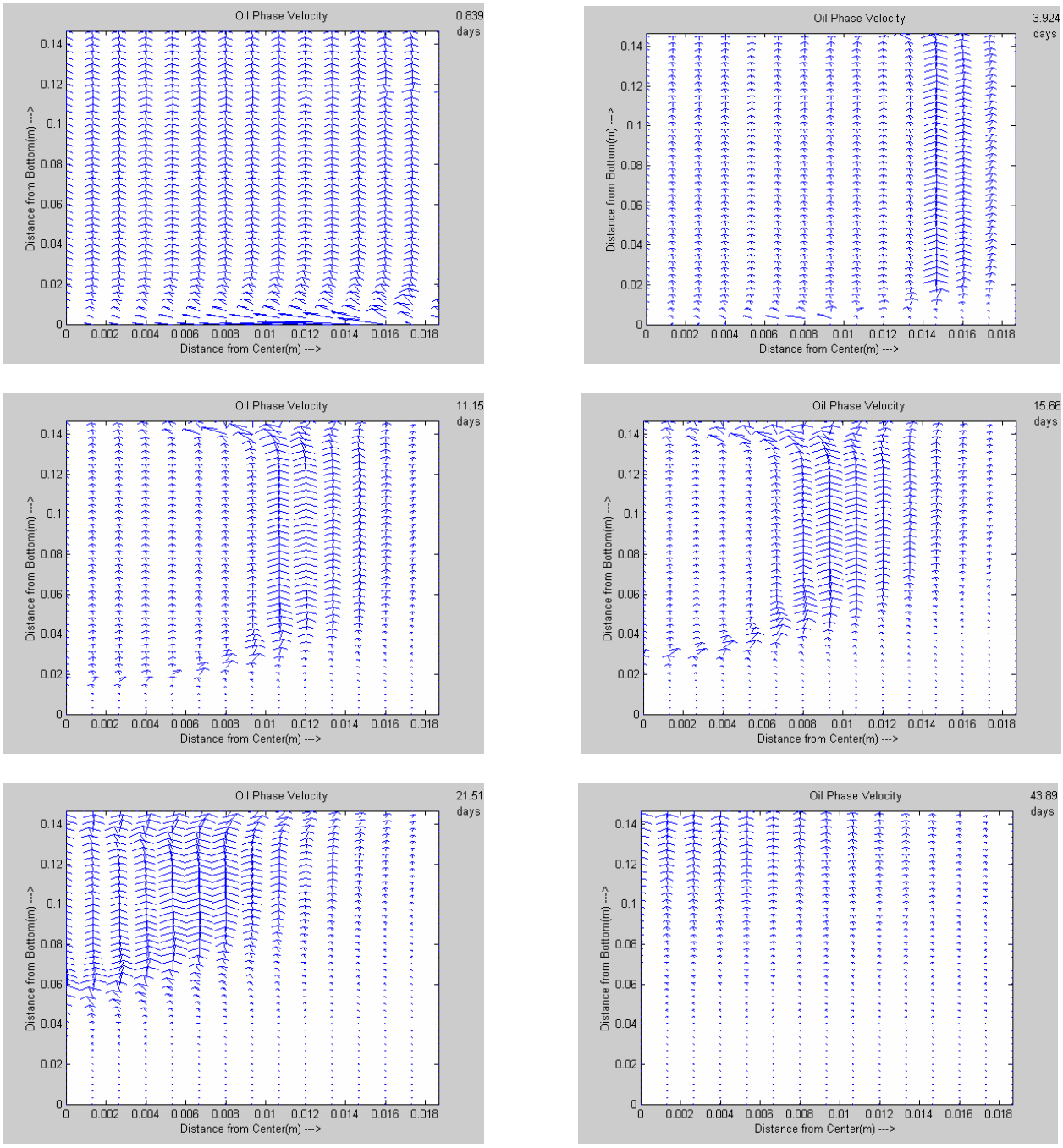

Fig. 46: Oil phase velocities at various times, t = 0.83, 3.9, 11.5, 15.16, 21.5, 43.89 days from top left, row-wise. Oil phase is seen to recover from the top of the core with prominent velocity streak traveling in the direction of highest oil relative permeability as seen in Fig. 44.

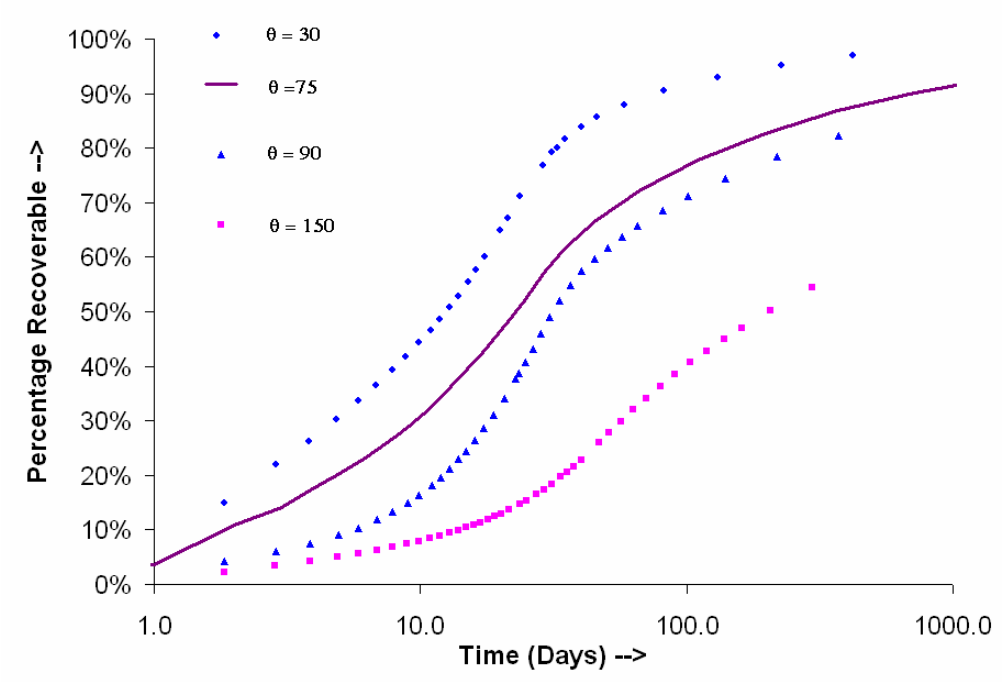

Fig. 47: Surfactant-brine imbibition: Effect of extent of wettability alteration

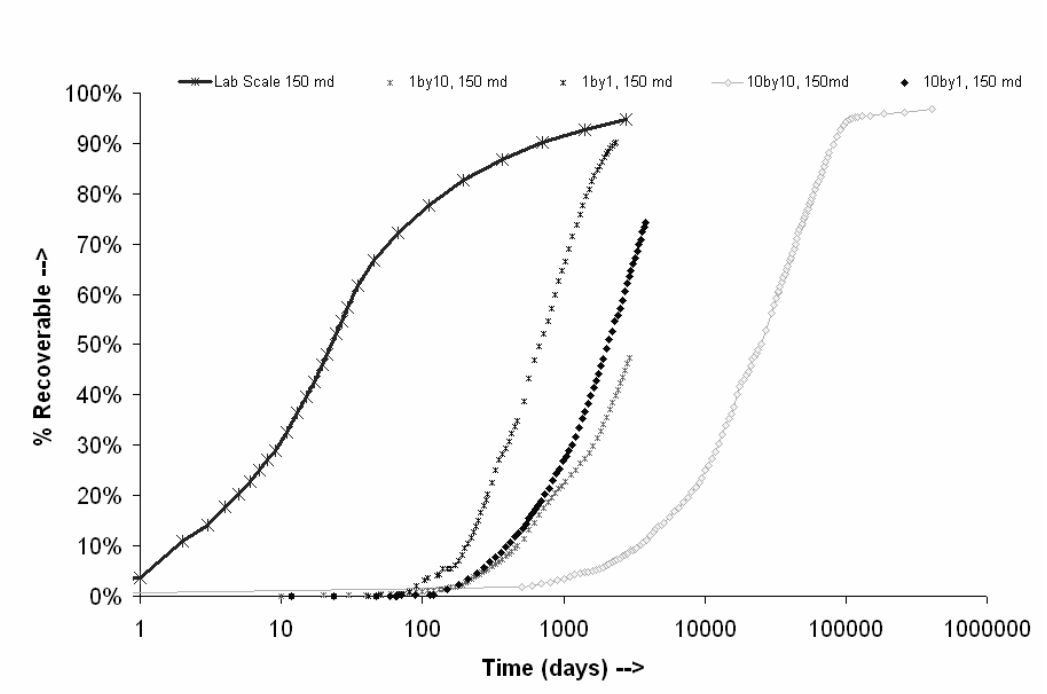

Fig. 48: Scale up of the imbibition process to 1 m wide X 1 m high, 1 m X 10 m, 10 m X 1 m, and 10 m X 10 m fracture blocks.

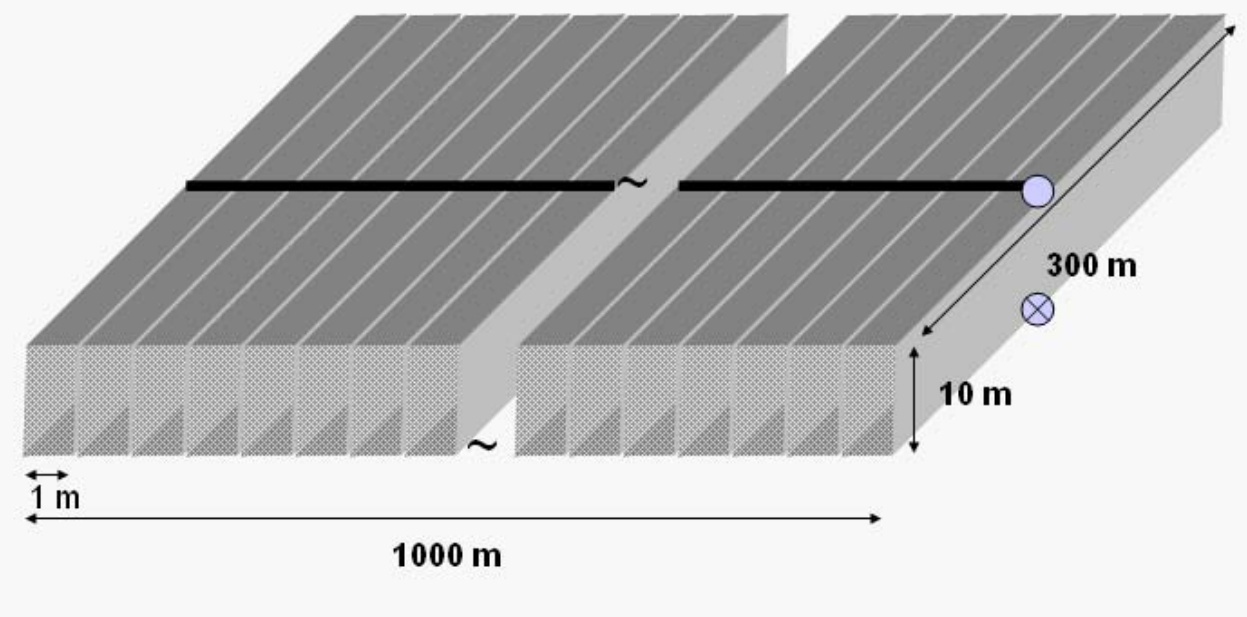

Fig. 49: Reservoir block used for simulation of surfactant huff-n-puff process of oil recovery from fractured oil-wet carbonate media

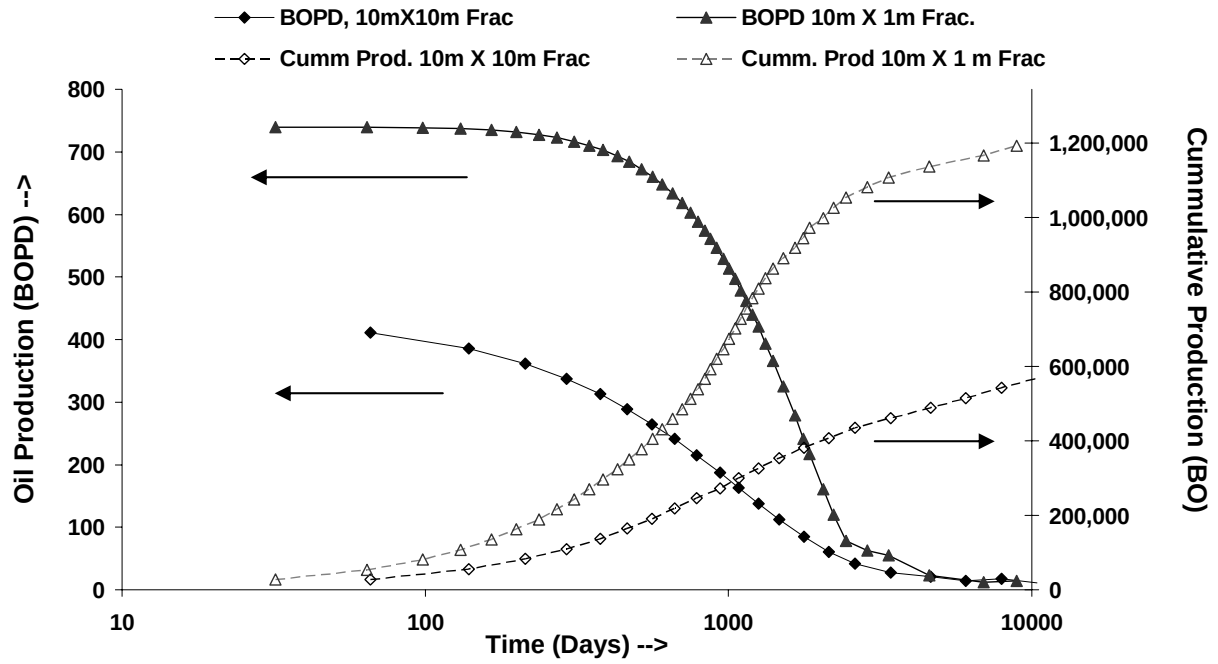

Fig. 50: Production from 1000 m x 300 m fractured oil-wet reservoir, with fracture spacing of 10 m and 1 m.